

2022-08-01

An Unmanned Surface Vehicle: Autonomous Sensor Integration System for Bathymetric Surveys

Fernando Sotelo Torres
University of Texas at El Paso

Follow this and additional works at: https://scholarworks.utep.edu/open_etd



Part of the [Electrical and Electronics Commons](#), and the [Water Resource Management Commons](#)

Recommended Citation

Sotelo Torres, Fernando, "An Unmanned Surface Vehicle: Autonomous Sensor Integration System for Bathymetric Surveys" (2022). *Open Access Theses & Dissertations*. 3730.
https://scholarworks.utep.edu/open_etd/3730

This is brought to you for free and open access by ScholarWorks@UTEP. It has been accepted for inclusion in Open Access Theses & Dissertations by an authorized administrator of ScholarWorks@UTEP. For more information, please contact lweber@utep.edu.

AN UNMANNED SURFACE VEHICLE: AUTONOMOUS SENSOR INTEGRATION
SYSTEM FOR BATHYMETRIC SURVEYS

FERNANDO SOTELO TORRES

Master's Program in Electrical Engineering

APPROVED:

Laura Alvarez, Ph.D., Chair

Robert Roberts, Ph.D., Co-Chair

Hector Erives-Contreras, Ph.D.

Miguel Velez-Reyes, Ph.D.

Virgilio Gonzalez, Ph.D.

Stephen L. Crites, Jr., Ph.D.
Dean of the Graduate School

Copyright ©

by

Fernando Sotelo Torres

2022

DEDICATION

This thesis is dedicated to my family.

For their endless love, support, and encouragement.

AN UNMANNED SURFACE VEHICLE: AUTONOMOUS SENSOR INTEGRATION
SYSTEM FOR BATHYMETRIC SURVEYS

by

FERNANDO SOTELO TORRES, B.S.

THESIS

Presented to the Faculty of the Graduate School of

The University of Texas at El Paso

in Partial Fulfillment

of the Requirements

for the Degree of

MASTER OF SCIENCE

Department of Electrical and Computer Engineering

THE UNIVERSITY OF TEXAS AT EL PASO

August 2022

ACKNOWLEDGEMENTS

Thank you to my parents, Cecilia and Guillermo, who teach me that everything worth in life comes with a cost, and for their unconditional support.

My sincere gratitude to my advisor Dr. Laura Alvarez for her treasure guidance and advice throughout the process. For giving me the tools and space to build a real-scale prototype. I would also like to thank my thesis co-advisor, Dr. Robert Roberts, for his valuable feedback on my research. Without their support, I could not be able to finish this research.

Finally, I would like to recognize the support of my friends and members of the GeSeoSE research group in developing this project. Especially to Jorge Mayo, Jayanga Thanuka, Santiago Hoyos, Dr. Hernan Moreno, and my little brother Pablo Sotelo that help me in the field campaigns and laboratory tests.

ABSTRACT

Unmanned Surface Vehicles (USVs) have been applied to earth sciences, with only a few studies conducted in water environments, as these systems provide autonomous measurement capabilities and transferability to other environmental settings. In this thesis, a reliable, yet economical, USV has been developed for bathymetric surveying of lakes. The system combines an autonomous navigation framework, environmental sensors and a multibeam echosounder to collect submerged topography, temperature, windspeed and monitor the vehicle status during prescribed path planning missions.

The main objective of this study is to provide a methodological framework to build a USV, with independent decision-making, efficient control, and long-range navigation capabilities. Integration of sensors with navigation control enabled the automatization of position, orientation, and velocity of the vehicle. A solar power integration was also tested to control the duration of the autonomous missions. Results of the solar power compared favorable against the standard LiPO Battery System. Extended and autonomous missions were achieved, with the developed platform, that is also capable of evaluating the danger level, weather circumstances, and energy consumption through real-time data analysis. With all incorporated sensors and controls, this USV is able to achieving self-governing decisions and improving its own safety. A technical evaluation of the proposed vehicle was conducted as a measurable metric of the reliability and robustness of the prototype. Overall, a reliable, economical and self-powered autonomous system has been designed and built to retrieve bathymetric surveys, as a first step to develop intelligent systems for reconnaissance that combines field robotics with machine learning to make decisions an adapt to unknown environments.

TABLE OF CONTENTS

DEDICATION.....	iii
ACKNOWLEDGEMENTS.....	v
ABSTRACT	vi
TABLE OF CONTENTS	vii
LIST OF TABLES	ix
LIST OF FIGURES	x
CHAPTER 1: INTRODUCTION AND BACKGROUND.....	1
CHAPTER 2: OBJECTIVES, SCIENCE QUESTIONS, AND TASKS.....	8
2.1. Navigation Subsystem	9
2.2. Guidance Subsystem.....	10
2.3. Control Subsystem.....	10
CHAPTER 3: METHODOLOGY	11
3.1. Unmanned Surface Vehicle Design.....	11
3.1.1. Wireless Communication System.....	12
3.1.2. Flight Controller.....	12
3.1.3. Rudderless Four Thrusters System	13
3.2. Power System.....	14
3.2.1. Electrical Components	14
3.2.2. Battery Analysis.....	18
3.2.3. Power System – Solar Power Management System (SPMS).....	20
3.3. Sensor Integration.....	28
3.3.1. Hardware	30
3.3.2. Software.....	33
3.4. Guidance, Navigation, and Control Capabilities.....	34
3.4.1. Navigation Capabilities	35
3.4.2. Guidance Capabilities	37
3.4.3. Control Capabilities	37
3.4.4. Echosounder Sensor	38

3.5. Study Area.....	39
3.5.1. GeoSenSE Laboratory.....	39
3.5.2. Ascarate Park.....	39
3.5.3. Grindstone Lake.....	40
CHAPTER 4: RESULTS AND DISCUSSION	41
4.1. Power System.....	41
4.1.1. Solar Power Simulation.....	42
4.1.2. Battery System.....	44
4.2. Sensor Integration.....	48
4.3. Capabilities.....	51
4.3.1. Navigation	51
4.3.2. Guidance.....	58
4.3.3. Control.....	61
4.4. Bathymetric Maps.....	66
4.4.1. Post-Processing Tools	66
4.5. Limitations of the Results	73
CHAPTER 5: FUTURE WORK	75
CHAPTER 6: SUMMARY AND CONCLUSIONS	76
REFERENCES	78
GLOSSARY	84
APPENDIX	85
VITA	88

LIST OF TABLES

Table 1. USV Platforms in Literature.	3
Table 2. ABES Physical Characteristics.	12
Table 3. List of Electronic Components.....	15
Table 4. Power Consumption of the Platform.	17
Table 5. LiPO Battery Specifications.....	19
Table 6. Solar Panel System Battery Specifications.	21
Table 7. Solar Panel Specifications.....	22
Table 8. Time to Charge a Battery with Different Solar Panel Configurations.	22
Table 9. Solar Charge Controller Technical Specifications.	27
Table 10. Signals Monitored by the Microprocessor.....	29
Table 11. Microprocessor (Raspberry Pi 4) – Pinout Configuration.	31
Table 12. List of the Field Campaigns.	41
Table 13. Cut-off Voltage and Safety Voltage Limit of the Power Systems.	45
Table 14. Capability Test Summary.	53
Table 15. Capability Test: RMSE, MAE, and Distance Evaluation.	55
Table 16. Euclidean Distance for Each Waypoint.	57
Table 17. Guidance Capabilities Calculations.....	61
Table 18. ABES GNC Capabilities.....	66

LIST OF FIGURES

Figure 1. Research Methodology Diagram: The Fundamental Elements of an Autonomous USV.	9
Figure 2. The First Validation of the Prototype in UTEP’s Swimming Pool.....	11
Figure 3. Thruster Configuration of the USV (Rudderless System).....	13
Figure 4. ABES Electrical Diagram.....	16
Figure 5. The Electrical Configuration of the Battery System. (a) Measured voltage. (b) Measured current.	18
Figure 6. Nominal Current Discharge Curve of a LiPO 20Ah Battery Capacity.	19
Figure 7. The electrical configuration of the battery system. (a) Measured voltage. (b) Measured current.....	21
Figure 8. USV with the Solar Panel Integration.	23
Figure 9. Nominal Current Discharge Curve. (a) LiPO 20Ah Battery Capacity. (b) LiPO 60Ah Battery Capacity.....	25
Figure 10. LiFePO ₄ Performance at Different Nominal Discharge Currents.....	25
Figure 11. RNG-50D-SS Solar Panel Characteristics. (a) Current vs. Voltage Performance. (b) Power vs. Voltage Performance.....	26
Figure 12. Equivalent Circuit of the Boost Converter.	28
Figure 13. Sensors Integrated into the Robotic System.	29
Figure 14. Sensor Integration Electrical Schematic.....	32
Figure 15. Sensor Integration Electrical PCB Layout.....	32
Figure 16. Sensor Integration Module Technical Drawing (PCB – Raspberry Pi 4).	33
Figure 17. USV Capabilities to be Evaluated.....	34
Figure 18. ABES Motion Control System.....	35
Figure 19. Failsafe Workflow.....	38
Figure 20. Satellite View of the Ascarate Lake Locates in El Paso, TX.	40
Figure 21. A Satellite View of the Grindstone Lake Locates in Ruidoso, NM.	40
Figure 22. Power System Current Consumption Versus PWM Configuration.	42
Figure 23. MATLAB – Simulink Model of the Boost Converter.	43
Figure 24. 20Ah LiFePO ₄ Battery State of Charge Powered by SPMS.....	43
Figure 25. 20Ah LiFePO ₄ Battery Charge Characteristics at 4.5 Amperes.	44
Figure 26. Power System Comparison in Ideal Conditions.	45
Figure 27. Power System Comparison at the Ascarate Lake. Blue Line: Lipo Battery System on Jan 21, 2022. Green: Solar Power System on April 27, 2022.	46
Figure 28. Power System Comparison at the Ascarate Lake. Blue: Lipo Battery System on May 6, 2022. Green: Solar Battery System on May 19, 2022.....	47
Figure 29. Solar Battery System Performance at the Grindstone Lake on May 18, 2022.	47
Figure 30. Wind Speed at Ascarate Lake.	48
Figure 31. Average Wind Speed Every 5 Minutes. (a) Location: Asarate Lake, El Paso, TX. (b) Location: Grindstone Lake, Ruidoso, NM.	49
Figure 32. Temperature Conditions in Different Locations.	50
Figure 33. Comparison of the GPS Calibration and the Rudderless Four Thrusters’ System Configuration. (a) Before Improvement. (b) After Improvement.	52
Figure 34. Capability Study. (a) The Path Follows in Mission 1 and Mission 4. (b) Path Follows in Mission 7 and 8.....	54

Figure 35. RMSE and MAE Calculations. (a) X Coordinates. (b) Y Coordinates.	55
Figure 36. Distance Between Coordinates Points.	56
Figure 37. ABES Prototype at Ascarate Lake.	57
Figure 38. Total Time Running in Autonomous Mode Without a Failure Through Time.	58
Figure 39. (a) Mission 1 – Horizontal Path. (b) Mission 2 – Vertical Path. (c) Mission 3 – Spiral Path. (d) Mission 4 – Diagonal Path.	60
Figure 40. GPS System Comparison Trajectory at the Grindstone Lake.	60
Figure 41. Platform Navigation Speed.	62
Figure 42. Base Station with Failsafe Command Activated.	63
Figure 43. ABES Moving Towards the Home Position. (a) The Wind Speed Limit at 10 km/h. (b) Trajectory Follows by the Vehicle When the Failsafe is Activated.	64
Figure 44. ABES Moving Towards the Home Position. (a) The Wind Speed Limit at 15 km/h. (b) Trajectory Follows by the Vehicle When the Failsafe is Activated.	65
Figure 45. Bathymetric Map of the Ascarate Lake on July 28, 2021.	67
Figure 46. 3D Bathymetric Map of the Ascarate Lake on March 03, 2022. (a) Mission 1 – Horizontal Path. (b) Mission 2 – Vertical Path.	68
Figure 47. Bathymetric Map (2D Map) of the Ascarate Lake on April 27, 2022.	69
Figure 48. Bathymetric Map (3D Map) of Grindstone Lake on May 25, 2022.	69
Figure 49. Bathymetric Map of the Ascarate Lake on July 28, 2021.	70
Figure 50. Bathymetric Map of the Ascarate Lake on March 03, 2022. (a) Mission 1 – Horizontal Path. (b) Mission 2 – Vertical Path. (c) Mission 3 – Spiral Path.	72
Figure 51. Bathymetric Maps. (a) South Section of the Ascarate Lake on May 19, 2022. (b). East Section of the Grindstone Lake on May 25, 2022.	73



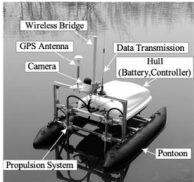
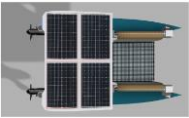
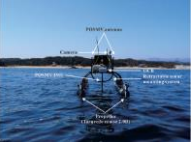
CHAPTER 1: INTRODUCTION AND BACKGROUND

The potential use of robots in environmental data collection is increasing as costs reduce, sensing capabilities are enhanced, and human life can be at risk (Kok Ping, Ling, Quan, & Dat, 2012). For instance, Unmanned Surface Vehicles (USVs) are a reliable option for scientific research, environmental missions, ocean resource exploration, and military uses. The new generation of vehicles offers significant advantages over the traditional surveying methods, for example, high mobility and low cost (Boukoberine, Zhou, & Benbouzid, 2019). Moreover, USVs are a precise and lightweight solution for hydrographic applications since they provide lower operation investment, improved personnel safety, extended operational range, offers greater autonomy, and increased flexibility in sophisticated environments, including muddy, harsh, and dangerous missions (Morten, 2010). However, USVs face some challenges, like the development of fully autonomous vehicles in a highly dynamic maritime environment (Liu, Zhang, Yu, & Yuan, 2016). Additionally, most existing USVs are confined to experimental platforms, comprised primarily of relatively small-scale USVs with limited autonomy, endurance, payloads, and power outputs (Savitz, et al., 2013).

The study of lakes, seas, and rivers provide essential resources for living organisms, including humans. Therefore, the analysis of physical features of water bodies plays a vital role in many applications in hydrology science, such as management of water resources (K. Anderson, 2016), fluvial modeling (Horrit, Bates, & Mattinson, 2016), water balance components (Versini, Gires, Schertzer, & Tchiguirinskaia, 2020), harmful algal bloom studies (Kislik, Dronova, & Kelly, 2018) and forecasting flood hazards in real-time flood (Contreras, Gironás, & Escauriaza, 2020). Furthermore, geomorphology as a science pursues to comprehend landforms and underwater terrain (Roy & Sinha, 2007). Hence, for marine research, bathymetric data is

indispensable. There is a diverse range of applications such as marine, and lacustrine research (Hell, et al., 2012), the distribution of organisms and coastal circulation study (da Silveira, Strenzel, Maida, Araújo, & Ferreira, 2020), management and protection of coastal areas (Šiljeg, Lozic, & Šiljeg, 2015) and bio-geophysical and socioeconomic processes (Traganos & Reinartz, 2018). The existing methods to conduct bathymetric surveys perform well in a specific environment but present some deficiencies. The Total Station Theodolite requires a significant investment and human power to perform measurements (Viney & Kirk, 2000). Aerial LiDAR is limited to clear water conditions with a high cost of equipment and sensors (Skinner, 2011). Even though the Multi-Beam Echo Sonar has a high cost is one of the more efficient technologies in the market. Remote sensing techniques provide an alternative means of mapping bathymetry more efficiently around broader areas, and image-based approaches play a central role in river-oriented data collection programs (Legleiter & Kinzel, 2021). Consequently, an Unmanned Surface Vehicle that integrates the Echo Sonar technology is a reliable solution to generate underwater terrain maps since it removes the need for an operator and enables new capabilities over existing techniques. Moreover, multibeam echo sounding systems are considered an emerging technique broadly applied in oceanography (Alvarez, et al., 2018). Table 1 compare the technical features of diverse platforms in the research area to discover the answers to the literature's flaws that will help to improve the study of the lentic and lotic ecosystems.

Table 1. USV Platforms in Literature.

Research Title	SONOBOT: Autonomous Unmanned Surface Vehicle for Hydrographic Surveys	Adaptive Path Planning for Depth Constrained Bathymetric Mapping	Modeling and Experimental Testing of an USV with Rudderless Double Thrusters	Autonomous Solar USV with an Automated Launch and Recovery System for UAV	Application of USV in Coastal Environments: Bathymetric Survey using a Multibeam Echosounder
Authors / Publication Year	(Kebkal, et al., 2014)	(Wilson & Williams, 2017)	(Chunyue, et al., 2019)	(Aissi, et al., 2020)	(Kum, et al., 2020)
Institution	Evologics GmbH	Australian Centre for Field Robotics	Tianjin University	Mohammed 1st University	Korea Institute of Ocean Science and Technology (KIOST)
Description	Lightweight surface vehicle for shallow water hydrographic surveys, research, monitoring, or surveillance.	Algorithms are introduced to partition convex polygons to allow efficient path planning for coverage.	Established a model and the proportional derivative + line of sight control algorithm, the path-following control of the USV	Creating a long-lasting mobile autonomous launch-and-recovery system for UAV	Bathymetric surveys of a shallow marine coastal area.
Technical Details	Boat type: Twin hull catamaran Propulsion: Hydro-jet thruster	Boat type: Twin hull (Differential thrust) Propulsion: Two Seabotix BTD150 thrusters	Boat type: Catamaran structure Propulsion: DC Brushless thrusters	Boat type: Unsinkable scalable catamaran Propulsion: Two differential motors	Boat type: Flexible double-hulled catamaran. Propulsion: 4 Torqeedo cruise 2.0 R
Picture					

Kum et al. (2020) created an ultra-light, flexible double-hulled catamaran, modified with position and orientation features for marine vessels. The Wave Adaptive Modular Vessel (WAM-V) integrated an R2SONIC 2022 multibeam echosounder (MBES) for bathymetric surveys. A power supply system composed of four Torqeedo Power batteries that provided 25.9 Volts of

nominal voltage, enough to cover a total distance of 76.6 kilometers in two operation modes (Manual and Autonomous). The operator control unit (OCU), remote control unit (RCU), and Sensor PC communicated in both directions through a radio-frequency (RF) modem and LTE router to improve the transmission of messages (Kum, et al., 2020). This vehicle is a highly effective platform for managing and monitoring shallow nearshore areas. However, it has some constraints, such as operating only in calm sea conditions to protect the instruments. Due to wind, the autonomous mode is unreliable, as it's has problems following the pre-programmed waypoints. The USV is limited to daytime for the safety of instruments and the power capacity of batteries. Furthermore, communication has sometimes failed due to environmental conditions and coverage interfering with USV operation.

The “Swordfish” is a catamaran design with two thrusters, a structure for a docking station, a GPS unit, and an IMU. The communication system contains a GSM, Wi-Fi, Freewave radios for wireless connections, and a Benthos acoustic modem for underwater connections (Ferreira, et al., 2007). The actuators and sensor integration are a solid effort in terms of engineering capabilities. Although, there is a lack of advanced path and trajectory following maneuvers. A similar platform, the twin-hull catamaran developed by Furfaro, Dusek, and Ellenrieder (2009), powered by six separate 12-Cell NiMH battery packs, provides energy for the propulsion system, PI controller, infrared camera, and GPS. The vehicle has autonomous features such as navigating between preset GPS waypoints (Furfaro, Dusek, & von Ellenrieder, 2009). The flaws in the Nereus ASV design are the lack of range and endurance capacities, like alternative power storage methods and autonomous failsafe solutions.

On the other hand, an adaptive path planning for depth-constrained bathymetric created by Wilson and Williams (2017) presents an algorithm in a twin hull, differential thrust (Seabotix

BTD150) design with two waterproof electronics enclosures. A Li-Ion battery pack in each hull provides six hours of operational time. The electronic system includes a leak and temperature sensor to enhance safety capabilities (Wilson & Williams, 2017). The novel part of this investigation is the generation of an efficient path that produces the ideal bathymetric map of an unknown area.

The research by Jungwook et al. (2020) proposed the control of a rigid monohull boat with sensors to provide autonomous navigation and collision avoidance abilities. It used a diesel engine with a single waterjet that gives the advantage of 15 operating hours per refuel. However, much noise and unwanted measurements were included, particularly in windy and rough sea conditions (Jungwook, et al., 2020). Sonnenburg and Woolsey (2013) utilized a similar method for the effective model-based control design and trajectory optimization of inflatable hull boats by incorporating a laser line scanner for obstacle detection, an attitude, and a heading system. The studies presented a solid integration of hardware and software components for USV autonomy (Sonnenburg & Woolsey, 2013). Nevertheless, both systems utilize fossil fuel to power the systems and have poor performance in inclement weather without the possibility of reaching aggressive and fast variable trajectories.

In his work, Kebal et al. (2012) developed a lightweight autonomous surface vehicle, the Sonobot, for shallow water hydrographic surveys, research, monitoring, or surveillance. A twin-hull catamaran craft and a hydro-jet thruster provide excellent stability and payload capacity. It uses four sets of 14.8V Lithium Polymer rechargeable batteries to feed the different sensors integrated as DGPS-System for location accuracy, a front-view camera for better control, and a single-beam echo-sounder for bathymetry purposes (Kebkal, et al., 2014). The platform is an

example of a state of the art of Unnamed Surface Vehicle, but a negative point is the propulsion system's high cost, which is four times the cost of the proposed USV design in this thesis.

The researcher by Chunyue et al. (2019) studied the three degrees of freedom (DOFs) dynamic model, a novel propeller thrust design, and evaluated the performance through some motion measurements. Including the acceleration test, circle test, and zigzag test, which is an excellent example of a control algorithm applied in a maritime platform. The FAS-01 USV is 1.5 meters long that adopts a catamaran structure that includes two main hulls symmetrically with a maximum speed of 1.5 m/s (Chunyue, et al., 2019). The propulsion system uses a rudderless double thrusters configuration, similar to this paper's proposed design. Taking out the rudder from the power system equation allows the platform to save energy.

Developing a platform with long-term and autonomous capabilities is one of the main goals of this research. The proposed design by Aissi et al. (2020) is an excellent approach that solves the challenge of extending the navigation capacities. The idea of integrating renewable energy is an intelligent solution to overcome the problem. A solar panel is installed on the roof of the docking platform as the primary energy source for the whole power system (Aissi, et al., 2020). This prototype demonstrated a fully autonomous system that can complete long-term missions. The approach covered in this research served as a foundation for one of the main tasks in this project.

The manuscripts showed the employment of a hull configuration as the most likely structural element used in literature. Rigid inflatable hulls are suitable for military applications primarily because of their greater endurance and payload capacity. Furthermore, due to their excellent system stability, decreasing the risk of capsizing in rough water, greater payload capacity, and redundancy, catamaran and trimaran USVs are primarily used (Campbell, Naeem, & Irwin, 2012). Different propeller configuration provides heading and speed control for most

USVs (Khare & Singh, 2012). Active sensors such as radar and lidar provide more consistent detection performance in marine environments than passive sensors such as cameras (Jungwook, et al., 2020). Wireless communication systems, such as IMUs and GPS sensors, are utilized to guarantee good operating conditions and improve the performance of the vessels (Roberts & Sutton, 2006). Finally, the ground station monitors the real-time status of the USV and its onboard equipment (Liu, Zhang, Yu, & Yuan, 2016), which enables the possibility of controlling the platform in case of an emergency.

The autonomy gained by sensor integration and predictive analytics in this research improved quick decision-making in complex environments by collecting meaningful data such as the system voltage, the electrical box temperature, and the depth of the underwater terrain. The construction of the proposed platform included the critical elements and capabilities mentioned in the literature, such as excellent system stability, large payload capacity, robust propeller configuration, IMUs, GPS sensors, and a ground station. A robust echosounder collected the data to create models that calculate the zone's depth, the water temperatures, salinity in the area, and other hydrologic applications. Capable of autonomous and remotely controlled operation, employing a fast and maneuverable Unmanned Surface Vehicle represents a cost-effective solution for surveys in harbors, inland and coastal waters, hard-to-reach, or dangerous locations. To sum up, the gaps found in the literature employed to build the suggested platform included limited endurance, restricted payload capacity, power restrictions, absence of long-range abilities, and lack of real-time navigation capabilities.

CHAPTER 2: OBJECTIVES, SCIENCE QUESTIONS, AND TASKS

This research seeks to develop a reliable platform to generate underwater terrain maps with self-governing commands. The platform's name is ABES, which stands for Autonomous Bathymetric Exploration System. It poses omnidirectional movements suitable for exploring shallow waters, natural reserves, and restricted areas. The system pursues to complete missions without unexpected events, supported by remote measuring devices. The ultimate objective is to generate meaningful underwater terrain data employing bathymetric instrumentation. However, the proposed vehicle deals with the limitation of the power capacity of batteries, communication stability, and hazardous environment management. Therefore, this investigation addresses these flaws.

Creating an autonomous crewless surface vehicle based on the literature review and solving the technical challenges such as designing an advanced path planning trajectory, long-range capabilities, and real-time navigation abilities is critical. In a real scenario, the boat is under constant environmental disturbances induced by hydrodynamic effects, winds, waves, and currents, which affect the ability to strictly follow the desired path within an acceptable deviation boundary (Villa, Aaltonen, & Koskinen, 2020). Consequently, the first objective was to enhance the state estimation and control of the USV by integrating varied sensor technologies.

One of the primary targets of literature pursues the creation of a long-lasting mobile autonomous system, independent battery charging, and mission planning (Aissi, et al., 2020). Therefore, the second research objective was to build an autonomous system capable of controlling energy consumption and employing green energy to increase the duration of a mission.

Finally, the third objective was to build an unfailing platform capable of making autonomous decisions based on real-time data. Guidance, Navigation, and Control composed the

three main components of these research objectives, which are vital components of a USV platform (Liu, Zhang, Yu, & Yuan, 2016). These subsystems work in interaction with each other to complete the final goal. Therefore, the scientific questions were answered through a series of tasks, as shown in Figure 1.

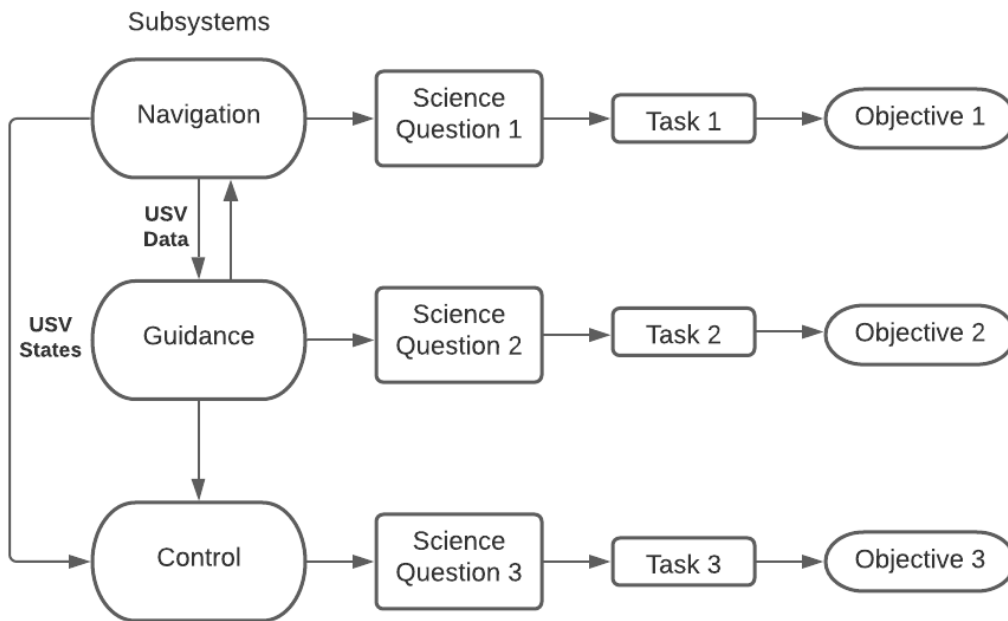


Figure 1. Research Methodology Diagram: The Fundamental Elements of an Autonomous USV.

2.1. Navigation Subsystem

Q1. How can active/passive remote sensors and actuators integrated into the system improve the data collection, navigation, and maneuverability of the USV?

Objective 1. Enhance the efficient control of the environment perception, navigation, and communication systems of the USV by incorporating heterogeneous sensors.

Task 1 – Sensor Integration: Development of a robotic system that integrates the echosounder system with high-resolution capabilities to build an accurate bathymetric model; GPS + IMU to reduce the communication limitations such as limited bandwidth, the transmission of noise, communication delays, and failures; and the integration of a microprocessor to control the power system, and monitors crucial signals.

2.2. Guidance Subsystem

Q2. How can an efficient energy consumption of the USV influence long-term mission plans?

Objective 2: Conducted long-term and autonomous missions, effectively evaluating the danger level, weather circumstances, sampling region, and energy consumption.

Task 2 – Power System: Design and integrate a solar power management system for battery control. Obtain electric energy from the photovoltaic (PV) cells to make the required power available for the onboard workstations and devices of the USV. As a result, the combination of Solar Panels with Lithium-Ion arrays provides energy for a more extended period.

2.3. Control Subsystem

Q3. How can rapid survey learning improve a robotic system's decision-making and data management process?

Objective 3: Optimize the USV safe and coverage control capabilities by analyzing real-time data to make autonomous decisions.

Task 3 – Safe and Coverage: Create a model to optimize the vehicle's capabilities (GPS Accuracy and DC Motor Control) to effectively complete the mission, covering the most extensive area autonomously without incidents. The data collected by the sensors deploy failsafe commands and prevent an event where the vehicle control is lost.

CHAPTER 3: METHODOLOGY

3.1. Unmanned Surface Vehicle Design

The prototype has a rectangular lightweight aluminum structure with four T200 Thrusters controlled by a speed driver, the Basic ESC developed by Blue Robotics ®. This configuration allows the vehicle to perform omnidirectional movements to explore different representations of water bodies. The vehicle has multiple applications due to its flexible capabilities. Figure 2 shows the first validation of the manual control of the prototype in a monitored environment.

The ABES design is 940mm long and adopts a rectangular structure with a thruster attached to each end, symmetrically calculated to prevent roll and pitch movements. An inflatable tube in the center for floating redundancy capabilities hives stability under excessive load. Table 2 summarizes the physical characteristics of the boat.

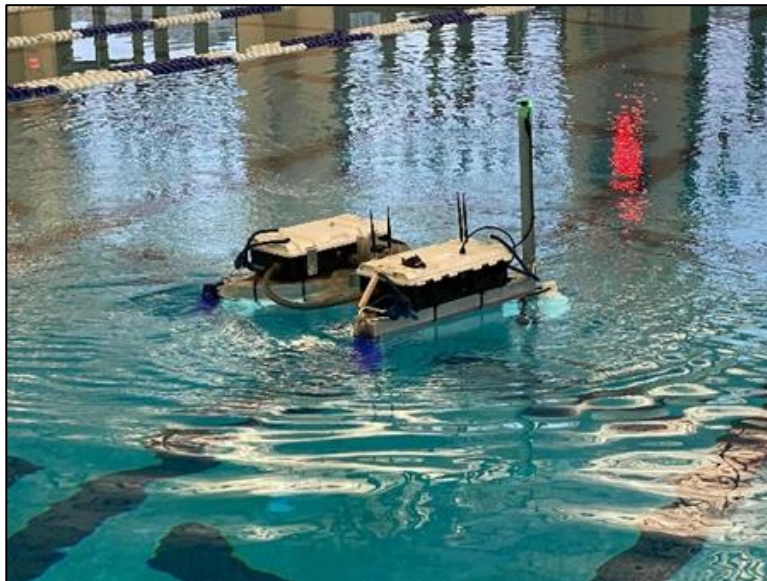


Figure 2. The First Validation of the Prototype in UTEP's Swimming Pool.

Table 2. ABES Physical Characteristics.

Parameter	Value
Length (L)	940 mm
Width (W)	950 mm
Height (H)	1000 mm
Draft with tube (DT)	500 mm
Draft without tube (DWT)	250 mm
Distance between thrusters (DBT)	840 mm
Weight (W)	25 kg
USV velocity (MAX)	1.5 m/s

3.1.1. Wireless Communication System

The ground control station included a PC for mission planning, a telemetry modem, bathymetric apparatuses, and live monitoring of the boat's real-time status. The wireless communication system performed cooperative control and monitoring tasks that gained flexibility.

The telemetry devices included:

- RFD900+ Telemetry Modem ®: reliable remote data transmission option. It possessed a line-of-sight-range over 40 km, a frequency band of 902MHz - 928MHz, a six pins configuration, and up to 50 frequency hopping channels.
- FrSky Taranis System ®: radio control allowed manual vessel operations. An 8-Channel 2.4 GHz worked as the receiver and the X9D Plus 2.4G as the transmitter.

3.1.2. Flight Controller

The Mission Planner controlled the navigation of the maritime vehicle, a platform developed by ARDUPILOT that gave flexible solutions to planned and loaded autonomous missions. The Pixhawk 2.1 provided navigation capabilities as a single-board flight controller with sufficient inputs and outputs for the most demanding applications. The previous sampling test guided the location of the waypoints in a grid within a range of 10 by 10 meters. Afterward, the “Auto grid” function from ARDUPILOT was employed to map the study area with the statistics found from the iterative subsets of data. The flight controller communicated with the telemetry

system, GPS, and radio control. The vehicle used the waypoints previously defined in the software to navigate. It employed the information received from the GPS (Here 2) to calculate the distance and direction to the next waypoint in the mission planner. In the approximation made by Furfaro, Dusek, and Ellenrieder (2009), the bearing is used as the set point for the PID controller, while a digital compass provides feedback at the control loop frequency. The control loop updated the electric motors via pulse-width modulation (PWM) to the electronic speed controller (ESC) at a rate of 20 Hz.

3.1.3. Rudderless Four Thrusters System

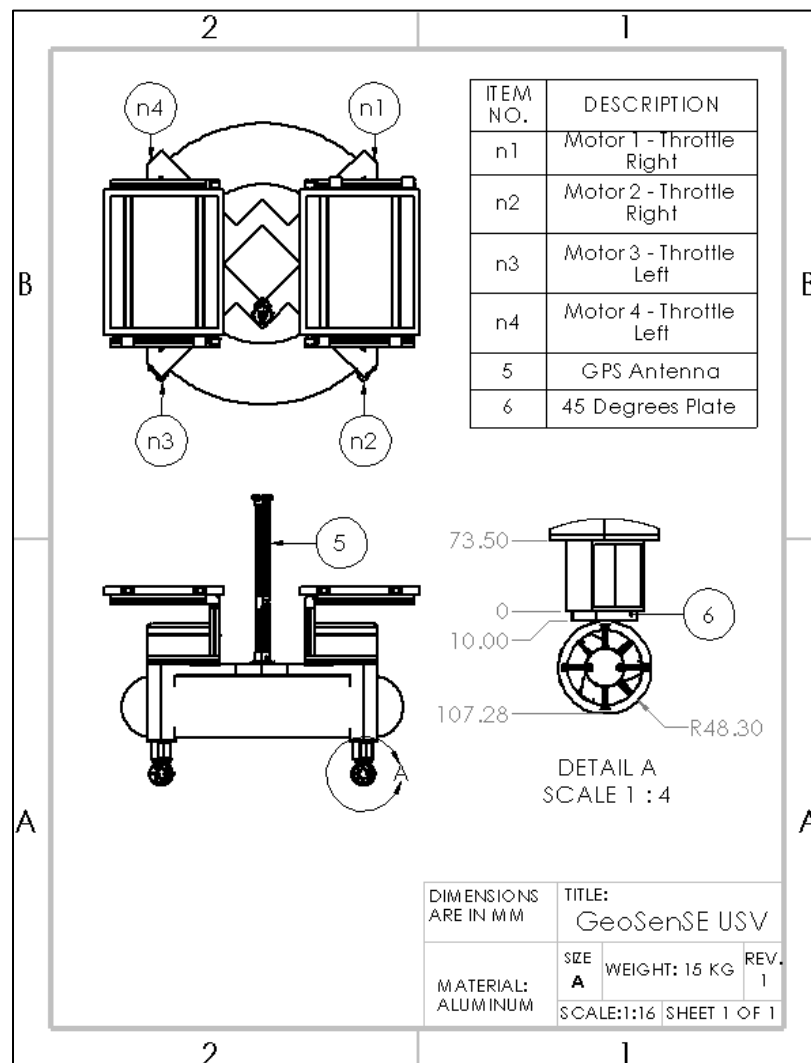


Figure 3. Thruster Configuration of the USV (Rudderless System).

The propulsion system with four T200 Thrusters worked together to move the vehicle's aluminum structure, the payload, and all the electrical components. The thrusters consist of a direct-current fully flooded brushless motor with clockwise and counterclockwise capabilities, enabling the possibility to move forward and backward without turning the platform 180° degrees. It has a differential steering mechanism that requires four inputs, n_1, n_2, n_3 , and n_4 , to adjust its direction, where n_1, n_2, n_3 , and n_4 are the four motor speeds in Revolutions Per Minute (RPM). The throttle of the four propellers controls the USV velocity, and the differential speed controls the steering of the USV. This configuration eliminated the need for a rudder in the propulsion system, as shown in Figure 3. To move in a straight line, the port and starboard thrusters need to run at the same speed, which means the differential thrust was zero in this scenario (Sharma, Naeem, & Sutton, 2012).

Based on the research made by Chunyue et al. (2019), Equation 1 and Equation 2 defined the speed of the propellers in straight and differential modes, respectively:

$$n_s = \frac{n_1 + n_2 + n_3 + n_4}{4}, \quad (1)$$

$$n_d = \frac{(n_1 + n_2) - (n_3 + n_4)}{4}, \quad (2)$$

The thruster configuration mentioned before was the base to define the functions of each motor in the Mission Planner Software ®. The USV with the rudderless fourth thrusters system needs to generate momentum by the differential thrust between the port and starboard propellers to change the heading (Chunyue, et al., 2019). During this process, to throttle right, the motors n_1 and n_2 are powered. On the contrary, to throttle left, motors n_3 and n_4 are activated.

3.2. Power System

3.2.1. Electrical Components

The isolated boxes on top of the aluminum structure carried the electronic devices required to control the vehicle. The power system integrated the following components listed in Table 3,

which contains the information of the manufacturer and the primary function of every item listed. The first control device of current and voltage was the Mauch Sensors Module connected to the batteries. A circuit breaker controlled the power distribution to the platform. The flight controller monitored and operated the speed controllers, radio receiver, telemetry modem, and GPS. A picture of the physical connections of the components is located in the appendix.

Table 3. List of Electronic Components.

Item	Part Number	Manufacturer	Function
Sensor board	Mauch 004 - PL-200	Mauch Electronics	Measured the current and voltage of each battery. Communicates with the sensor hub.
Sensor hub	Mauch Sensor Hub X8	Mauch Electronics	Collects the current of the sensor board and passes the controlled current to the power supply.
Power supply	Mauch 017 - PL 4-6S BEC	Mauch Electronics	It received the current from the sensor Hub X8 and supply voltage to the flight controller.
Circuit breaker	CB185-150	Bussmann	Control switch.
Flight controller	Pixhawk 2.1	Hex Technology	Used sensors' data to calculate the USD's desired speed and direction.
Speed controller	Basic ESC	BlueRobotics	Bidirectional electronic speed controller for the T200 thruster.
Thruster	T200	BlueRobotics	Underwater thruster.
Radio receiver	FrSky Taranis Receiver X8R 8	FrSky	Communication with remote control with a channel of 2.4GHz
Telemetry modem	RFD900+	RFDDesign	Long-range communication between the rover and the base station.
GPS	Here 2 GNSS	Hex Technology	Accurate determination of the geographical locations.

Figure 4 displays the electrical diagram of the platform. All the electronic components listed in Table 3 are interconnected to make the boat able to navigate. Four antennas installed on the top of the electric enclosure box transmit and receive the radio waves of the telemetry modem and radio receiver. The flight controller served as the brain of the electronic system to control the different functions and parameters of the driver, modules, and receivers.

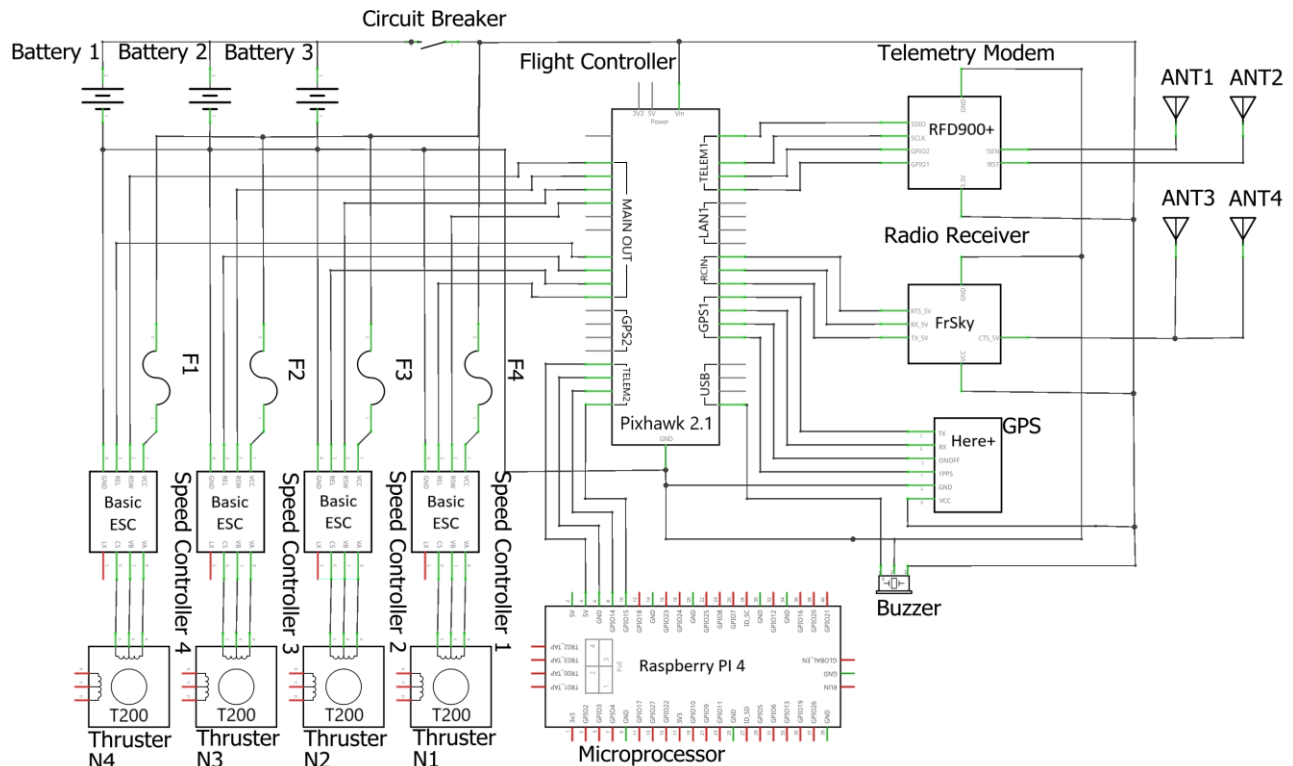


Figure 4. ABES Electrical Diagram.

A series of calculations in Table 4 shows how much power each platform component consumes, divided by the central electronic sections. The first device of every section's row is the one that powers the rest connected to it, which works as peripheral devices. Formula 3 calculated the applied electric power, where "V" is the voltage in volts, "I" is the current in amperes, and "P" is the power in watts.

$$P(\text{Watts}) = V(\text{Volts}) \cdot I(\text{Amperes}), \quad (3)$$

Table 4. Power Consumption of the Platform.

Component / Section	Devices	Number of Devices	Operating Voltage (V)	Operating Current (A)	Total Current (A)	Power (W)	Total Power (Watts)
Microprocessor and Sensors	Voltage Regulator	1					
	Raspberry Pi 4*	1					
	Anemometer*	1					
	Temperature Sensor*	1	5	2	2	10	10
	Current Power Supply Sensor*	1					
Solar Charge Controller	Solar Charge Controller	1	5	0.01	0.01	0.05	0.05
Current / Voltage Control Board	Mauch Control Structure	1					
	Flight Controller*	1					
	Telemetry Modem*	1	5.4	2.5	2.5	13.5	13.5
	Radio Receiver *	1					
	GPS Here 2 GNSS*	1					
Propulsion System	T200 (At 1700 PWM)	4	12.8	3.6	14.4	46.08	184.32
	Basic ESC	4					

*Devices powered by the first one of every section.

Total Power	207.87	Watts
-------------	--------	-------

The total power required by the system is 207.87 Watts, which is the amount of power needed to run the boat for an hour. Four times the battery system required power is the goal because of reliability and safety reasons. Based on the research, the maximum voltage capacity in solar batteries available in the market is 12.8 Volts, which is needed to integrate the PV cell. Formula 4 and Formula 5 show that at least 60 Ampere-Hour (Ah) is required to power the vehicle for 4 hours of operation.

$$Total\ Power = 4 \cdot 207.87\ Watts = 831.48\ Watts, \quad (4)$$

$$I = \frac{P}{V} = \frac{831.48\ Watts}{12.8\ Volts} = 64.95\ Amperes, \quad (5)$$

3.2.2. Battery Analysis

There were two battery systems analyzed during the development of the platform. The lithium-polymer (LiPO) batteries were selected as the first option to power the vehicle since they offer flexibility and simplicity. This type of battery is usually utilized in drone architectures effectively. A parallel configuration was selected to increase the current (Ampere-Hour) capacity and keep the voltage at the same level, based on the power calculation explained in the previous section, a capacity of 60 Ah. The following circuit simulated in NI Multisim [®] illustrates the configuration utilized in the vehicle to power all the electronic devices. The DC power supplies (V1, V2, and V3) represent the batteries. The parallel configuration supplies the same voltage but the triple current capacity with a total of 60 Amperes.

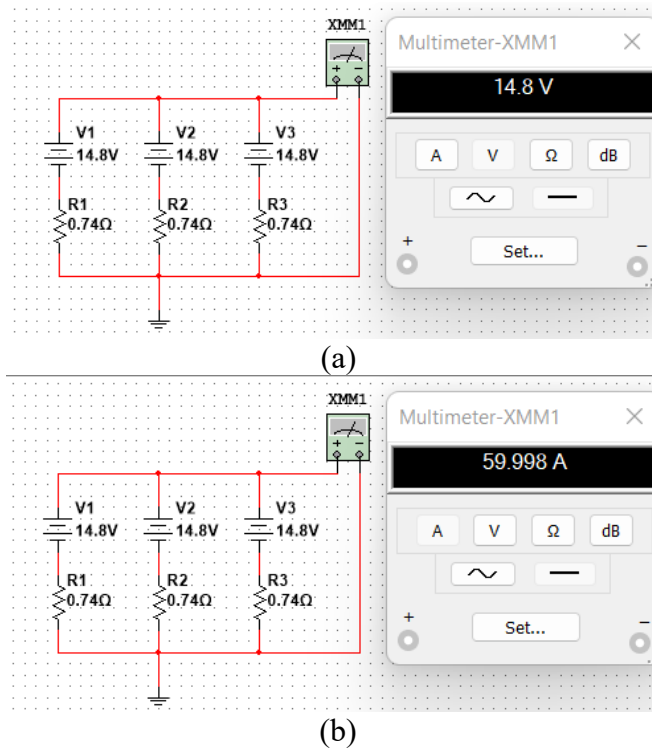


Figure 5. The Electrical Configuration of the Battery System. (a) Measured voltage. (b) Measured current.

The specification of the batteries utilized in the LiPO power system is listed in Table 5. As specified in the electrical circuit in Figure 5, three batteries were needed to reach the 60,000 mAh capacity required by the system.

Table 5. LiPO Battery Specifications.

Specification	Value
Brand	Turnigy
Type	LiPO
Minimum Capacity	20000mAh
Cell Count	4 / 14.8V
Constant Discharge	12C
Peak Discharge (10sec)	24C
Pack Weight	1775g
Charge Plug	JST-XH
Discharge Plug	XT90

The discharge cut-off voltage is at which a battery is considered fully discharged, beyond which further discharge could cause harm or directly affects the electrochemical performance (Beattie, 2016). The manufacturer of the Turnigy LiPo battery does not provide the cut-off voltage specification. Thus, a theoretical and practical calculation was performed. Figure 6 shows the calculation using the simulator in MATLAB – Simulink ® to find the theoretical nominal current discharge curve. Hence, the safety voltage limit point was defined as 13.5 Volts because it is 2.4 V above the cut-off voltage and gives sufficient time to react in an emergency. Theoretically, at a nominal discharge current rate of 14.4 Amperes, 79 minutes of operation are obtainable with a 20Ah LiPO battery in safe mode.

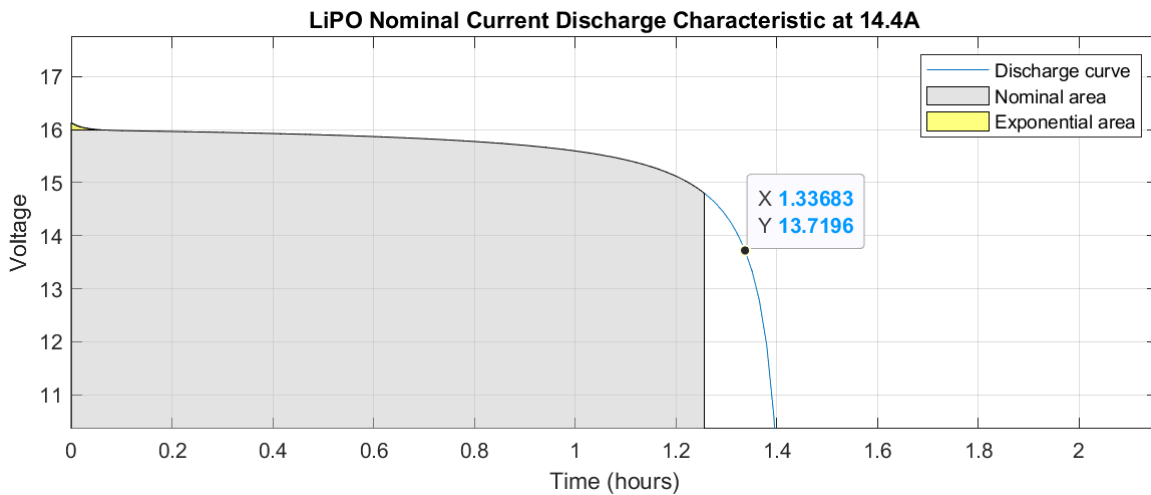


Figure 6. Nominal Current Discharge Curve of a LiPO 20Ah Battery Capacity.

However, LiPo batteries can ensure drone operation for a maximum of 90 min (Boukoberine, Zhou, & Benbouzid, 2019). These constraints motivated the analysis of a second option, the Solar Battery System. The following section explains the selection of different components and the calculation to build a reliable second source of power for the USV.

3.2.3. Power System – Solar Power Management System (SPMS)

Alternative source energy was required to increase the navigation capabilities. Thus, a solar panel was integrated into the power system to fulfill the goal of completing a long-distance mission. For a fundamental surveillance mission, the solar cells were estimated to provide an energy saving of 59%, despite an increase in the vehicle weight (Harvey, et al., 2012). ABES is the perfect platform to integrate a solar panel because of the space available and the weight load capacity. A storage element (Battery) is required in all solar power systems because solar cells can only generate power at certain times. The Solar Power Management System (SPMS) design considered three stages: The first phase was the solar cell panels and battery selection; the second stage was the study of the solar charge controller requirements; and finally, the live monitoring of voltage to deploy a safety command in case of lower levels.

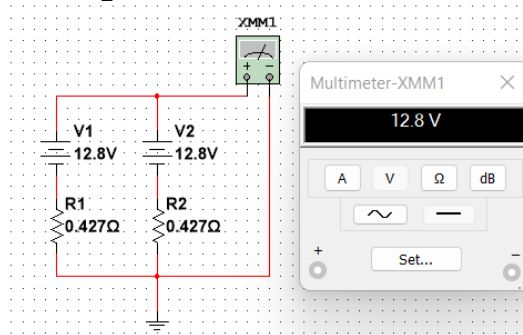
The SPMS obtained the electric energy from the solar system and made the necessary power available for the onboard computers and other electronic circuitries (Jaw-Kuen, Der-Ming, Pin-Ying, Geng-Feng, & Jhij Hua, 2009) of the USV. Based on the calculation in section 3.2.1., the power consumed by all the electronic items was discussed, especially the voltage drop when the T200 thrusters were in use. The battery technology chosen for this USV application study was the Lithium Iron Phosphate Battery (LiFePO₄). Even though the industry extensively used lead-acid batteries, it is not suitable for USV applications considering their weight and volumetric capacity. Table 6 shows the specifications of the selected batteries for the SPMS. The selected battery capacity was 30,000 mAh for a single piece. Therefore, the required batteries were reduced

to two compared to the LiPO system. Based on the supplier specifications, the discharge cut-off voltage for this type of battery is 10 volts.

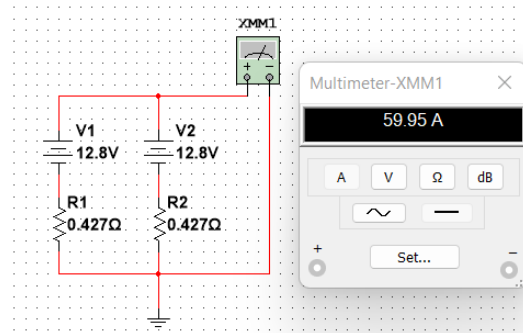
Table 6. Solar Panel System Battery Specifications.

Specification	Value
Brand	Eco-Worthy
Type	LiFePO ₄
Minimum Capacity	30000mAh / 360Wh
Nominal Voltage	12.8 V
Continuous Charge/Discharge Current	30 A
Size	180mm x 76.2mm x 160 mm
Weight	3.265 kg
Maximum Charge Voltage	14.5 V
Discharge Cut-Off Voltage	10 V
Operating Temperature	-20 °C to 60 °C

A configuration of two 30 Ampere-Hour LiFePO₄ batteries was required to fulfill the demand of the 60 Ampere-Hour. Figure 7 shows the results of the simulation.



(a)



(b)

Figure 7. The electrical configuration of the battery system. (a) Measured voltage. (b) Measured current.

Table 7. Solar Panel Specifications.

Item	Value
Brand	Renogy
Serial Number	RNG-50D-SS
Maximum Power at Standard Test Conditions	50 W
Optimum Operating Voltage (Vmp)	18.6 V
Optimum Operating Current (Imp)	2.69 A
Open Circuit Voltage (Voc)	22.3 V
Short Circuit Current (Isc)	2.94 A
Module Efficiency	16.90%
Maximum System Voltage	600 VDC UL
Maximum Series Fuse Rating	15 A
Solar Cell Type	Monocrystalline (6.25 x 1.9in)
Number of Cells	33 (3 x 11)
Dimensions	581 x 509 x 30 mm
Weight	3.5 kg
Operating Temperature	-40°C to +90°C
Nominal Operating Cell Temperature (NOCT)	47±2°C
Junction Box - IP Rating	IP 65
Junction Box – Output Cables	14 AWG

Table 7 enlisted the photovoltaic panel specification needed in the solar power system design based on the power specification, available space, and weight limits. Table 8 shows the time required to charge one battery with the power supply by the solar panel. It took approximately 7 hours to charge a battery with one PV Panel completely. Even though the solar panel is a continuous energy source, no technology is available to supply the amount of current required to charge a battery in a short period. Therefore, the batteries needed to be previously charged, with the advantage that they were constantly charged in a campaign.

Table 8. Time to Charge a Battery with Different Solar Panel Configurations.

Panel Configuration	Total Power Provide (Watts)	Hours to fully charge by PV	Total Weight (Kg)
One Renogy 12V Solar Panel	50	7.24	5.64
Two Renogy 12V Solar Panels	100	3.84	11.28

Based on Tables 7 and 8, the ideal solar panel to be installed in ABES are two 50W 12V Solar Panels that provide an additional power source and leave space for the payload, the River Surveyor M9 ®. The PV panels charge two 12.8 Volts Lithium Iron Phosphate Battery with a maximum charger current of 30 Amperes each. As shown in Figure 8, the solar panel installed uses an aluminum profile that enables foldable capabilities to access the isolated electrical boxes.

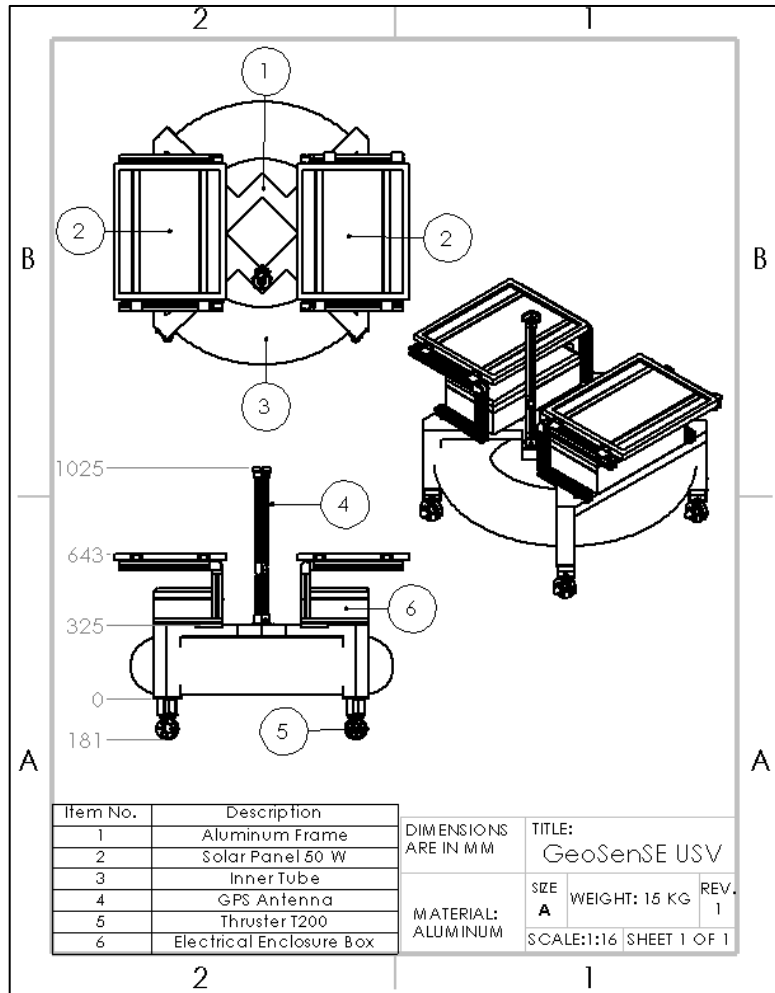
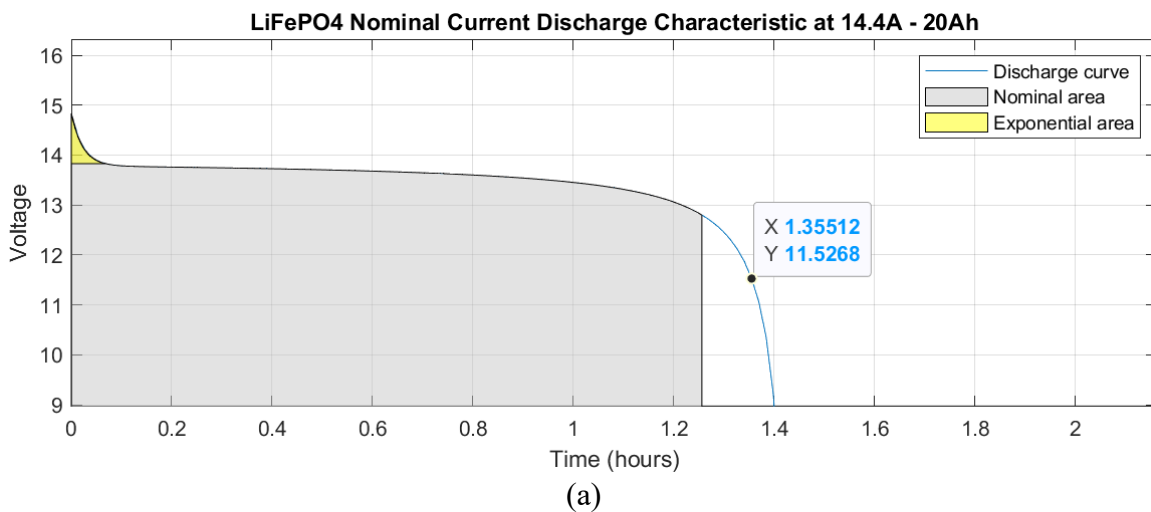


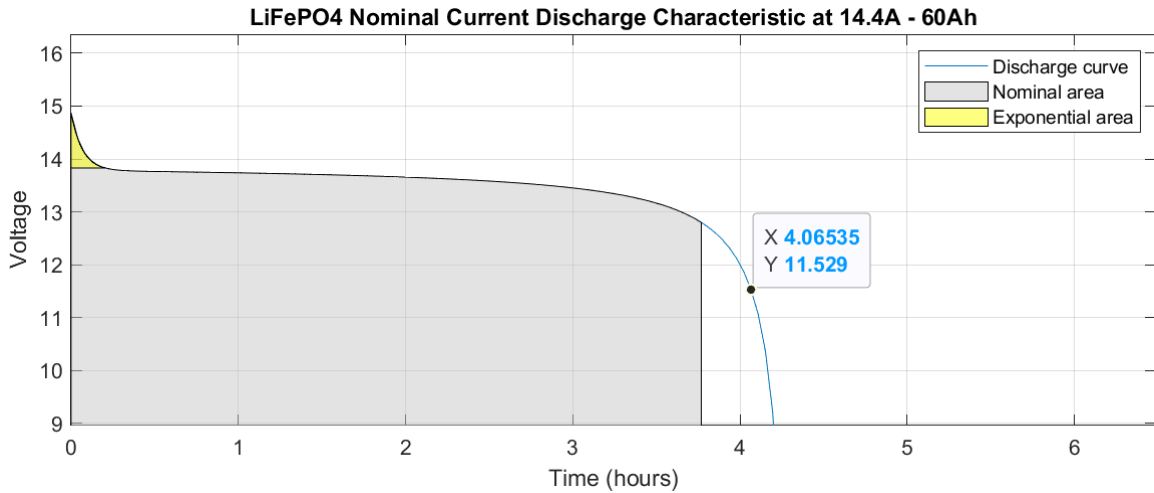
Figure 8. USV with the Solar Panel Integration.

The behavior of the components of the system was studied in MATLAB – Simulink. The first step was the simulation of the characteristics of the battery. The simulation was done with two different battery configurations to compare it with the LiPO system. Figures 9a and 9b show the current discharge characteristic of a 20Ah (One battery) and a 60 Ah (Two batteries in parallel

configuration) Lithium-Ion Battery configuration, respectively, divided into three areas. The first area shows the exponential voltage drop when the battery is fully charged (Yellow). The second area (Nominal area) represents the energy that can be extracted from the battery until the voltage drops below the nominal voltage (12.8 V), around 1.25 hours for one battery and 3.7 hours of operation for the 60Ah battery configuration. Finally, the third section represents the total discharge of the battery, when the voltage drops rapidly, which goes from 12.8 V to 9.2 V in 20 to 30 minutes approximately. All the values are plotted considering a nominal discharge current of 14.4 amperes, sufficient to power the four thrusters and all the electric components in the vehicle. The theoretical safety voltage level selected is 11.5 Volts since it gave sufficient time to return the boat to its home position. This value is congruent to the theoretical discharge cut-off voltage of 10 volts provided by the supplier in the datasheet of the LiFePO₄ battery (See Table 6). As expected, the operational time is around four hours with the triple current capacity.

Figure 10 shows the voltage drop process with three different discharge current values, which does not have a linear behavior. The less current consumption, the longer the vehicle can navigate. The second step was to know the PV's power, current, and voltage characteristics with the “PV Array Block in Simulink.”





(b)

Figure 9. Nominal Current Discharge Curve. (a) LiPO 20Ah Battery Capacity. (b) LiPO 60Ah Battery Capacity.

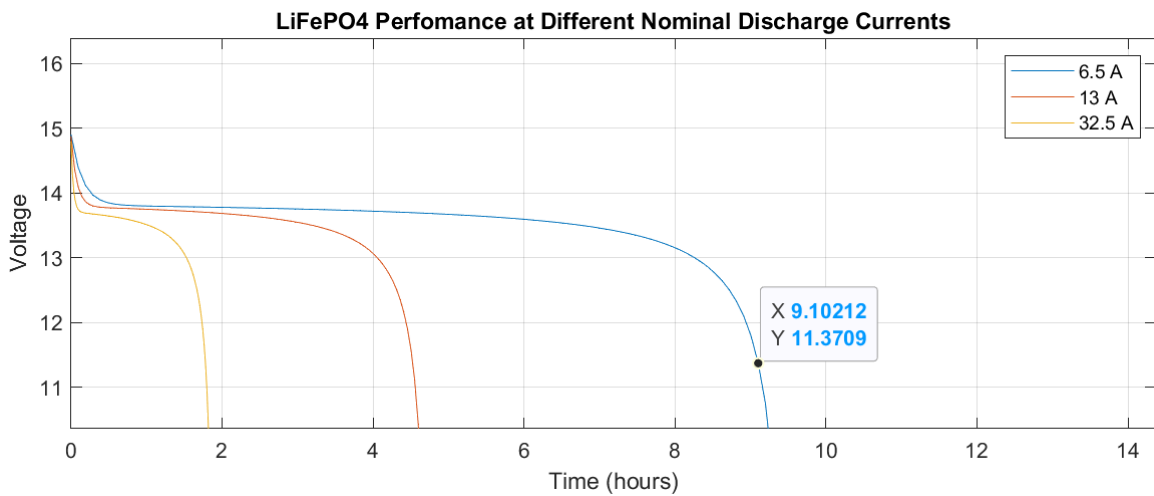


Figure 10. LiFePO₄ Performance at Different Nominal Discharge Currents.

Figure 11 displays the critical features of the solar panel. The plot on top shows the current versus voltage where the voltage and current at the maximum power point are 18.6 Volts and 2.69 Amperes, respectively. At the bottom, the power versus voltage indicates that 18.6 volts generate the maximum power of 50.034 Watts as anticipated at a 1000 irradiation level and a temperature of 25 °C.

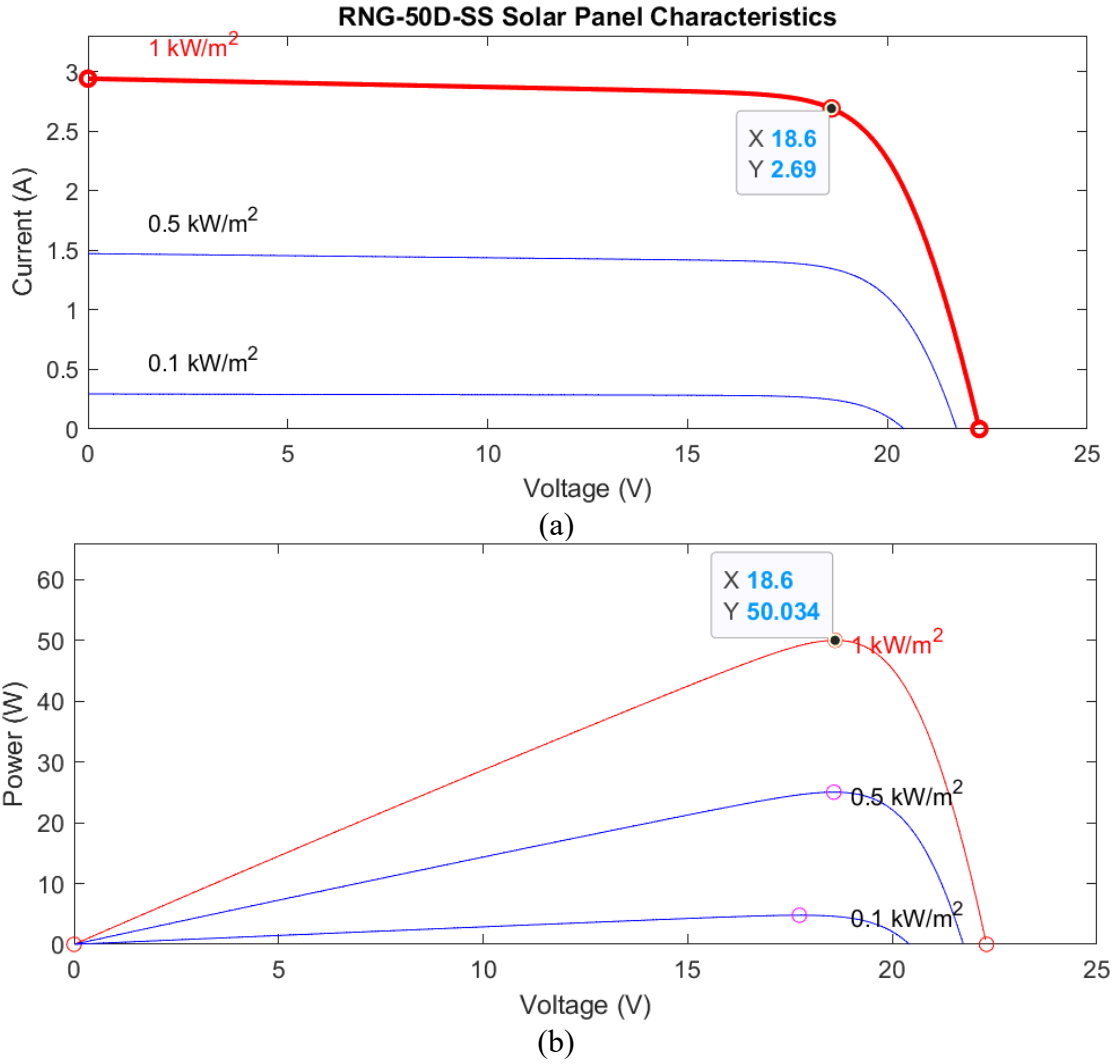


Figure 11. RNG-50D-SS Solar Panel Characteristics. (a) Current vs. Voltage Performance. (b) Power vs. Voltage Performance.

The controller is the final component of the Solar Power Management System (SPMS). The controller's goal is to monitor and regulate the delivery of energy drawn from the solar panels. It is connected to the panels to supply voltage to the LiFePO₄ batteries. The theoretical design of the solar charge controller can be calculated with the following formulas to find the ideal electrical components value.

$$Inductance(L) = \frac{V_{op}(V_{ip} - V_{op})}{f_{sw} \cdot I_{ripple} \cdot V_{ip}} = \frac{12(18.6 - 12)}{5000 \cdot 0.269 \cdot 18.6} = 3.166mH, \quad (6)$$

$$Capacitance (C) = \frac{I_{ripple}}{8 \cdot f_{sw} \cdot V_{ripple}} = \frac{0.269}{8 \cdot 5000 \cdot 0.12} = 56.041 \mu F, \quad (7)$$

The different controller options were studied based on the values obtained from the previous formula. Two charge controllers are primarily used in today’s solar power systems: pulse width modulation (PWM) and maximum power point tracking (MPPT). The pulse width modulation (PWM) charge controller is the most effective means to achieve constant voltage battery charging by adjusting the duty ratio of the switches (MOSFET) (Osaretin, 2015). This system offers the following advantages: higher charging efficiency, longer battery life, reduced battery overheating, minimized stress on the battery, and the ability to de-sulfate a battery. Based on Osaretin (2015) work, the Wanderer controller from Renogy ® was selected to fulfill the requirement. The device is an advanced charge controller for off-grid solar applications, with highly efficient PWM charging, increasing battery life and improving system performance. It was utilized for 12V/24V battery bank applications, including a 4-stage (Bulk Charge, Boost Charge, Float Charge, and Equalization) battery charging algorithm for rapid, efficient, and safe battery charging. Table 9 shows the technical specifications of the device.

Table 9. Solar Charge Controller Technical Specifications.

Item	Value
Brand	Renogy ®
Model	Wanderer 10A PWM
Nominal Voltage	12V/24V Auto Recognition
Rated Charge Current	10A
Max. PV Input Voltage	50 VDC
USB Output	5V, 2A max
Self-consumption	≤10mA
Operating Temperature	-25 °C to +45 °C / -31 °F to 113 °F
Terminals	Up to #12 AWG
Weight	0.12 kg.

The Solar Charge Controller with four charging stages offered the following advantage. The charge control operation remains uninterrupted even when the PV panel gives a low output current at a low insolation level because the bulk converter boosts the current up to the required level of charging (Bhattacharjee, 2012) to optimize the available current. An equivalent circuit representation of the selected controller is made based on models on the equivalent circuits

proposed by Rashid (2001) and the other components of the SPMS. The circuit includes the MOSFET to control the conductivity, an inductor to store energy, and a diode that carries the current during the switching cycle when the switch is off (Rashid, 2001).

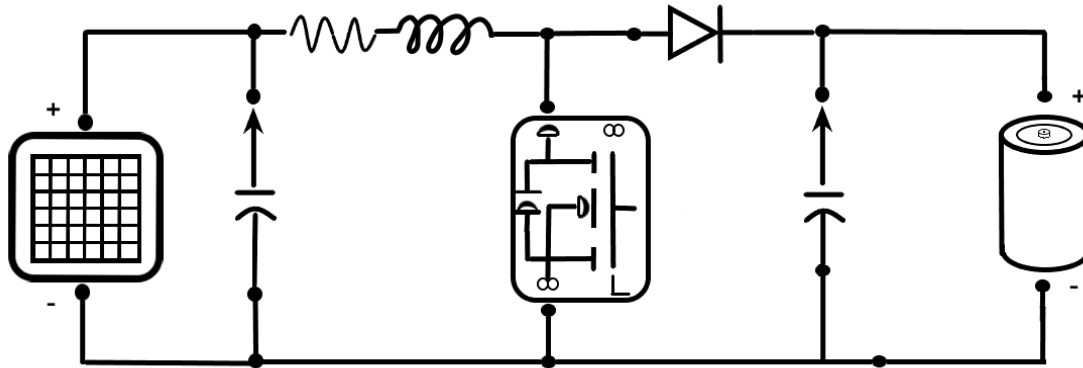


Figure 12. Equivalent Circuit of the Boost Converter.

3.3. Sensor Integration

The robotic system integrated different devices to enhance the capabilities of the boat. As the primary payload, the echosounder sensor carried out high-resolution capabilities to build a bathymetry model. A microprocessor was incorporated to control the power system, monitor crucial signals, and deploy failsafe commands. The objective was to send a command to Pixhawk 2.1 to control the critical function of the platform, with the overall goal to cover the most significant area possible without incidents. Figure 13 displays an overview of the sensors integrated into the robotic system. One of the goals of this research was to provide a reliable platform to measure the danger level to deploy a recovery system in an emergency. The Raspberry Pi 4[®] was the selected microprocessor to collect data from different sensors and make decisions autonomously. The integration of the second controller was implemented to cover its significant drawbacks by working cooperatively to achieve and perform the desired tasks and missions (Aissi, et al., 2020) as high-level control computer companion.

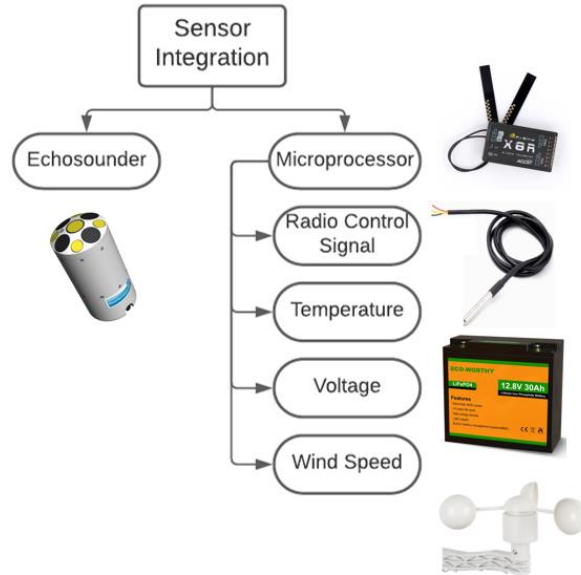


Figure 13. Sensors Integrated into the Robotic System.

Table 10 shows the signals selected to collect real-time data in the first column, the normal operating conditions of the signals located in the second column, the sensors used to monitor those signals in the third column, and the functionalities displayed in the fourth column.

Table 10. Signals Monitored by the Microprocessor.

Signal	Operating Range	Sensor	Function
Battery voltage and current (Power System)	Operating voltage: 11V – 14.5 V. Operating current: 0A – 20A.	INA219 I2C bi-directional DC power supply sensor	With a 12-bit resolution, the module can measure a bus voltage range of 0 to 26 V. It monitors the state of the batteries to prevent running out of power.
The temperature of enclosure box	Operating temperature: -Lithium battery (LiFePOA4): 0°C – 55°C. -Lipo battery: 0°C – 35°C.	DS18B20 temperature sensor waterproof	A high-quality stainless-steel probe can measure temperatures from -55°C to 125°C with an accuracy of ±0.5°C. The battery temperature was monitored to prevent fire and damage.
Wind Speed	Wind speed possible to navigate the boat: 0 to 25 km/h.	Anemometer	The cup-type anemometer measures wind speed by closing a contact as a magnet moves past a switch
Radio Signal	RC transmitters turn off for more than 0.5 seconds (System on hold)	FrSky Taranis System	The base station monitors the radio control signal.

3.3.1. Hardware

This section studied the data collected by the microprocessor during a mission. The measured parameters served as an indicator to decide when the vehicle operated under normal conditions. The microprocessor continuously monitored three of the four signals, which were unified in the sensor integration system. Only the radio signal was observed directly by the base station. The first step in the designing process was the definition of the inputs and outputs required. The communications between the microprocessor and the sensors used different interface alternatives. The INA219 used I2C1 clock bus communication through two cables connected to pin GPIO2 (SDA) and pin GPIO3 (SLC); the temperature sensor DS18B20 used a 1-Wire connection to pin GPIO4, and the anemometer used 1-Wire communication in pin GPIO5. A LED and a push-button were included to enable more functions to help the user interact with the system.

After defining the inputs and outputs configuration, the circuit was tested on a breadboard. The test of the electric circuit with this approach offers a series of advantages, such as the possibility to test the sensors' integration and make changes quickly. Plus, it is a safe and affordable way to test circuit functioning. Table 11 shows a detailed description of the connections between the components and the microprocessor.

Once the circuit was validated, the third step was the electrical schematic design incorporating each device's hardware requirements and physical connections. Raspberry Pi gave a +3V DC to power all the devices. As illustrated, the red line represents the positive terminal and the blue line the ground, respectively. Different electrical resistances were added to the layout to protect or filter the signal. Fritzing ® software was employed to make the schematic and the PCB layout illustrated in Figure 14. The PCB design was manufactured by JLCPCB ®. Figure 15 illustrates the Printed Circuit Board (PCB) designed to support the body of electronic components to carry the electrical connection and components. The PCB offered a permanent solution to have the electronic devices working, a better current carrying capacity than a breadboard, and a robust solution.

Table 11. Microprocessor (Raspberry Pi 4) – Pinout Configuration.

#	Function	Output	Color Cable	#	Function	Output	Color Cable
1	3v3 Power	Power to PCB	White	2	5v Power	Pixhawk-Telem2-Power	Red
3	GPIO 2 (I2C Data)	INA219-Sda	Blue	4	5v Power	Fan +	Red
5	GPIO 3 (I2C Clock)	INA219-Scl	Green	6	Ground	Pixhawk-Telem2-Ground	Black
7	GPIO 4	DS18B20-Signal	Yellow	8	GPIO 14 (UART Transmit)-Tx	Pixhawk-Telem2-Rx	Blue
9	Ground	Ground the protoboard	Black	10	GPIO 15 (UART Receive)-Rx	Pixhawk-Telem2-Tx	Green
:				12	GPIO 18 (PCM Clock)	Led-Output	Gray
29	GPIO 5	Annenometer-3	Purple	14	Ground	Fan -	Black
				22	GPIO 25	Pushbutton-Input	

The final step was the connection of the sensors to the PCB and the microprocessor. A fixture designed in SolidWorks ® and 3D printed served as the base of the circuit board (See Figure 16). A switching regulator was employed to give the 5V DC voltage necessary to power the Raspberry Pi 4. The proposed solution offered the flexibility to install the sensors on different platforms or expand their capabilities. The communication between microprocessors was made through the second telemetry port of the flight controller to the Transmit (Tx) and Receive (Rx) pins in the Raspberry Pi ®, which worked like a serial communication protocol (Communication method that uses one or two transmission lines to send and received data).

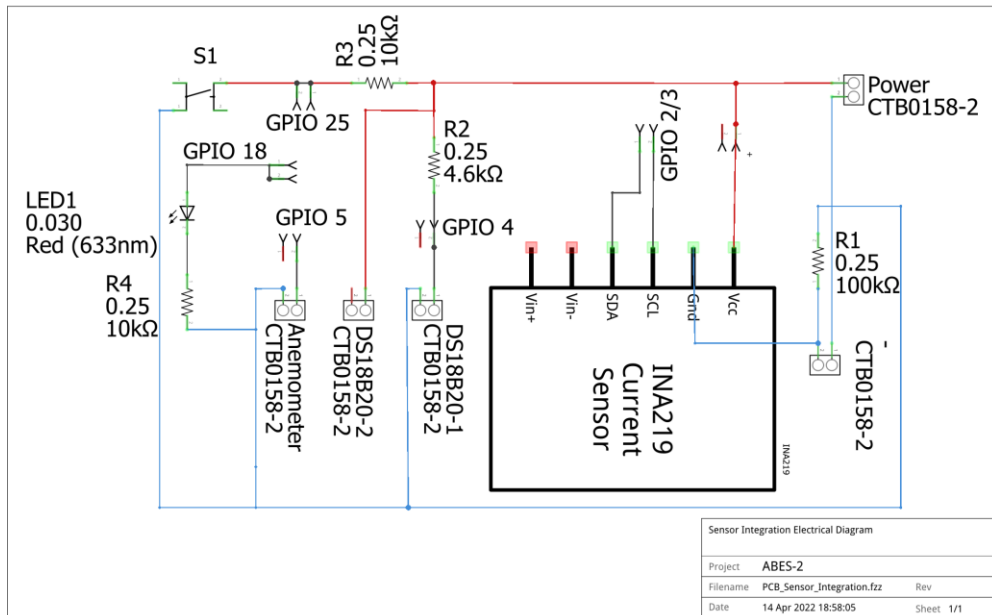


Figure 14. Sensor Integration Electrical Schematic.

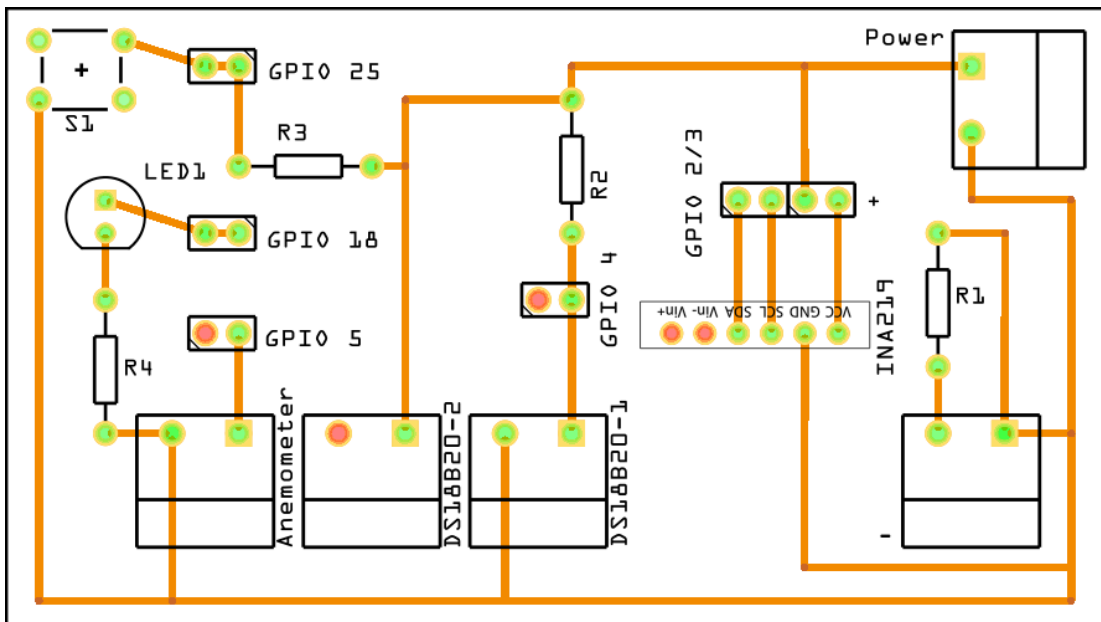


Figure 15. Sensor Integration Electrical PCB Layout.

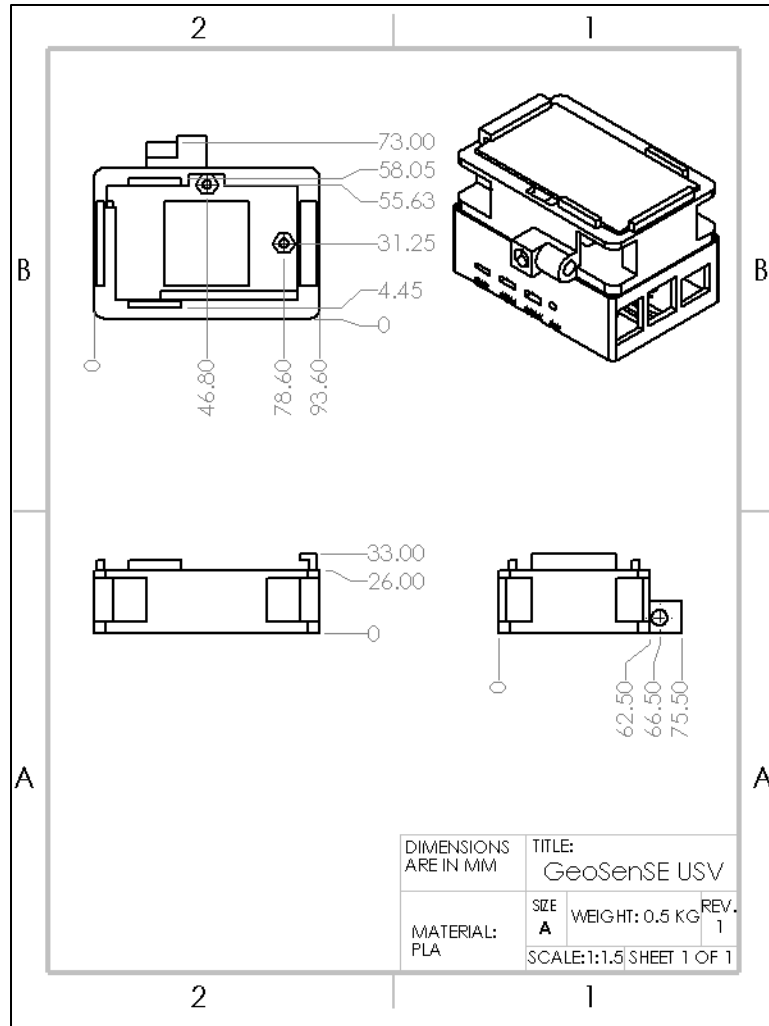


Figure 16. Sensor Integration Module Technical Drawing (PCB – Raspberry Pi 4).

3.3.2. Software

The sensor generated a millivolts scale (mV) signal that was acquired and interpreted by the microprocessor. Transforming that physical signal into meaningful data was possible through calculations and interpretation defined in the program's code. Python®, a high-level, interpreted, general-purpose programming language, was selected to complete the task of the sensors system. Different integrated development environments (IDE) for Python were used, such as Thonny®, which enabled detailed visualization of every line of the code, and Geany, which allowed the possibility to visualize the variables with code highlighting and line numbers.

Six sections constituted the code. The first section included the needed libraries of the sensors; then the variables were defined like the failsafe limits; the third section involved the input and output pin-out number; the fourth was the individual code section of each sensor to collect the data; the fifth was the main section of the program with a “while loop” that runs until the failsafe command was activated; finally the exception statement was defined to stop the program and log the data. The Python® script is in the appendix section.

3.4. Guidance, Navigation, and Control Capabilities

The objective was to create a model to improve the vehicle's capabilities to complete the mission effectively. A list of different capabilities was analyzed and measured to evaluate the vehicle's performance. This section summarizes some methods or tools employed to measure or specify the platform's limits. Several factors affected the results of every test. Hence, the first step was to obtain an idea of the values through model simulations, research, or tests in ideal conditions.

Figure 17 represents a list of the evaluated capabilities divided by subsystems.

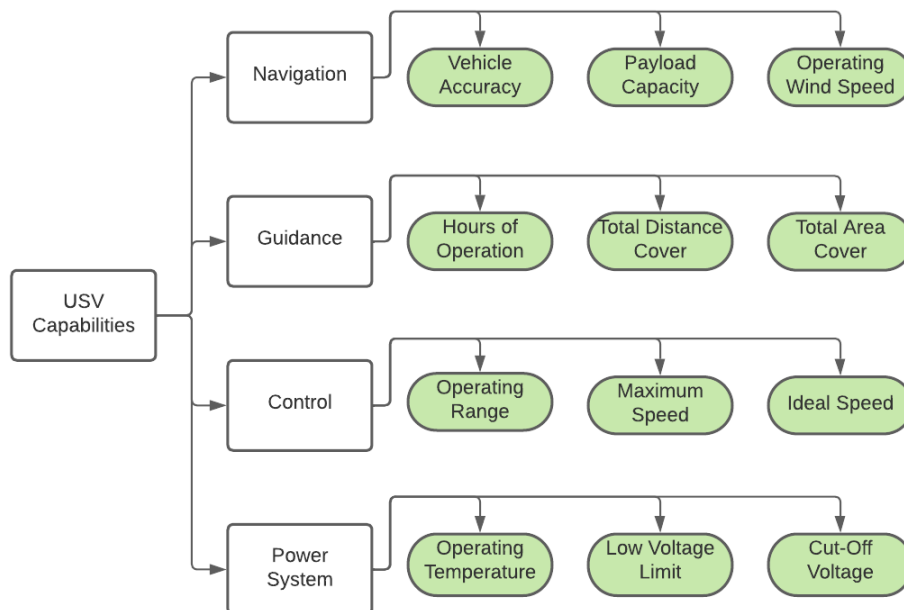


Figure 17. USV Capabilities to be Evaluated.

3.4.1. Navigation Capabilities

The PID tuning configuration helped to reach an improved navigation pattern. The most important configuration is Yaw, Roll, and Pitch tuning, which is essential for responsive and stable routing. The proportional-integral-derivative (PID) algorithm combines the three natural ways of taking into account the error: the actual (proportional), the accumulated (integral), and the predicted (derivative) values; the three gains depend on the magnitude of the error, the time required to eliminate the accumulated error, and the prediction horizon of the error (Tejado, Vinagre, Traver, Prieto-Arranz, & Nuevo-Gallardo, 2019). Figure 18 shows the USV model integrated with the PID control algorithm in the mission planner software.

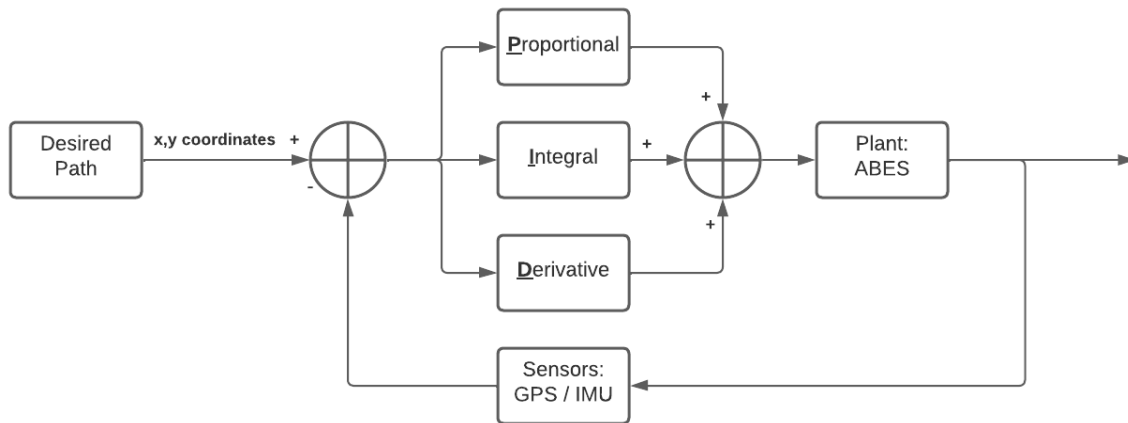


Figure 18. ABES Motion Control System.

Based on the PID algorithm USV model, the gains K_P , K_I , and K_D of the controller were manually adjusted. The steps followed were: (1) set $K_I = 0$ and $K_D = 0$ and adjust K_P gradually from small to large until the closed-loop response curve appeared to equal amplitude oscillation. (2) Document the current value K_P and the oscillation period T_o of the closed-loop response curve as presented in the rule of Ziegler-Nichols (Åström & Hägglund, 2004). (3) The K_I and K_D values were adjusted following a similar procedure for K_P in step (1). The PID control was defined based on the system response to the changes in the values. The PID Controller Tuning tool in MATLAB – Simulink ® was employed to validate the theory. The final parameters of the PID controller obtain were $K_P = 0.15$, $K_I = 0.15$, and $K_D = 0.10$.

The capacity to follow a predefined path can determine the success of a mission. The location of the boat relies on the accuracy of the global positioning system. Hence, considering the accuracy of the GPS, the deviation between points should be below < two meters 95% of the time. Given that the area to cover was extensive (14,400 m²), the error above two meters between coordinated points is irrelevant. Additionally, a calculation of the Mean Absolute Error (MAE) (Brassington, 2017), Root Mean Square Error (RMSE) (Chunyue, et al., 2019), and the Euclidean Distance (O'Neill, 2006) between the desired waypoints and the actual position of the system, by comparing the nominal coordinates desired against the absolute coordinates collected by the payload utilizing Formula 8, 9 and 10 were made.

$$MAE = \frac{1}{n} \sum_{i=1}^n |y_i - y_{di}|, \quad (8)$$

$$RMSE = \sqrt{\frac{1}{n} \sum_{i=1}^n (y_i - y_{di})^2}, \quad (9)$$

$$d = \sqrt{(x_2 - x_1)^2 + (y_2 - y_1)^2}, \quad (10)$$

Equations 8 and 9, the y_{di} are the coordinates of the i desired waypoint. n is the number of the points to be evaluated and y_i are the actual coordinates of the vehicle. These metrics statistically evaluate how accurate the model was and the amount of deviation from the actual and desired locations. The Euclidean Distance is the space between two points in the coordinate system. The (y_2, x_2) are the coordinates of the desired waypoint and (y_1, x_1) the absolute coordinates of the USV.

3.4.2. Guidance Capabilities

One of the main goals of this research was to be able to complete long-term missions. The power system integrated with the LiFePO₄ batteries, solar charge controller, and solar photovoltaic panel provides a 60 Ah capacity. It can safely survey areas for four hours on a partially cloudy day at an average speed of 1.2 m/s (4.32 km/h). Based on the hour of operation provided by the power system, in a 20-minute mission, ABES covered 1,500 meters. Theoretically, 15,795 meters and 12 missions can be covered in four hours.

3.4.3. Control Capabilities

The control of the vehicle sought to collect the most significant amount of data possible in the shortest time. Therefore, the system was built with the proper control forces to be generated in conjunction with instruction provided by the guidance and navigation systems while simultaneously satisfying desired control objectives. The telemetry system allowed precise steering and maneuvering of the USV within up to 20,000 meters.

The failsafe command (An automatic recovery response) was a model that used different signals such as temperature, wind speed, and battery voltage to deploy a command to return home position. This step also endorsed the live monitoring of the variables affecting performance to define the platform's limits. The signals that activate the failsafe command are Voltage Level, Wind Speed, Electronic Box Temperature, and Radio Signal.

The diagram and the code follow simple if-clause statements to prevent further difficulties within the boat. First, running out of power in the middle of the water due to a low battery or weak signal, and second, preventing unworthily losing too much energy due to the strong wind or high temperature.

In short, the diagram and code follow this logic: the mission starts, and the code continuously asks: “Is the battery low?” If not, it continues. Then, “Is the radio control signal low?” If not, it continues. Finally, “Is the wind speed or the temperature above the limit?” If not, go back

to the mission starts until the mission ends. Note that the internal sensors within the boat respond to previous questions. Hence, there are two possibilities:

- The mission ends, and the boat returns home without meeting the conditions. Completion of a successful mission.
- Alternatively, the boat returns home, activating the failsafe command before completing the mission because a yes confirmed either of the three conditions. Failsafe activated.

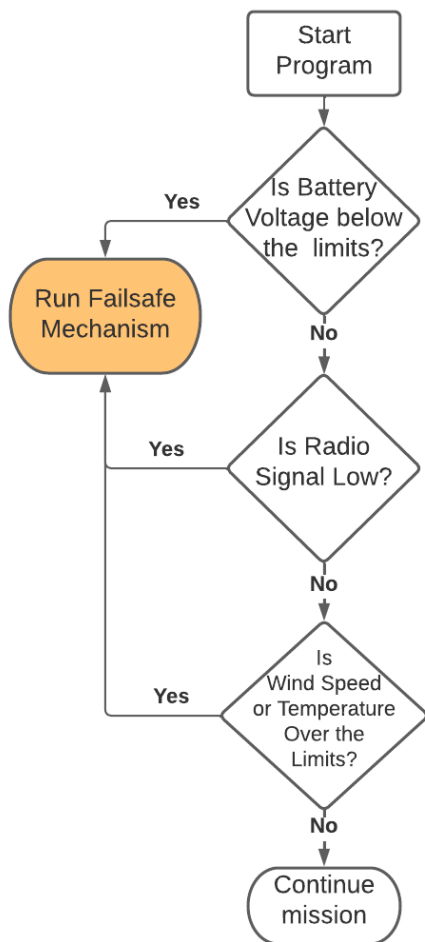


Figure 19. Failsafe Workflow.

3.4.4. Echosounder Sensor

The payload is the echosounder sensor manufactured by SONTEK ®. The RiverSurveyor M9 ® system is a robust and highly accurate Acoustic Current Doppler Profiler (ACDP) system specifically designed to measure 3-Dimensional water currents, depths, and bathymetry for

moving or stationary vessels. It was selected because the RiverSurveyor system combines proven state-of-the-art acoustic doppler velocity profiler instrumentation with a Windows-Based Software package perfect for the applications in the research. The M9 has a nine-beam system with two sets of four profiling beams and one vertical beam. It has a velocity profiling range of up to 30 m and a discharge measurement range of 80 m. It has two sets of velocity measurement transducers in a Janus configuration, four 3.0-MHz transducers and four 1.0-MHz transducers. Therefore, the device offers a sampling rate of 1 hertz, which means that data is collected every second. The sensor integrated a GPS-RTK feature that offers precise positioning and fast data sampling rates, which was perfect for evaluating the waypoints followed by the vehicle as a second locating method.

3.5. Study Area

3.5.1. GeoSenSE Laboratory

Located in the Geological Sciences Building at UTEP. A sensor laboratory was equipped with engineering tools to integrate the new features, fabricate the prototype parts, and validate the platform under ideal conditions. A 3D printer was utilized to model and simulate the modified parts of the platform.

3.5.2. Ascarate Park

It is a 1.1-mile perimeter route located in El Paso, Texas. Due to its proximity to UTEP, the area was used to validate the new features integrated into the system. It poses different water conditions like wind, vegetation, and clean water, making it a suitable place to test the changes to the platform and an easy-to-access area.

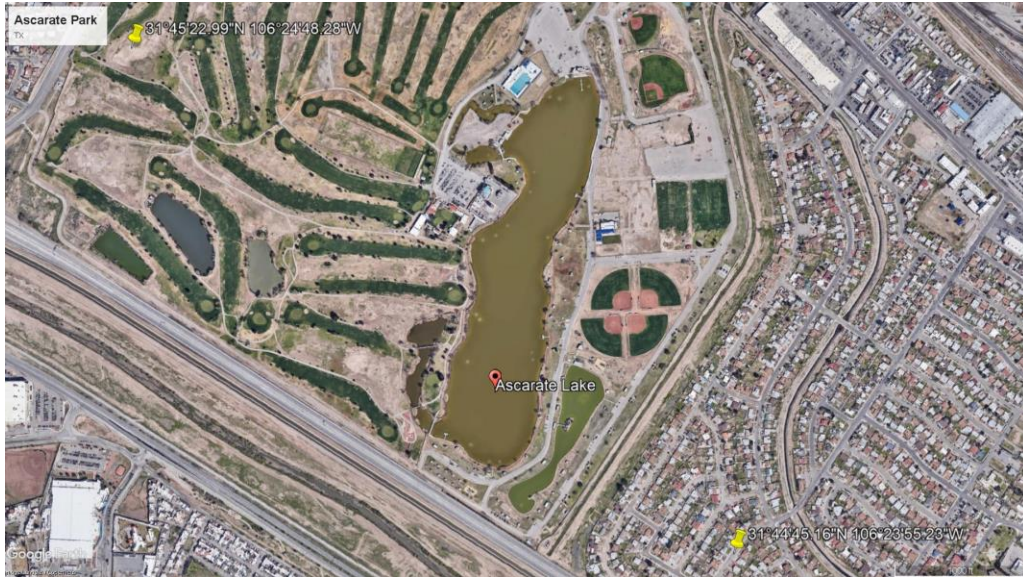


Figure 20. Satellite View of the Ascarate Lake Locates in El Paso, TX.

3.5.3. Grindstone Lake

The location of Grindstone Lake is in Lincoln County, near Ruidoso, New Mexico, a perfect zone for boating, given the excellent weather, the free algae waters, and ample space of 16 hectares (40 ac), having the longest side to the east where is the dam of 35 meters (115 ft). Finally, the lake is 2,108 meters (6,918 ft) above sea level (Davis, 2003).



Figure 21. A Satellite View of the Grindstone Lake Locates in Ruidoso, NM.

CHAPTER 4: RESULTS AND DISCUSSION

This section shows the outcome of the different mathematical models, laboratory testing, and campaigns. Most of the findings come from the field trips. Hence, Table 12 lists the campaigns, locations, and results. Every campaign provided data and answers to validate a specific feature of the prototype.

Table 12. List of the Field Campaigns.

#	Date	Location	Results
1	June 04, 2022	Elephant Butte Dam	Manual mode evaluated.
2	July 28, 2021	Ascarate Lake	Thruster's functions were defined.
3	August 12, 2021	Ascarate Lake	Battery consumption analysis.
4	August 19, 2021	Ascarate Lake	PWM and 60Ah battery configured.
5	September 24, 2021	Ascarate Lake	Thruster's modification and GPS calibrated.
6	January 21, 2022	Ascarate Lake	LiPO battery voltage monitored.
7	February 2, 2022	Ascarate Lake	PID tuning validated.
8	February 16, 2022	Ascarate Lake	Tested paths of guidance and control #1
9	March 3, 2022	Ascarate Lake	Tested paths of guidance and control #2
10	April 27, 2022	Ascarate Lake	Solar power system voltage and wind measured.
11	May 6, 2022	Ascarate Lake	Accelerometer relocated and validated.
12	May 19, 2022	Ascarate Lake	Failsafe and capability study test.
13	May 25, 2022	Grindstone Lake	Complete sensor integrated and long-term mission validated

4.1. Power System

The first step defined the power required for ideal vehicle navigation without compromising the payload. The pulse-width modulation (PWM) is a parameter that can be controlled in the platform to reduce the average power delivered by the electrical signal coming from the drivers. Because the thrusters were the devices that consume more power, this study was focused only on the current drop-by propulsion system. The PWM value is plotted against the current consumption, as shown in Figure 24. In the "X-axis," the pulse width modulation at a fixed voltage of 14.8 V, and the variable current in the "Y-axis." The ideal configuration was 1700

because it gave the maximum possible speed without an electrical circuit overcurrent and power waste. The truster utilized an average of 5.23 Amperes at ideal pwm.

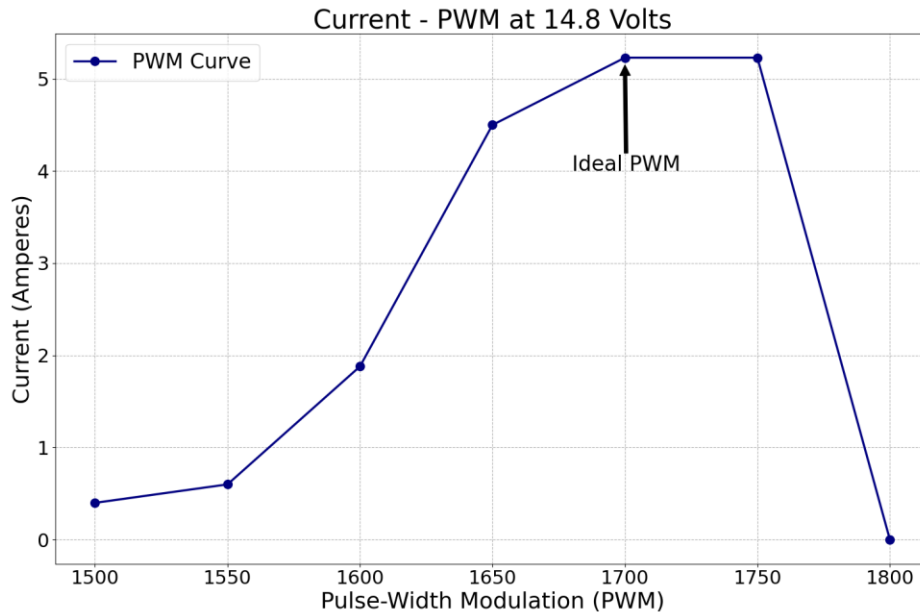


Figure 22. Power System Current Consumption Versus PWM Configuration.

4.1.1. Solar Power Simulation

Figure 23 represents the equivalent circuit of the proposed Solar Power Management System configuration in MATLAB – Simulink ®. The calculation in the methodology section defined the value of the Inductance (L), and Capacitance (C) used to configure the solar panel design parameters. The maximum power was around 50 Watts, as illustrated in the display box in the upper right corner. The model simulated one of the 20Ah LiFePO₄ batteries to understand the behavior. The simulation starts at the battery's 15% State of Charge (SOC), which represents the normal battery discharge condition, around 12.5 Volts.

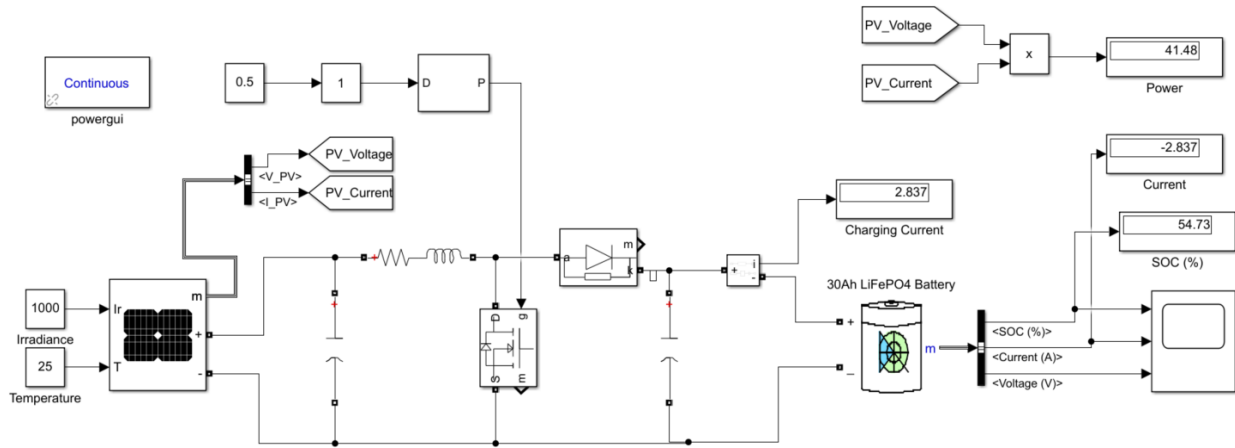


Figure 23. MATLAB – Simulink Model of the Boost Converter.

Figure 24 shows the results of the 20Ah battery starting at a 15% state of charge. At the end of a mission, a battery was usually at this charge level; therefore, starting at 12.5 Volts was an excellent approximation. As estimated, with an average charge current of 2.837 Amperes provided by the solar panel, it took to charge the battery 21,594 seconds (5.99 Hours). The SPMS does not work as a battery charger but as a second power source to extend the missions' duration.

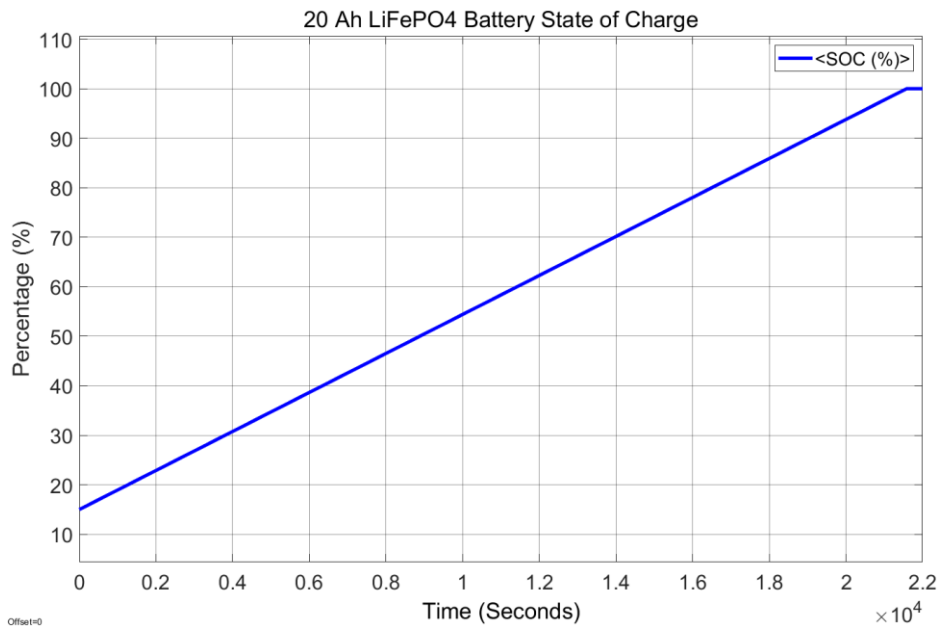


Figure 24. 20Ah LiFePO₄ Battery State of Charge Powered by SPMS.

However, the SPMS was designed to have two 50 Watts panels installed on the platform. This parallel configuration provided a current charging rate of 4.5 A, the same output of an A/C

Battery Charger. Figure 25 shows the behavior of 20Ah LiFePO₄ battery charged by a Battery Charger until it reaches the maximum charge voltage (14.25 Volts). The results showed that it took 4.4 hours to fully charge a 20Ah battery and 6.6 hours to charge a 30Ah battery.

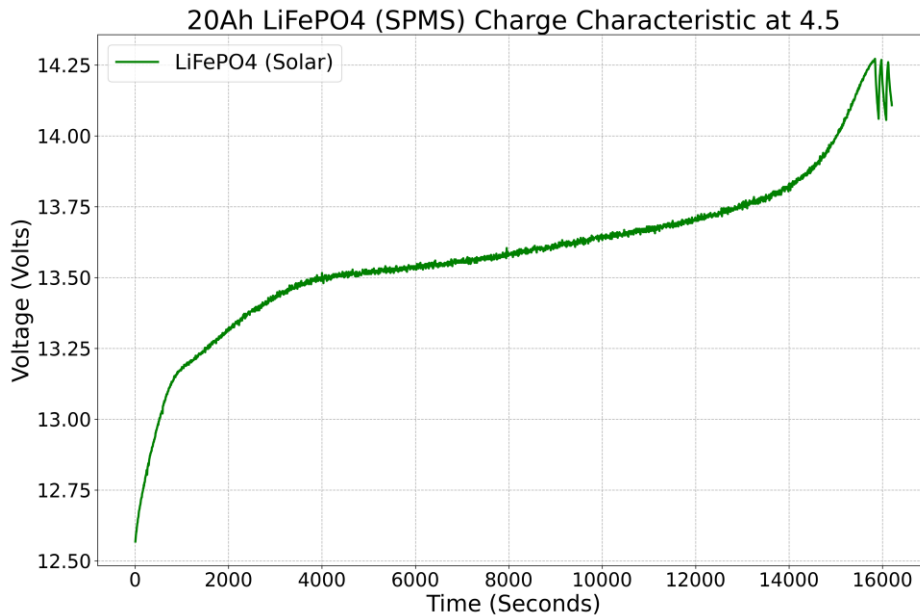


Figure 25. 20Ah LiFePO₄ Battery Charge Characteristics at 4.5 Amperes.

4.1.2. Battery System

This section compared the performance of the two battery systems. The voltage versus time is displayed to compare the behavior of both approaches. The first step was to test the power consumption in a controlled environment at the same PWM configuration for the four thrusters. The same electric charge capacity of 20 Ah was utilized for a transparent comparison between the two battery systems. The available LiPO battery within that current range capacity was 14.8 Volts. On the other hand, the LiFePO₄ batteries, ideal for solar applications, have a nominal voltage of 12.8 Volts. The plots in Figure 14 show a comparison of the two-battery system, on the “Y-axis” the voltage and “X-axis” the time. One LiPO Battery with the four thrusters at full power can last 77 minutes before it reaches the cut-off voltage (11.5 Volts). However, the SPMS with the panel constantly charging the battery can last up to 122.1 minutes before the cut-off voltage (10 Volts) is reached. The Solar Power Management System (SPMS) estimates to increase 37% the duration

of a mission over the standard LiPO battery system based on the laboratory results. These estimations confirmed the simulation calculations presented in the methodology section. Hence, as designed, a power system that triplicates the capacity to 60Ah was sufficient to power the platform for more than four hours.

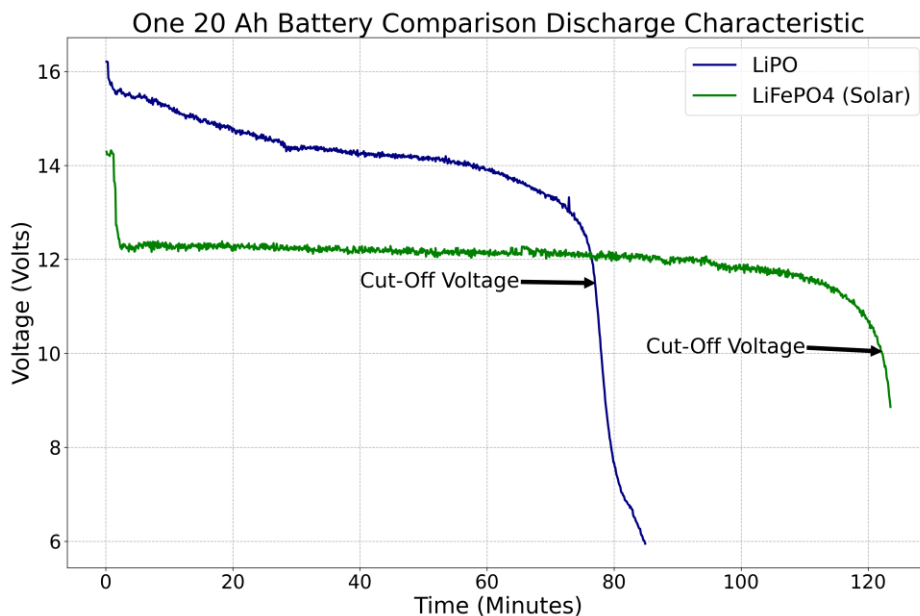


Figure 26. Power System Comparison in Ideal Conditions.

Based on the cut-off voltage highlighted in Figure 26, the low voltage limit was defined 10 minutes before the cut-off voltage was reached. Table 13 summarizes the limits of each power system, such as the theoretical and absolute cut-off voltage. The higher the battery capacity, the higher the cut-off value will be. Additionally, it was proof that the SPMS increased the available power with a smaller slope at the end of the discharge curve. The solar panel charged the batteries continuously, increasing significantly when the vehicle was in loiter mode.

Table 13. Cut-off Voltage and Safety Voltage Limit of the Power Systems.

	Solar Power Management System (Volts)	Time to reach voltage (Minutes)	LiPO (Volts)	Time to reach voltage (Minutes)
Nominal Voltage	12.8		14.8	
Low voltage limit	<u>11.5</u>	112.1	<u>13.5</u>	67
Cut-off Voltage	10	122.1	11.5	77

The low voltage limits acted as the minimum allowed operating voltage of the platform. So once that level was reached, the failsafe was activated. A series of tests were carried out to test the behavior of both systems in the field. The following plot in Figure 27 shows the performance of the battery voltage across time in different scenarios. The LiPO battery system presents a decreasing negative trend, contrary to the LiFePO₄ battery system, which reveals a positive trend at some points during the test.

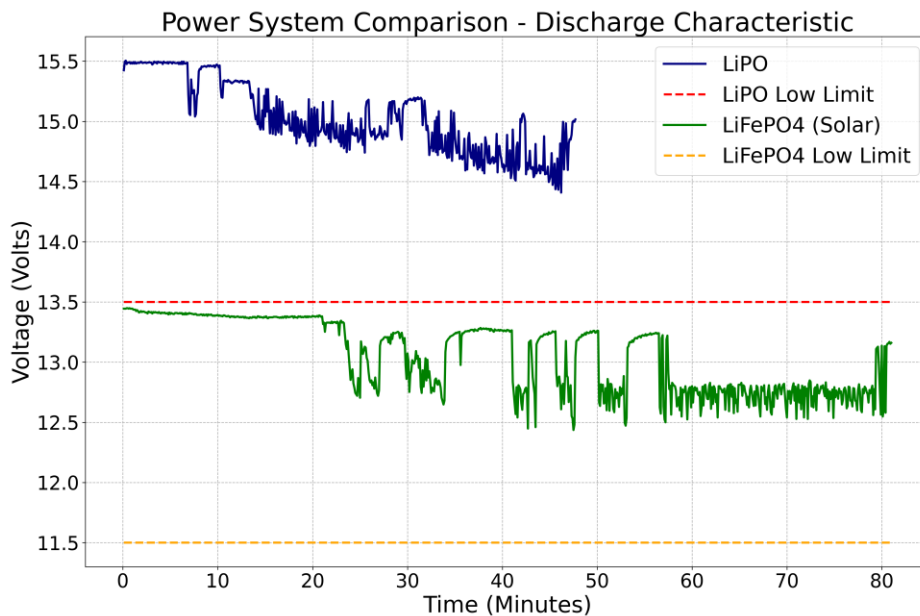


Figure 27. Power System Comparison at the Ascarate Lake. Blue Line: Lipo Battery System on Jan 21, 2022. Green: Solar Power System on April 27, 2022.

Two additional missions took place to compare the behavior of the systems. Figure 28 shows the operation of the two battery systems for extended periods. The LiFePO₄ battery system did not show a representative power decrease during the 140 minutes of operation. An average voltage of 12.966 volts confirmed that the system was stable and could survey areas for more than two hours without failure.

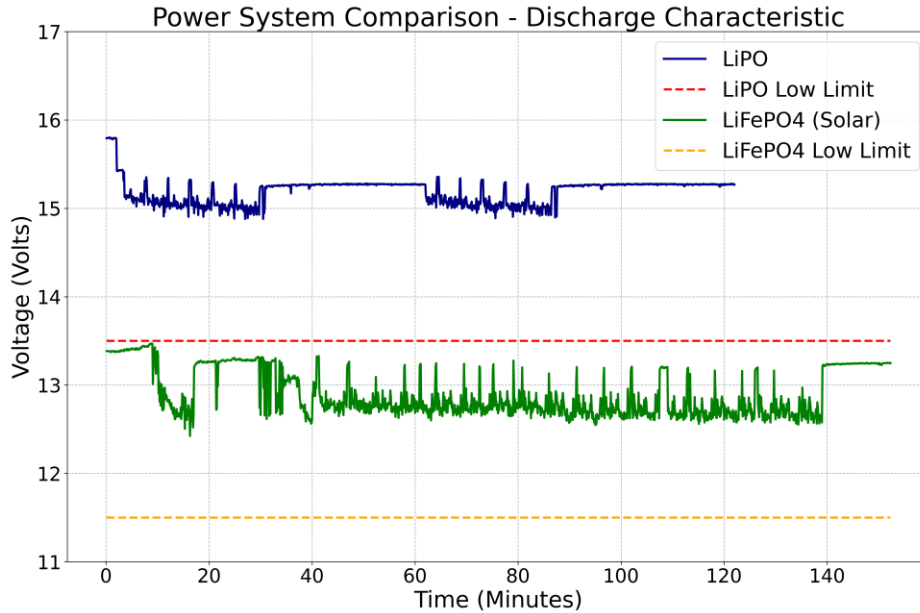


Figure 28. Power System Comparison at the Ascarate Lake. Blue: Lipo Battery System on May 6, 2022. Green: Solar Battery System on May 19, 2022.

Figure 29 shows the voltage behavior at Grindstone Lake during three separate missions with a length of 30 minutes each. The arrows in the plot indicate when a mission ends, where the prototype returns to its home position. While there is no current discharge, the voltage increases until the next mission start because the SPMG charges the batteries while the thrusters are not in use.

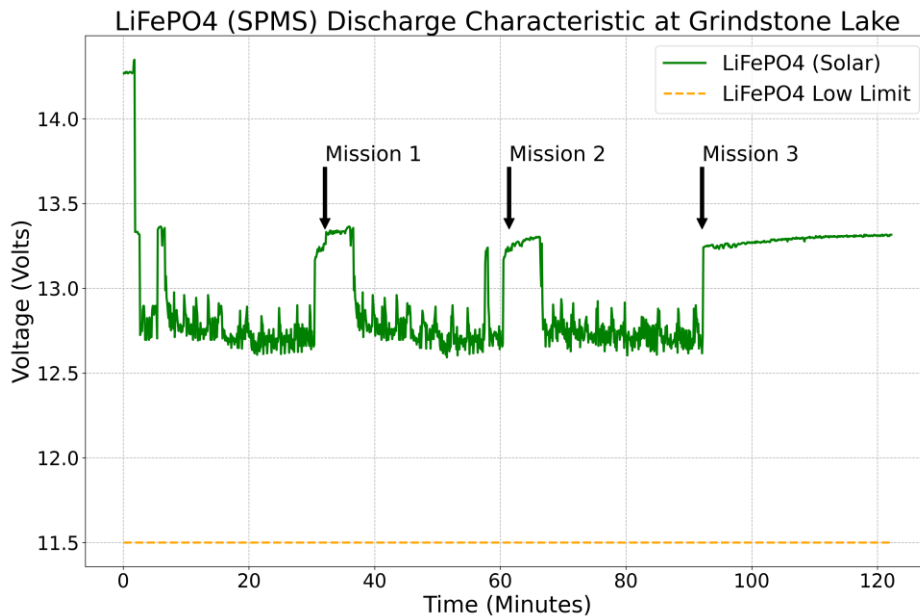


Figure 29. Solar Battery System Performance at the Grindstone Lake on May 18, 2022.

4.2. Sensor Integration

One of the goals of the system was to be able to make decisions autonomously. Hence, sensors to collect meaningful data were required to control the boat based on safety restrictions. The upcoming section presents the wind and temperature behavior in different scenarios. The microprocessor reads a value of the voltage (Volts), wind speed (km/h), and temperature (°C) of the system every 6 seconds. Figure 30 shows a plot of the wind conditions in the Ascarate Lake with the defined interval and the average during 80 minutes of the day. The anemometer provides the wind speed data to react quickly in case of rapid weather changes during a mission.

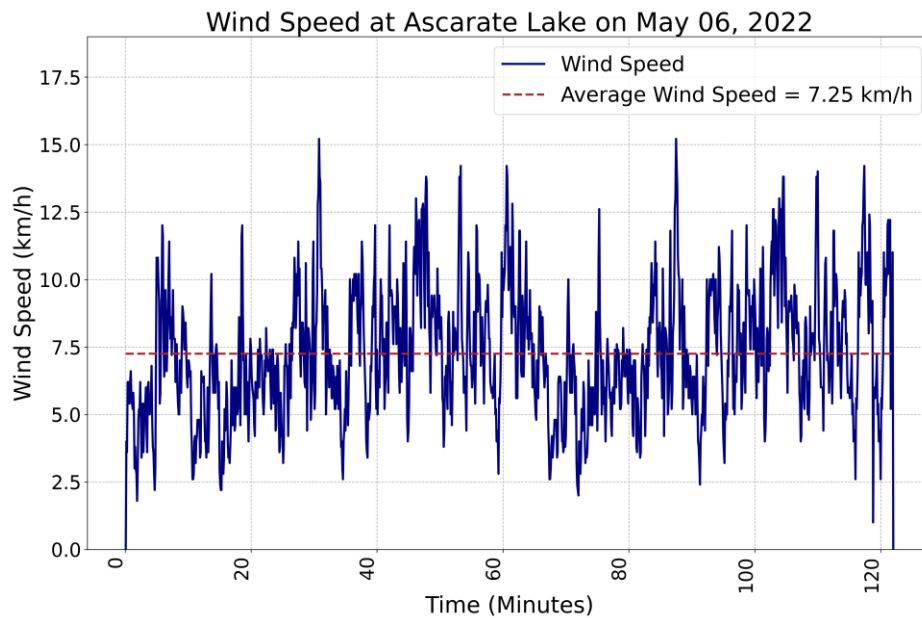
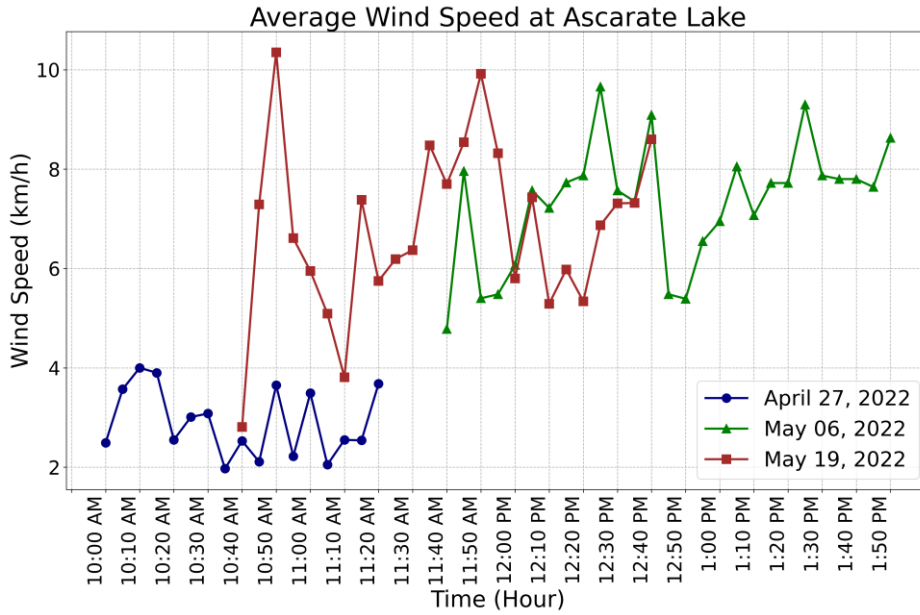
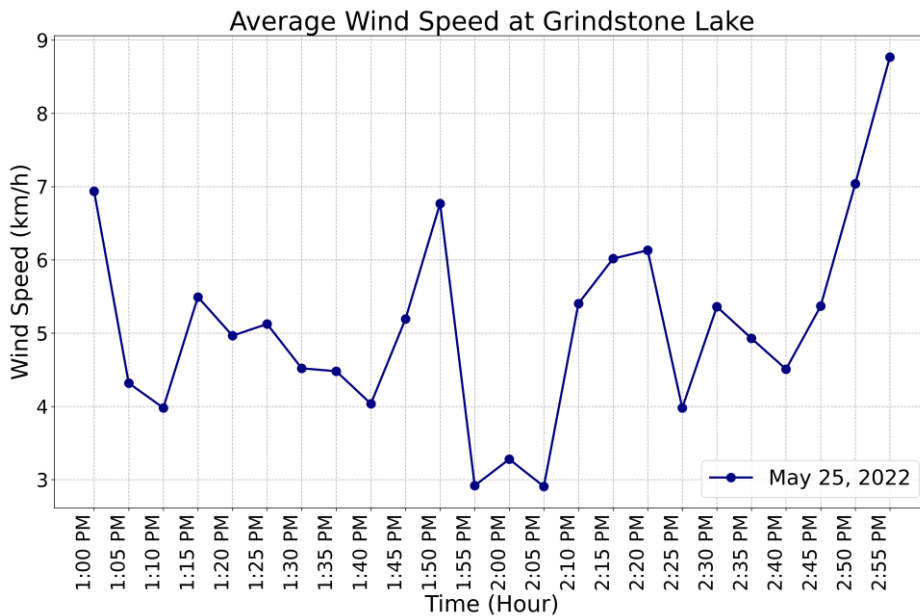


Figure 30. Wind Speed at Ascarate Lake.

The plots in Figure 31 show the average wind speed every 5 minutes at different locations and days. Figure 31 (a) reveals the wind condition in three different missions at the Ascarate Lake with a maximum average of 11 km/h, and Figure 31 (b) uses the same parameters but at Grindstone Lake. The data collected served as the basis for determining the platform's operational speed limit at 20 km/h. However, the vehicle demonstrated to navigate for 20 minutes in hazardous weather conditions where the wind was around 25 km/h.



(a)

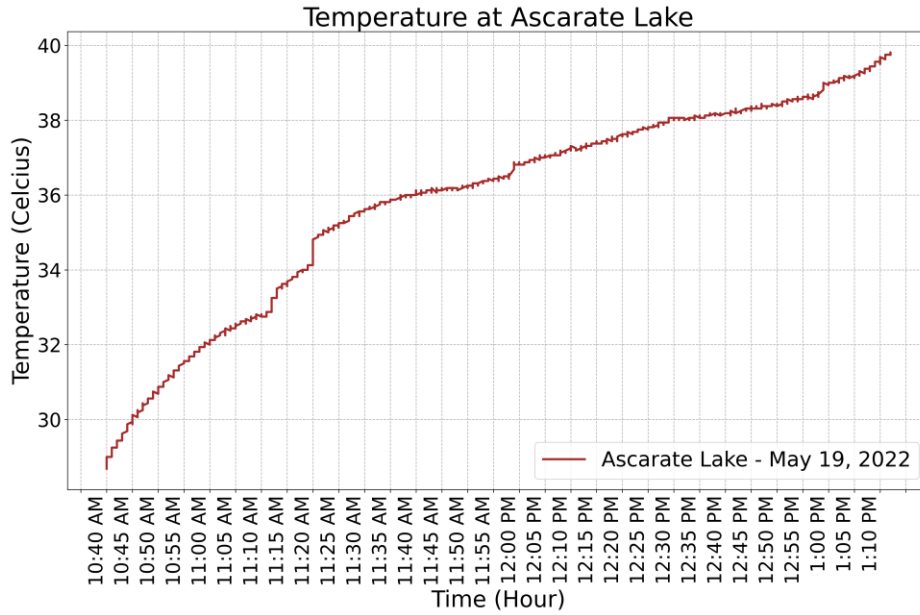


(b)

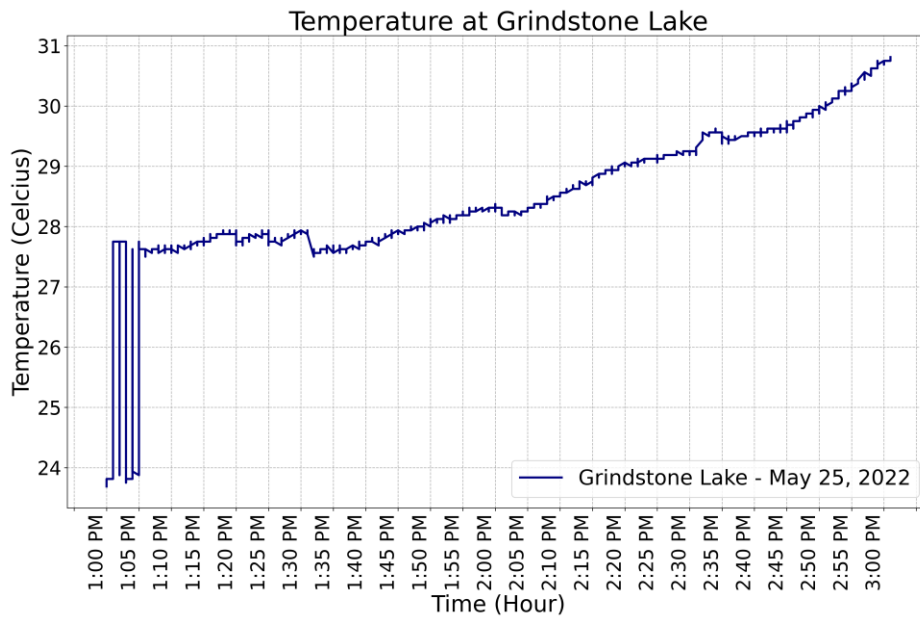
Figure 31. Average Wind Speed Every 5 Minutes. (a) Location: Asarate Lake, El Paso, TX. (b) Location: Grindstone Lake, Ruidoso, NM.

The temperature of the enclosure box was monitored during the missions to prevent damage to the power system. Moreover, thereby the temperature affects the device performance parameters. The plots in Figure 32 shows that the temperature increase due to the sun's position. The results obtained in the field test demonstrated that the electronic devices could be operated well in temperatures close to 40 °C. However, the maximum operating temperature in the

electronic box was set to 45 °C because it is the solar controller's maximum permissible temperature, the lowest limit temperature of all the devices that make up the electronic system.



(a)



(b)

Figure 32. Temperature Conditions in Different Locations.

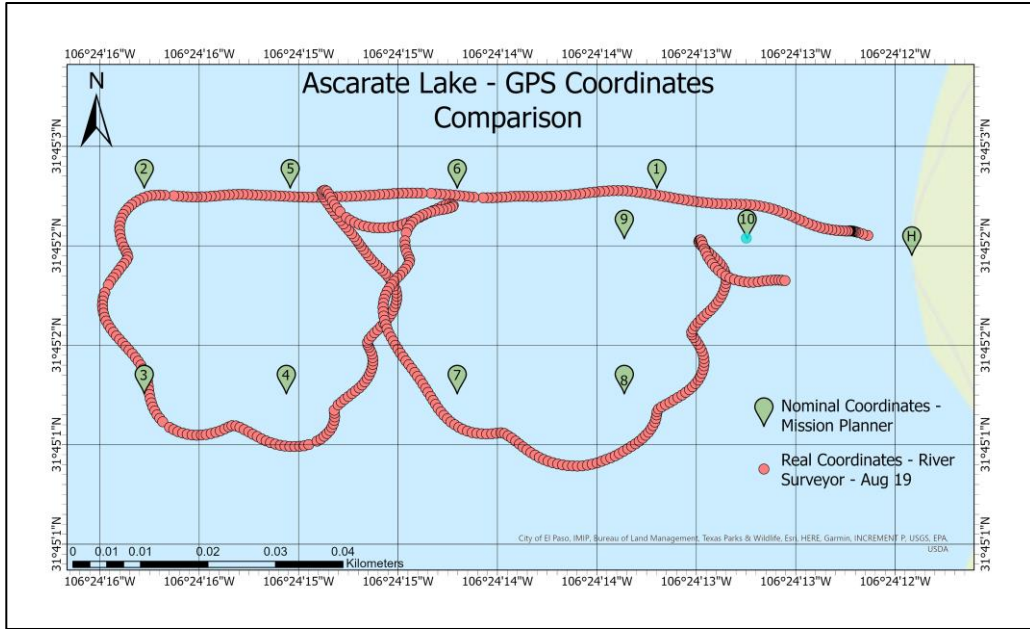
4.3. Capabilities

This section demonstrates the platform's capabilities through a series of validations in the field, divided into three subsystems: Navigation, Guidance, and Control.

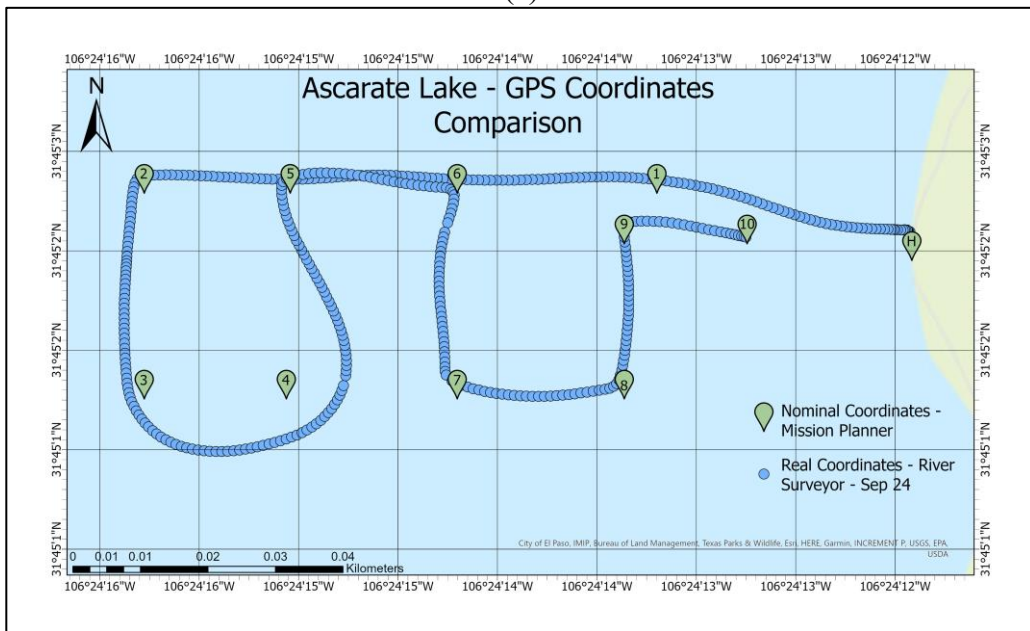
4.3.1. Navigation

The primary perception positioning system was the Here 2 GNSS ® GPS. During the first test, the boat lack of consistency in tracking programmed waypoints. Hence, a comparison before the GPS calibration and the rudderless four thrusters' system configuration is shown in Figure 14 to demonstrate the improvement. The Ascarate Lake map compares the program's GPS coordinates in the mission planner and absolute coordinates. At a scale from 0 to 40 m. In green are the 10 points of the mission. The red dots represent the vehicle's absolute coordinates, which come from the River Surveyor M9 device (GPS-RTK). The vehicle did not follow the programmed path, covering the mission of 323 meters in 10 minutes. The changes in the thruster's configuration to gain control, the GPS, and IMU calibration improved the results in the tracking system, represented with the blue dots in Figure 33 (b). The above actions almost eliminated zig-zagging and reduced the time to finish the same mission from 10 to 7 minutes.

Additionally, a PID tuning procedure, explained in the methodology section, was implemented in the navigation software to improve the ability to follow the predefined path. The practical experiment at the Ascarate Lake needed adjustments to reach ideal tuning conditions. A capability test was applied to analyze the steering control and yaw capacity to follow a determined path after implementing the PID tuning and accelerometer calibration. The calculation of the Root Mean Square Error (RMSE), Mean Absolute Error (MAE), and the distance between the nominal and absolute coordinates demonstrated the vehicle's capacity in the next figures.



(a)



(b)

Figure 33. Comparison of the GPS Calibration and the Rudderless Four Thrusters' System Configuration. (a) Before Improvement. (b) After Improvement.

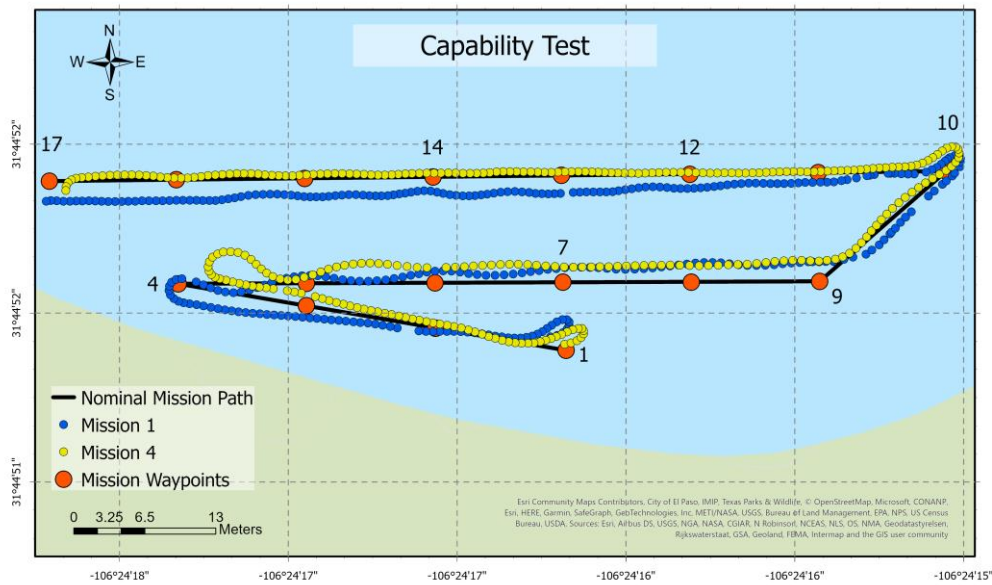
The mission was composed of seventeenth waypoints with a length of 164.83 meters. Eight different trials were tested in the field to compare outcomes. Table 14 shows that the time to complete the path is 298.38 seconds with an average speed of 0.55 m/s.

Table 14. Capability Test Summary.

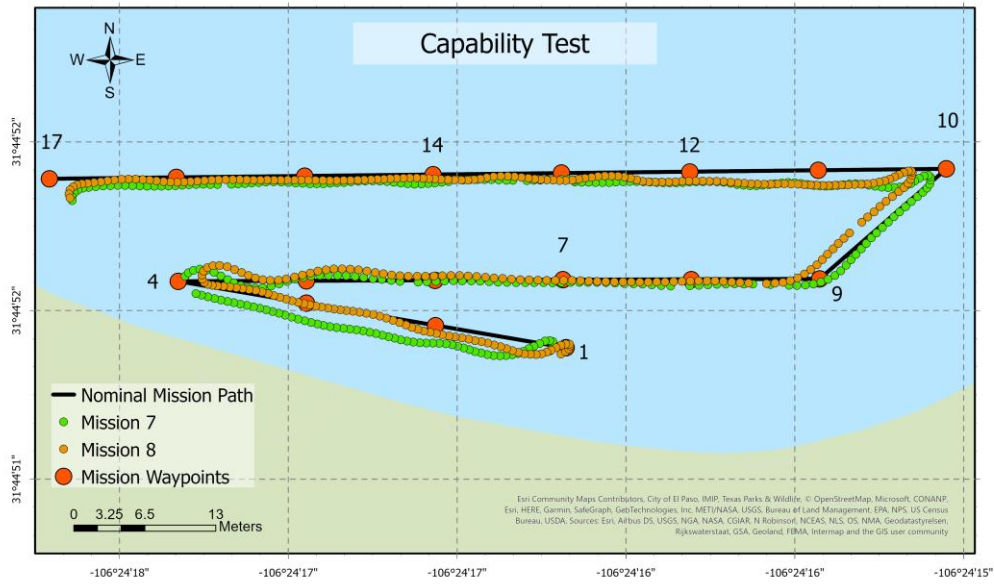
Mission #	Start Time	End Time	Mission Duration (Minutes)	Mission Duration (Seconds)	Average Speed (m/s)	
<u>1</u>	10:50:42 AM	10:55:54 AM	0:05:12	312	0.53	
2	11:04:18 AM	11:09:28 AM	0:05:10	310	0.53	
3	11:33:24 AM	11:38:15 AM	0:04:51	291	0.57	
<u>4</u>	11:39:23 AM	11:44:21 AM	0:04:58	298	0.55	
5	11:51:36 AM	11:56:26 AM	0:04:50	290	0.57	
6	11:57:45 AM	12:02:40 PM	0:04:55	295	0.56	
<u>7</u>	12:09:40 PM	12:14:35 PM	0:04:55	295	0.56	
<u>8</u>	12:15:52 PM	12:20:48 PM	0:04:56	296	0.56	
Mission Length (m)			164.83401	Average	298.38	0.55

Four missions were analyzed to determine the error between the nominal and real paths.

Maps (See Figure 34) show the tracking lines of missions 1, 4, 7, and 8, respectively.

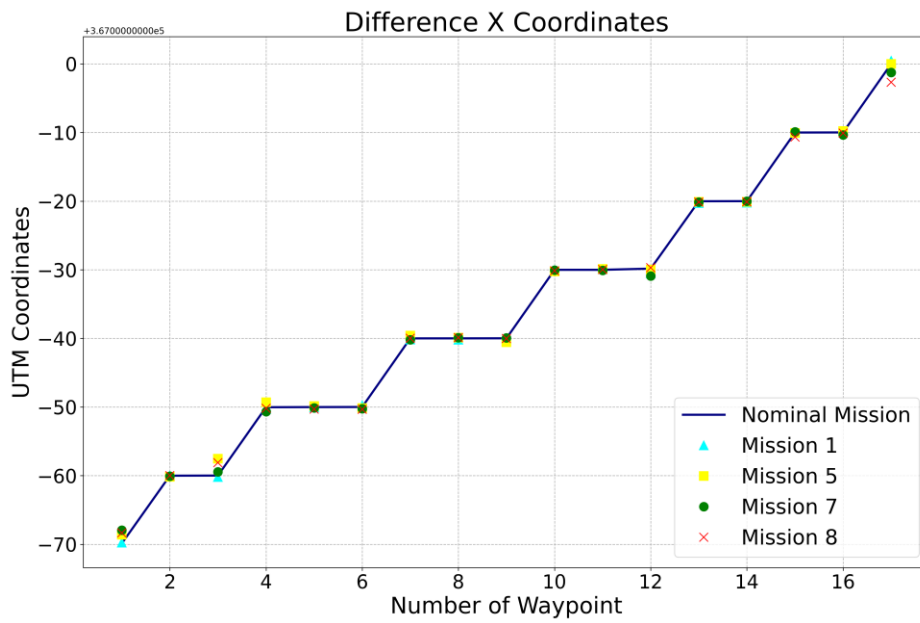


(a)

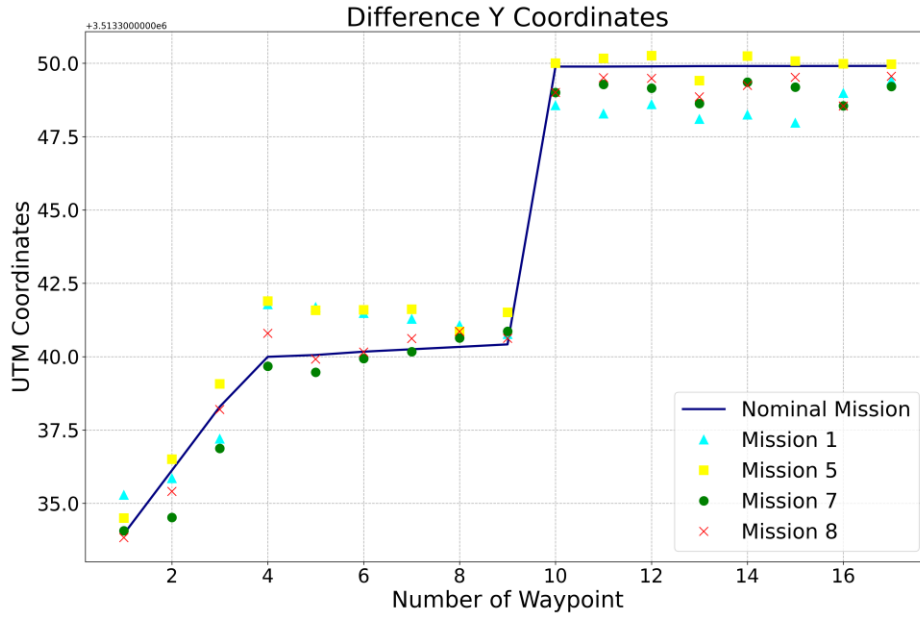


(b)

Figure 34. Capability Study. (a) The Path Follows in Mission 1 and Mission 4. (b) Path Follows in Mission 7 and 8.



(a)



(b)

Figure 35. RMSE and MAE Calculations. (a) X Coordinates. (b) Y Coordinates.

Table 15 summarizes the RMSE, MAE, and Euclidean distance between the missions' coordinates. Both statistical measurements show that the model presents a higher deviation in Y (Longitude) direction than the X (Latitude) collected points. The more significant changes in the vehicle's direction happened in the Y direction, which explained the variation.

Table 15. Capability Test: RMSE, MAE, and Distance Evaluation.

Mission #	RMSE		MAE		Distance Between Coordinates (m)
	Latitude (X)	Latitude (Y)	Latitude (X)	Latitude (Y)	
1	0.256	1.311	0.198	1.211	1.247
4	0.726	0.872	0.012	0.071	0.877
7	0.666	0.836	0.411	0.703	0.903
8	0.904	0.614	0.491	0.499	0.825
Average	0.638	0.908	0.278	0.621	0.963

Figure 36 analyzed the Euclidean distance between each waypoint of the mission. The outliers are highlighted with a red circle. The waypoints 4, 10, and 17 illustrated an average deviation of 2.5 meters. These were turning points where the platform struggled to maintain the yaw control

due to the weight and wind. Future work in the steering control is required to optimize the turning capabilities.

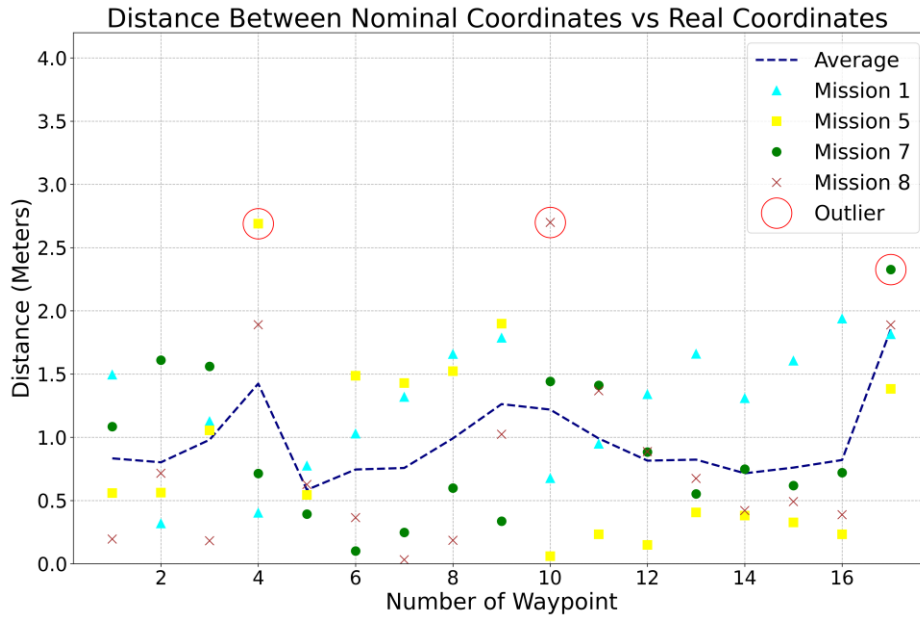


Figure 36. Distance Between Coordinates Points.

Table 16 listed every waypoint's numerical Euclidean distance deviation against the absolute coordinates system. The underlined values are the most significant deviation presented in the study. The average distance between the desired and actual points is 0.963 meters. Considering the accuracy of 2 meters of the GPS positioning system, the distance deviations in the tests can be accepted in practice. Therefore, the ABES platform achieved a satisfactory path following.

The platform successfully carried a payload with a weight of 8 kilograms. Theoretically, it can operate with payloads up to 20 kg with the inner tube integrated. The boat included a Bubble Level (Vials) to give the user a level reading of the platform. It gave the possibility to know if there is an unbalance in the “X” or “Y” direction. Figure 37 shows the integrated final stable prototype, with a closer look at the Level Vial.

Table 16. Euclidean Distance for Each Waypoint.

Waypoint #	Mission 1	Mission 4	Mission 7	Mission 8	Average
1	1.494	0.559	1.084	0.195	0.833
2	0.319	0.562	1.61	0.715	0.802
3	1.125	1.054	1.561	0.181	0.98
4	0.402	<u>2.689</u>	0.713	1.89	1.424
5	0.775	0.544	0.392	0.626	0.584
6	1.029	1.487	0.101	0.364	0.745
7	1.318	1.429	0.248	0.032	0.757
8	1.657	1.523	0.599	0.184	0.991
9	1.787	1.898	0.337	1.024	1.262
10	0.675	0.059	1.442	<u>2.699</u>	1.219
11	0.948	0.232	1.41	1.368	0.99
12	1.34	0.149	0.883	0.887	0.815
13	1.66	0.405	0.552	0.674	0.823
14	1.308	0.381	0.749	0.421	0.715
15	1.605	0.326	0.618	0.492	0.76
16	1.938	0.233	0.721	0.387	0.82
17	1.814	1.382	<u>2.326</u>	1.888	1.853
Average	1.247	0.877	0.903	0.825	<u>0.963</u>



Figure 37. ABES Prototype at Ascarate Lake.

4.3.2. Guidance

Through the campaigns, the hours of operation were able to be improved. Figure 38 shows the improvement of the ABES prototype. The vertical axis represents the total duration of the vehicle running in autonomous mode without incident in different dates.

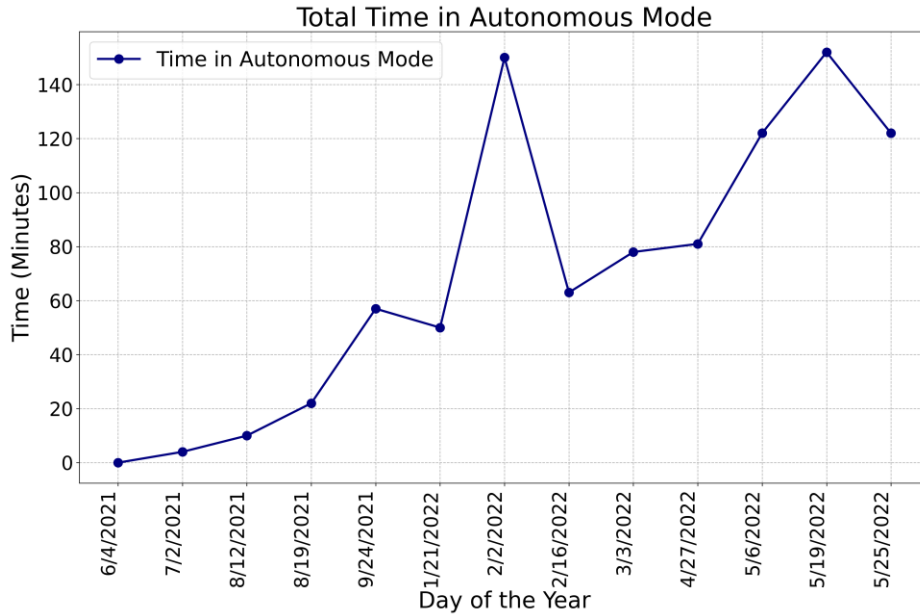
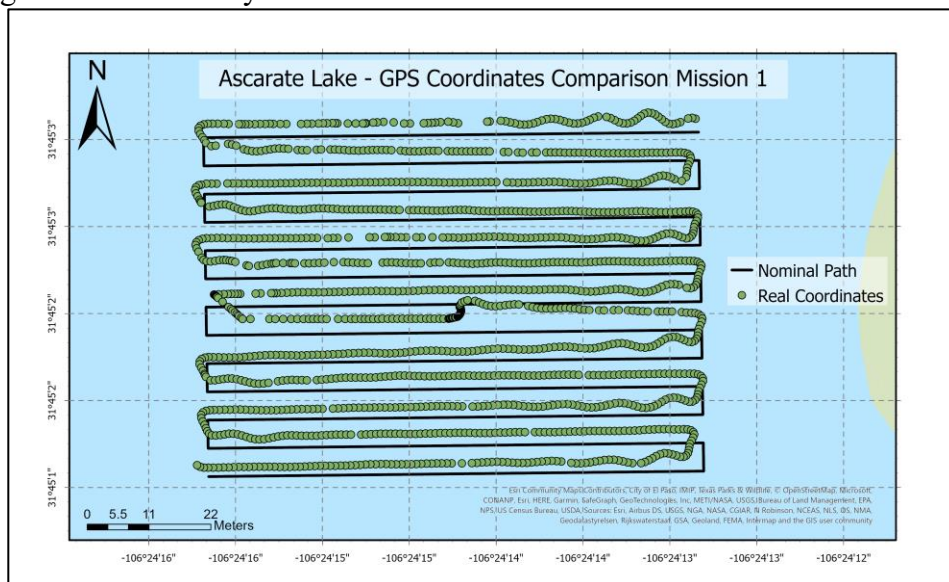
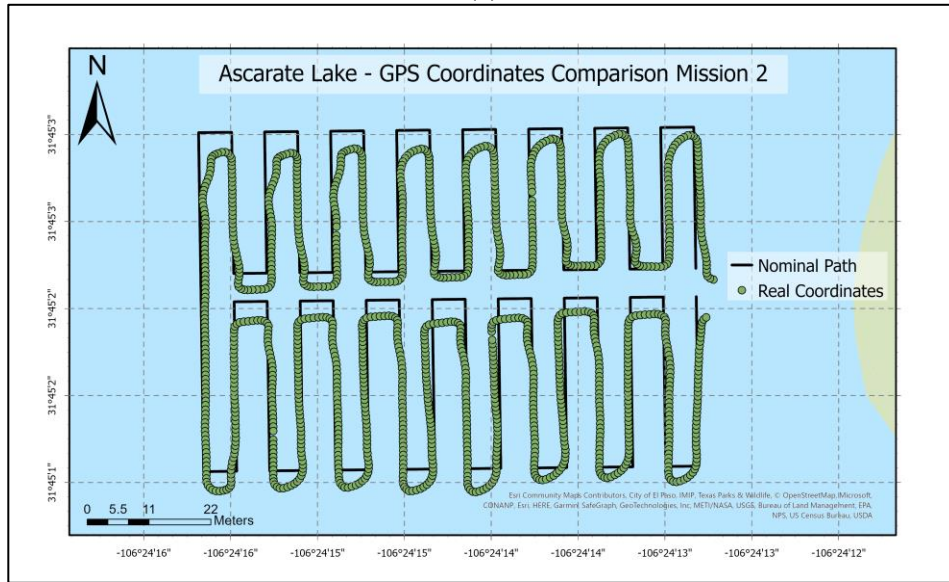


Figure 38. Total Time Running in Autonomous Mode Without a Failure Through Time.

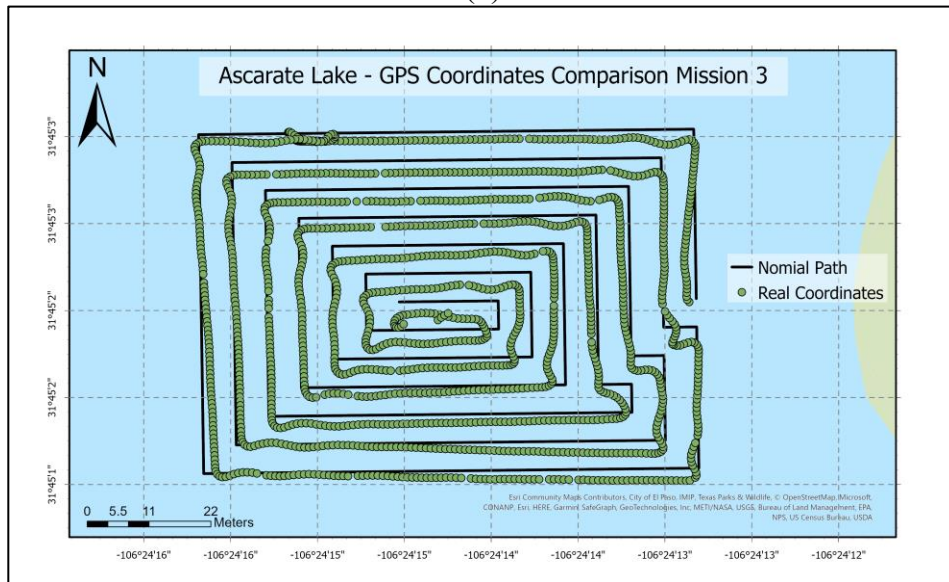
The control of the platform was tested at the Ascarate Lake with four different paths. The objective was to verify the control of the vehicle in different scenarios and conditions. The missions were made on a grid of 10 meters by 10 meters distance to facilitate the calculations.



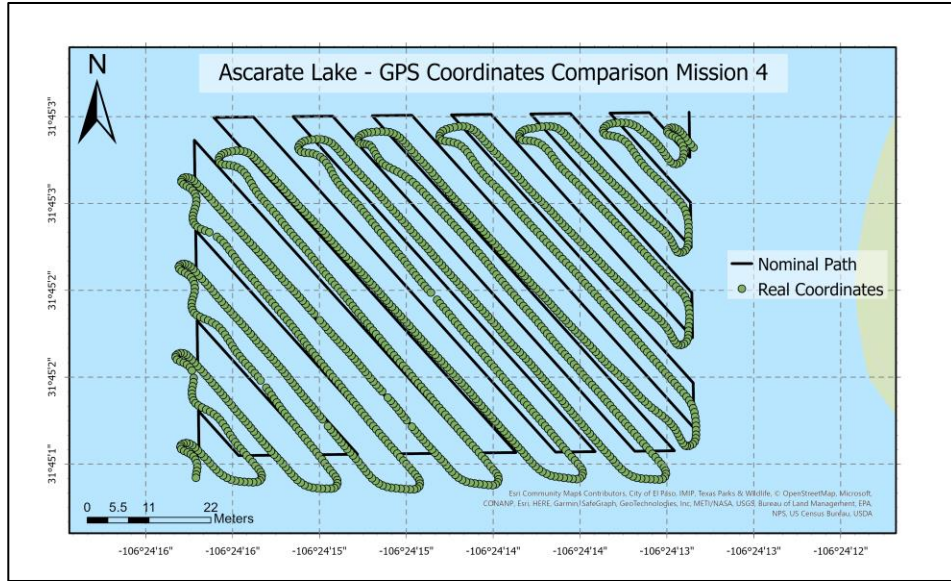
(a)



(b)



(c)



(d)

Figure 39. (a) Mission 1 – Horizontal Path. (b) Mission 2 – Vertical Path. (c) Mission 3 – Spiral Path. (d) Mission 4 – Diagonal Path.

Three successful missions at Grindstone Lake provided a scenario to validate the product under real conditions in a broader area. The length of each mission was 1316.26 meters, with a horizontal path from east to west and a total of 24 waypoints. Figure 40 shows the path followed by the vehicle reaching every programmed waypoint in a radius of 2.5 meters, between 01:20 pm to 03:40 pm.

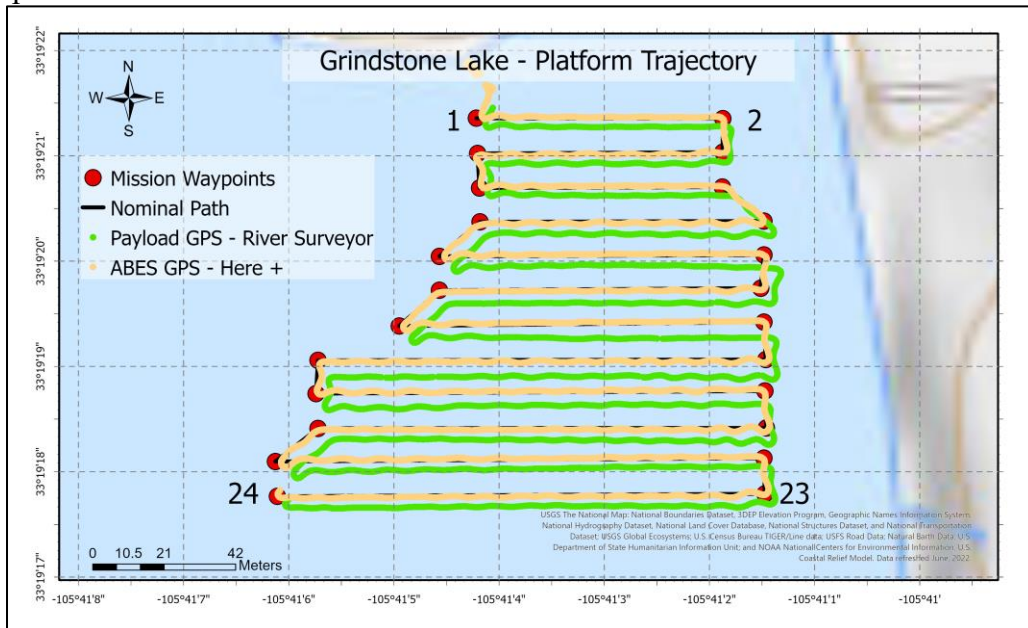


Figure 40. GPS System Comparison Trajectory at the Grindstone Lake.

The map compares the path trajectory between the two GPS systems. The yellow line illustrates the path measured by the location device (GPS Here 2) of the platform, which demonstrates that the vehicle can effectively follow the programmed path. However, the GPS of the payload (River Surveyor) in green presents an offset of 2 meters compared to the nominal path. The deviation among the localization systems is further discussed in chapter 5.

The estimation of the prototype parameters was defined based on the results obtained in the previous missions. In 20 minutes, a distance of 1300 meters was clearly covered at an average speed of 1.25 m/s. Table 17 recaps the calculations to define the ABES prototype guidance capabilities, considering that ten missions with an approximate length of 1316 meters each can be completed in four hours with the SPMG system. The missions were strategically divided into sections of the lake to enable the possibility of reviewing the collected data and giving time to charge the battery system. The ABES can cover a total distance of 13,160 meters and an area of 144,000 square meters (m²). For example, in 12 hours of operation, the platform can cover Grindstone Lake, which has a total area of 16 Hectares (160,000 square meters m²). Hence, three battery sets (180 Ah) are required to cover the lake without a break.

Table 17. Guidance Capabilities Calculations.

Parameter	Value
Hours of Operation	4 Hours
Completed Missions (Length: 1300 m)	10
Total Distance Cover	13,160 m
Total Area Cover	144,000 m ²

4.3.3. Control

With the four-thruster powered in one direction, the vehicle can speed up to 1.7 m/s (6.12 km/s), but for survey purposes, the ideal speed was set to 1.2 m/s (4.32 km/h) to keep the balance between measurement accuracy and propulsion speed. The vehicle's speed was measured by the GPS-RTK and compared to the base station software to calculate a suitable platform speed to

collect the most significant quantity of data without compromising the sample quality of 1 hertz. The plot in Figure 41 shows the vehicle's speed during a sample of 5 minutes during a mission at Grindstone Lake. The results demonstrated that an average speed of 1.27 m/s (Brown dashed line) did not compromise the data quality.

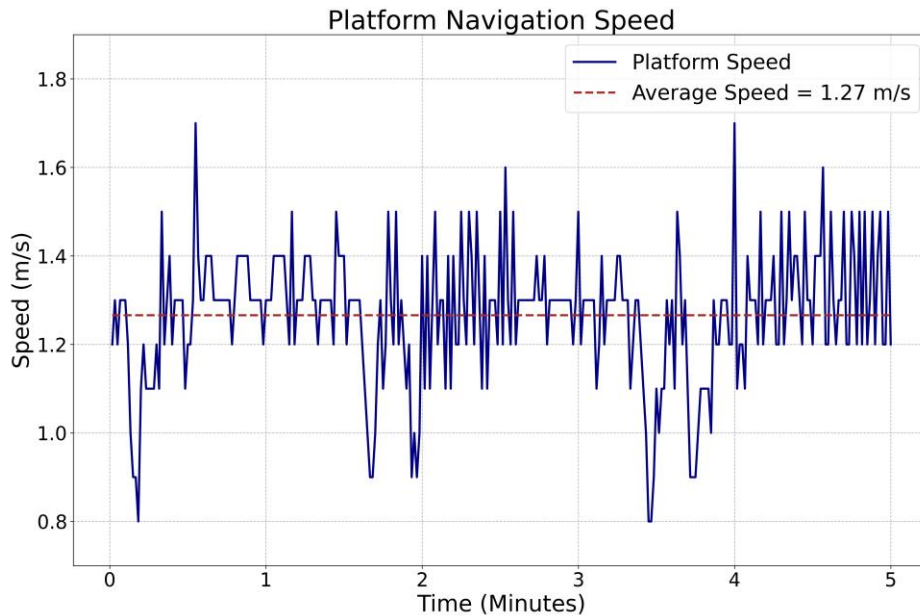


Figure 41. Platform Navigation Speed.

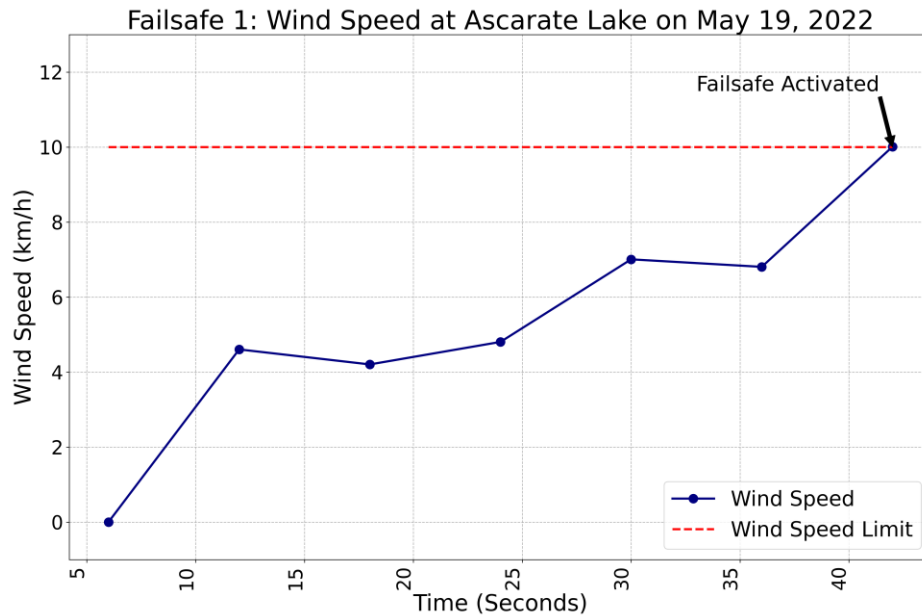
This section demonstrated the ability to deploy the failsafe command. The programmed function was tested by reducing the wind speed limit in two missions. The microprocessor sent the signal, via a serial port, to the flight controller to activate the failsafe command. Figure 29 shows the microcontroller's terminal window with the steps followed to activate the failsafe. As designed, the automatic recovery system was activated once the wind speed limit was reached (10 km/h). In the back, the flight-controller software indicated that the platform was in mode return to launch (RTL) when the alarm was triggered.

The test intended to activate the command if the wind speed exceeded the limit. Hence, the limit was adjusted to 10 km/h and 15 km/h, forcing the failsafe. Figures 43 and 44 show the results of the experiment. As programmed, the vehicle moved toward the home position illustrated in the following maps, where the green points represent the tracked position of the vehicle. Figure 43 (a)

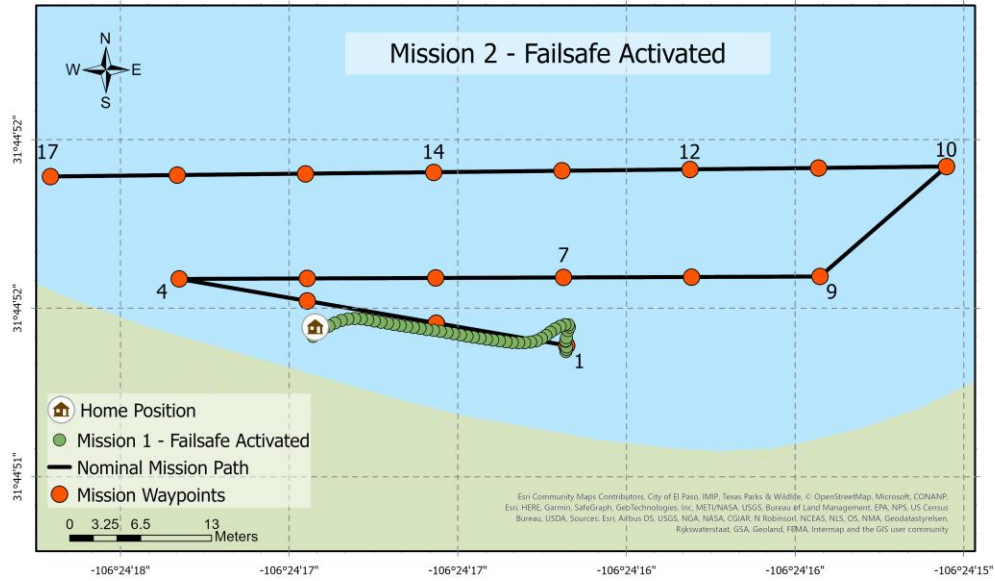
shows the wind speed measured by the controller during the activation sequence of the failsafe command. The red dashed line represents the limit established in both missions.



Figure 42. Base Station with Failsafe Command Activated.

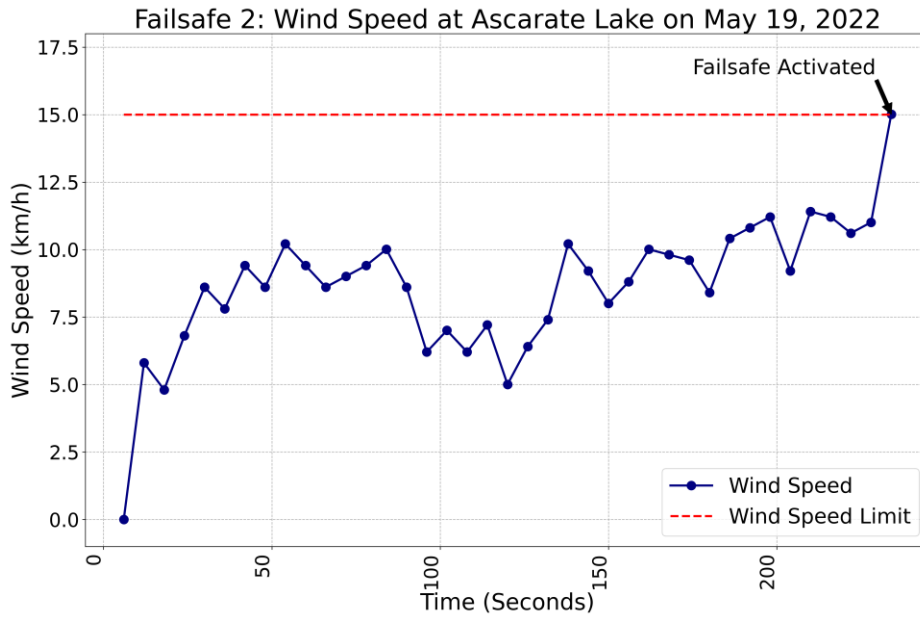


(a)

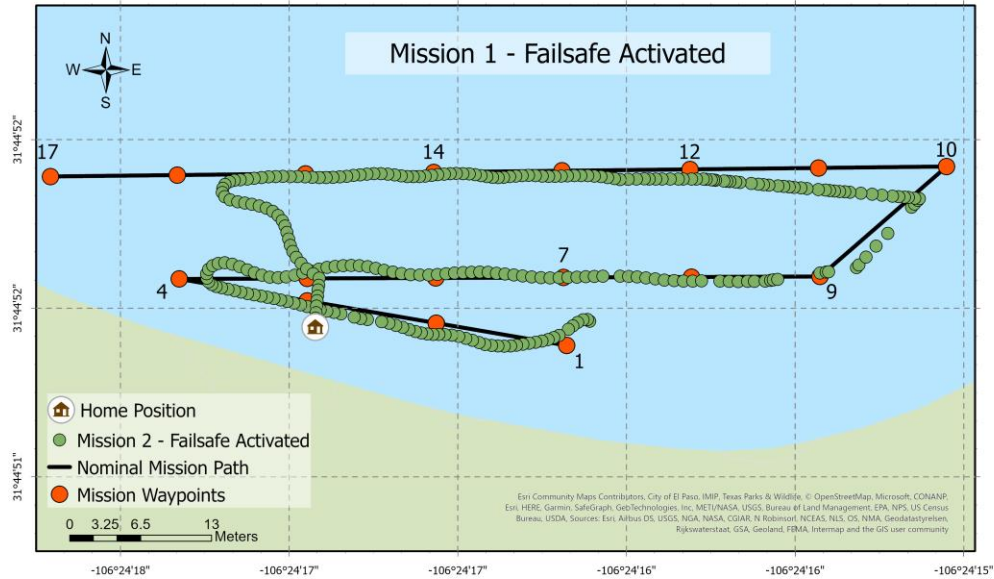


(b)

Figure 43. ABES Moving Towards the Home Position. (a) The Wind Speed Limit at 10 km/h. (b) Trajectory Follows by the Vehicle When the Failsafe is Activated.



(a)



(b)

Figure 44. ABES Moving Towards the Home Position. (a) The Wind Speed Limit at 15 km/h. (b) Trajectory Follows by the Vehicle When the Failsafe is Activated.

A second test with a higher wind speed limit (15km/h) confirmed the effective operation of the algorithm. It took an average of five seconds to communicate the instruction of Returning to Launch (RTL - Home Position) when the failsafe command was activated between the microprocessor and flight controller. Figure 44 (a) shows the measured values of the wind speed through time until the failsafe is triggered because it reached the limit of 15 km/h. Figure 44 (b) illustrates the vehicle's trajectory to reach the home position effectively.

Table 18 reveals an overview of the measurable capabilities of the system based on the previous sections. The technical capabilities of ABES were divided into the subsystems of the platform to achieve the best possible parameters separately. The platform demonstrated capable of following a path with an average error of 1 meter, carrying a payload up to 8 kg. The Solar Power Management System (SPMS) proved to increase the duration of a mission over the standard LiPO battery system. At an ideal speed, the ABES can cover an area of 144,000 square meters and collect 14,400 samples in four hours of operation.

Table 18. ABES GNC Capabilities.

System	Parameter	Value
Navigation	Distance Accuracy	1 m
	Payload Capacity	8 kg
	Maximum Operating Wind Speed	25 km/h
Guidance	Hours of Operation	4 Hours
	Total Distance Cover	13,160 m
	Total Area Cover	144,000 m ²
Control	Operating Range Manual Mode (Distance from the base)	1,500 m
	Operating Range Auto Mode (Distance from the base)	20,000 m
	Maximum Speed	1.7 m/s
	Ideal Speed	1.2 m/s
	Ideal PWM Configuration	1,700
	Maximum Points Collected (Sampling Frequency 1 Hz)	14,400 points
Power System	Maximum Operating Temperature (Electronic Box)	45 °C
	Low Voltage Limit	11.5 V
	SPMS Cut-Off Voltage	10 V

4.4. Bathymetric Maps

Two tools were used to generate this research's final product: bathymetric maps representing the lakes' depth based on geographical coordinates. The following section shows the process and the representations made with data collected during the mission with the ABES platform.

4.4.1. Post-Processing Tools

The first software selected for the hydrographic data collection and processing was HYPACK ®. It provides all the tools needed to design their survey, collect data, process it, reduce it, and generate results. Additionally, multiple acoustic frequencies fused with precise bandwidth control for robust and continuous shallow-to-deep measurements and automated cell size adjustments to optimize performance and resolution. First, a project was created to define the surveying zones and paths to follow. Then, it runs the survey parallel to the mission program in

the mission planner with live monitoring features. Lastly, it was used for post-processing purposes to filter the data, separate errors, and create the final 2D or 3D maps.

Figure 45 shows the first result of the bathymetric data collected in the Ascarate Lake. The scale goes from zero in red, one meter in green, and two meters in purple, representing the depth of the water. The UMT coordinates are displayed on the X and Y axis: a two-dimensional and three-dimensional space representation with a water depth between 0.5 m to 1.5m.

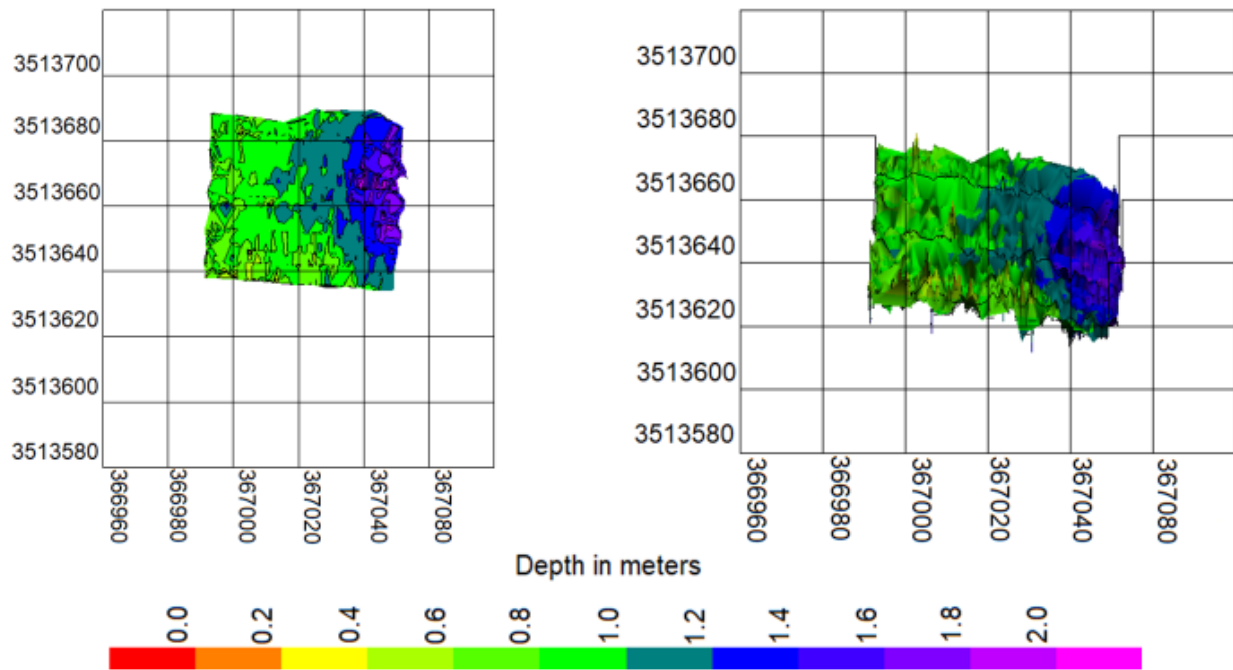
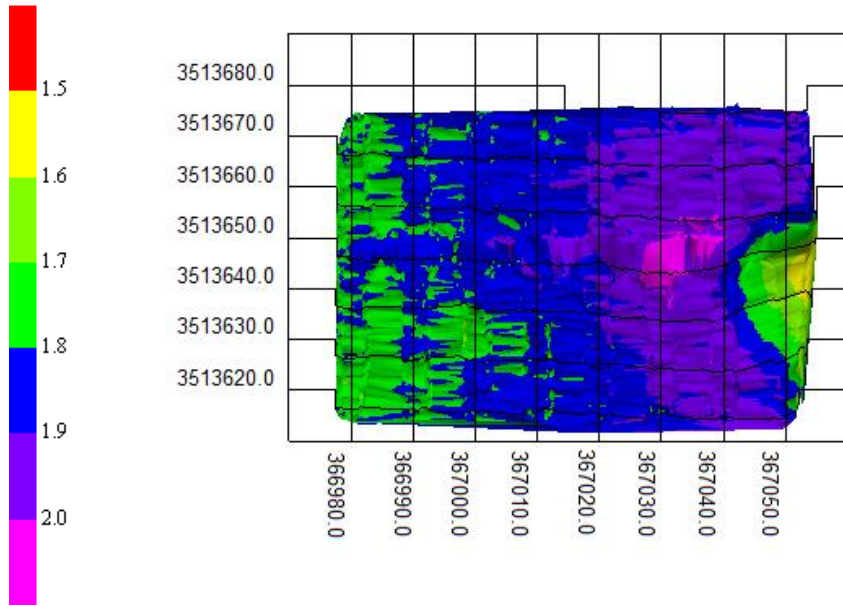
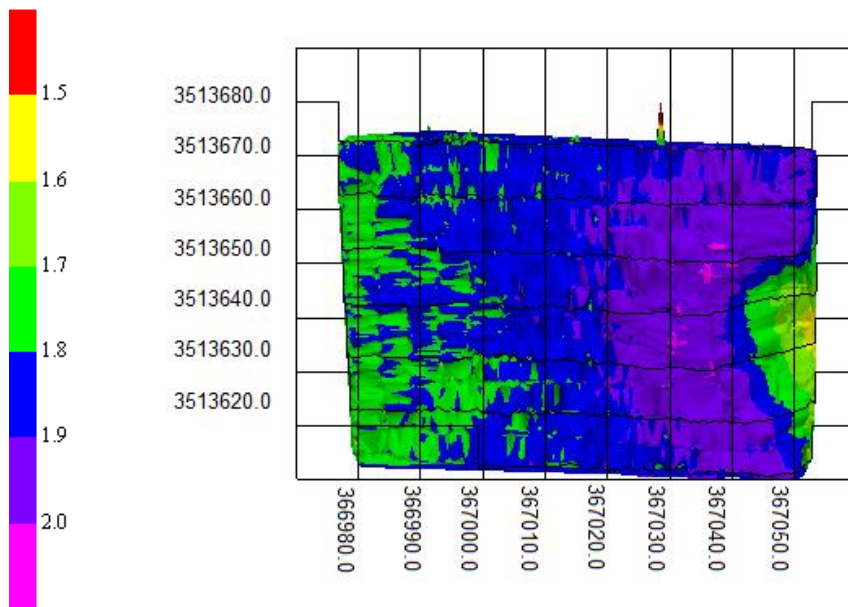


Figure 45. Bathymetric Map of the Ascarate Lake on July 28, 2021.



(a)



(b)

Figure 46. 3D Bathymetric Map of the Ascarate Lake on March 03, 2022. (a) Mission 1 – Horizontal Path. (b) Mission 2 – Vertical Path.

Figure 47 shows the surveyed south section of Ascarate Lake. The mission covers 1500 meters, the most extended area covered with ABES. The deepest sections were located around the center and closer to shore.

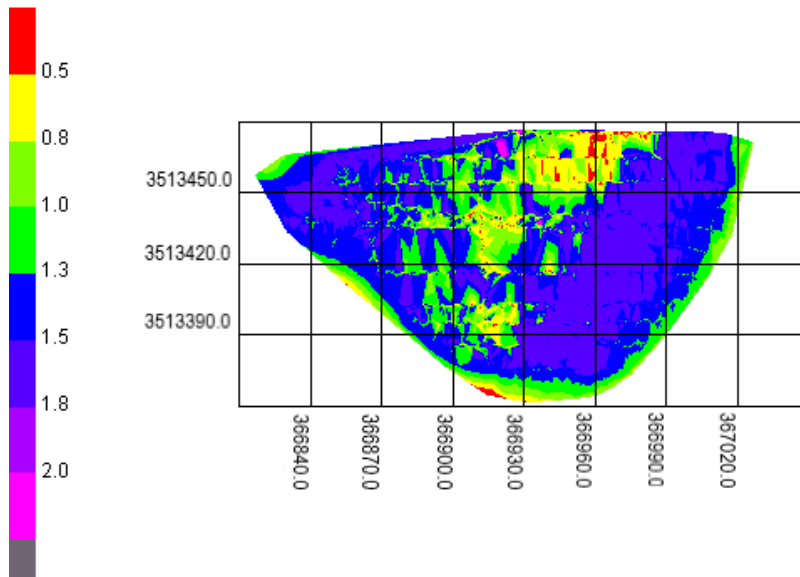


Figure 47. Bathymetric Map (2D Map) of the Ascarate Lake on April 27, 2022.

Figure 48 displays the results of the surveying mission at Grindstone Lake. It was the second biggest area covered by the platform for 120 minutes. The maps show that the depth goes from 0 to 23 meters, from yellow to purple.

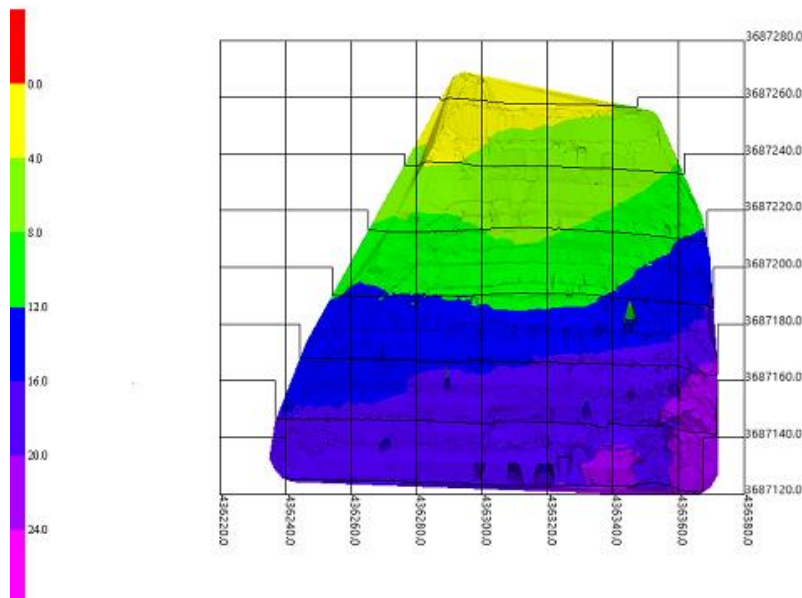


Figure 48. Bathymetric Map (3D Map) of Grindstone Lake on May 25, 2022.

A second post-processing software, ArcGIS Pro ® was employed to create the final products of this research. It combines multiple data sources to make intelligent maps. The software provides exploration, visualization, editing, and analyzing tools used to generate the different figures in this document. The maps include a legend that displays the different classes used to represent the depth of the water bodies, the scale to represent the distance ratio, a picture with more details of the study area, and the results in the center. Two different symbologies were employed to represent the data: graduated symbols represented the various classes by size and graduated colors that divided the classes by color.

The employed method to categorize the data was the “Natural Breaks (Jenks),” the numerical values of ranked data examined to account for non-uniform distributions, which generated the different classes of depth values. The legend included five classes. In red measurements below 0.73 meters, then in yellow values with an average depth of 1.02 meters, in light green values between 1.11 to 1.32 meters, and deeper areas in dark green values up to 1.97 meters. The map in the bottom right corner is El Paso with the location of the Ascarate Park and a scale of 40 meters. The study area is deeper in the center, and shallow areas are located close to the west side of the lake.

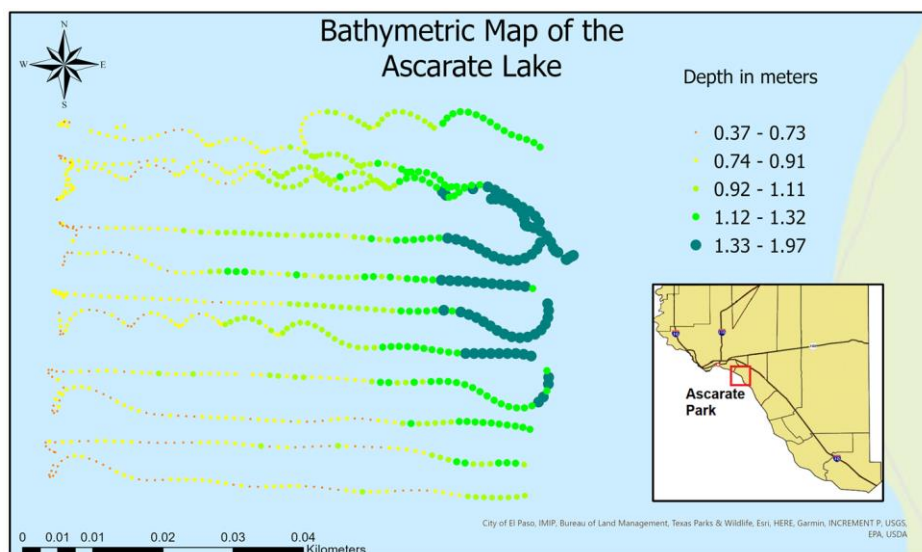
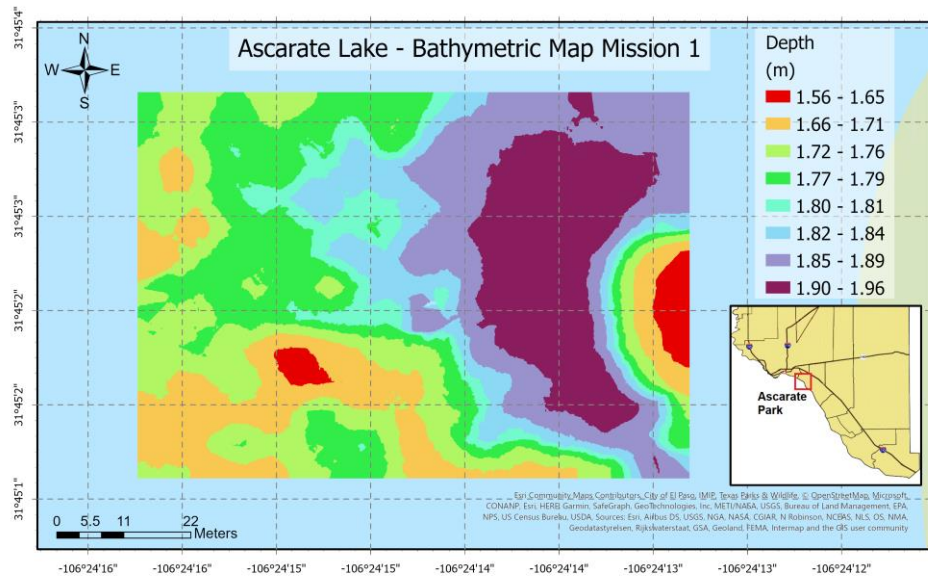
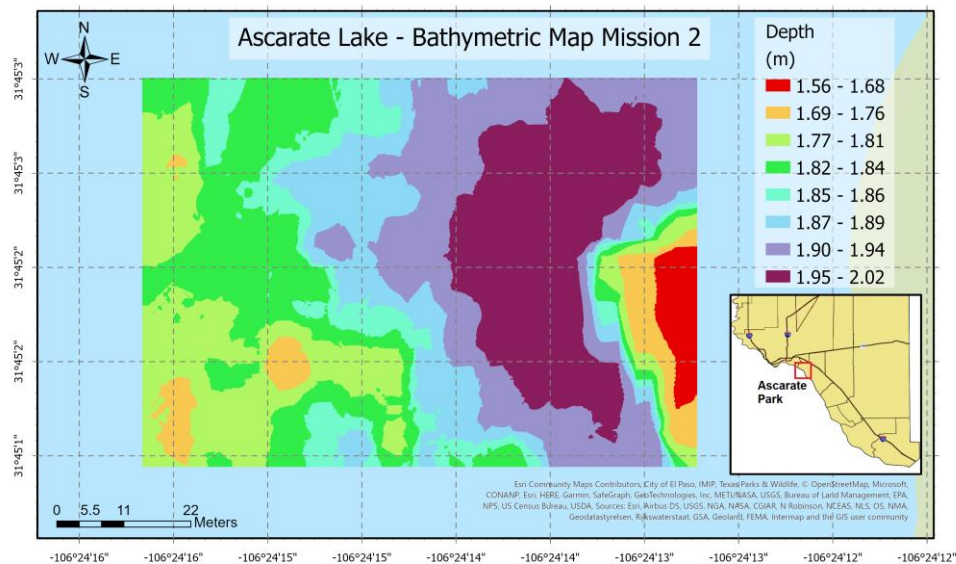


Figure 49. Bathymetric Map of the Ascarate Lake on July 28, 2021.

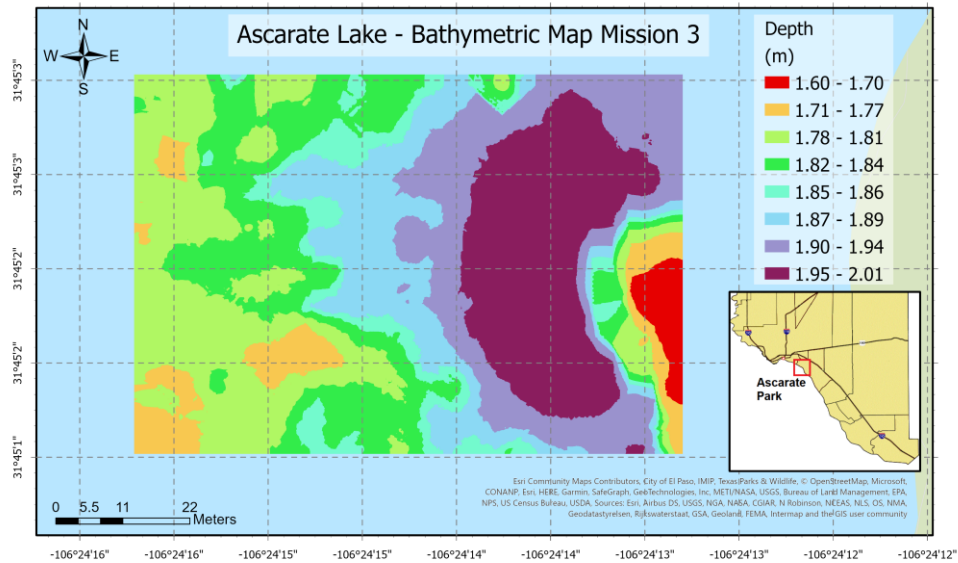
The following maps display a 2D representation (See Figure 50), utilizing the Kriging Interpolation Method to generate a depth map. The data was taken from the same area but with a different path followed by the autonomous boat. In the legend, there are eight different classes. Red measurements represent values below 1.5 meters, and the deeper areas are colored in purple between 1.95 to 2.02 meters. The scale is 22 meters. The deeper areas of the study are located in the center. Furthermore, shallow water sections were situated close to both sides of the lake.



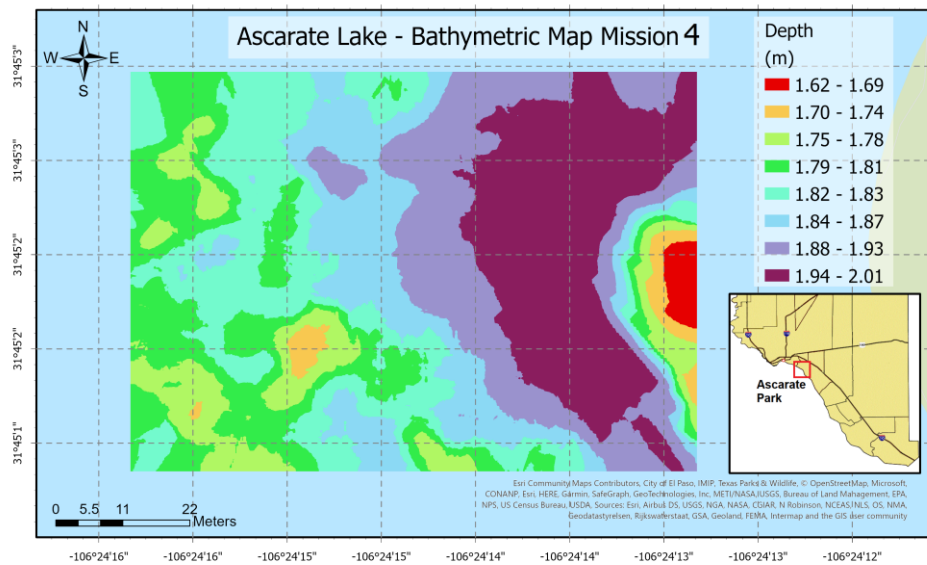
(a)



(b)



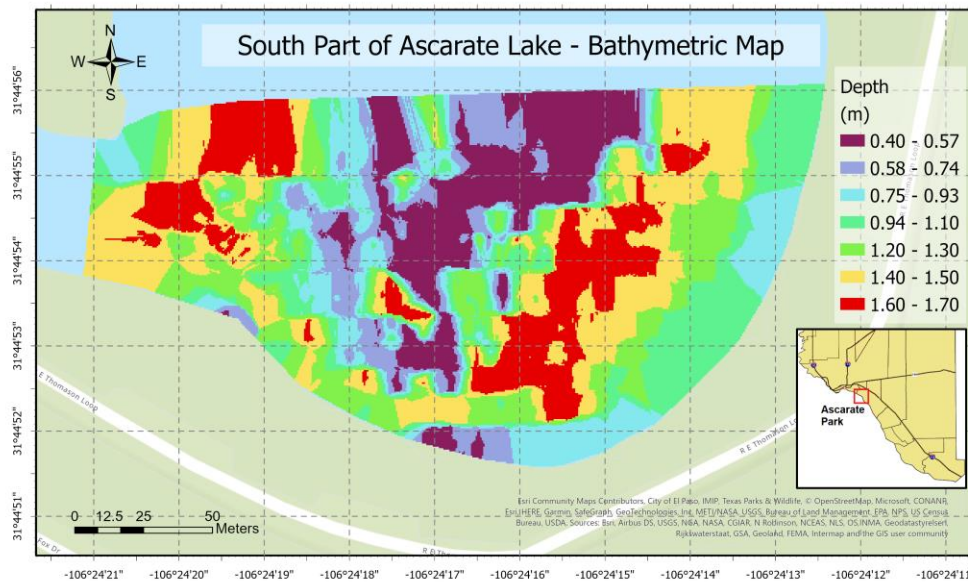
(c)



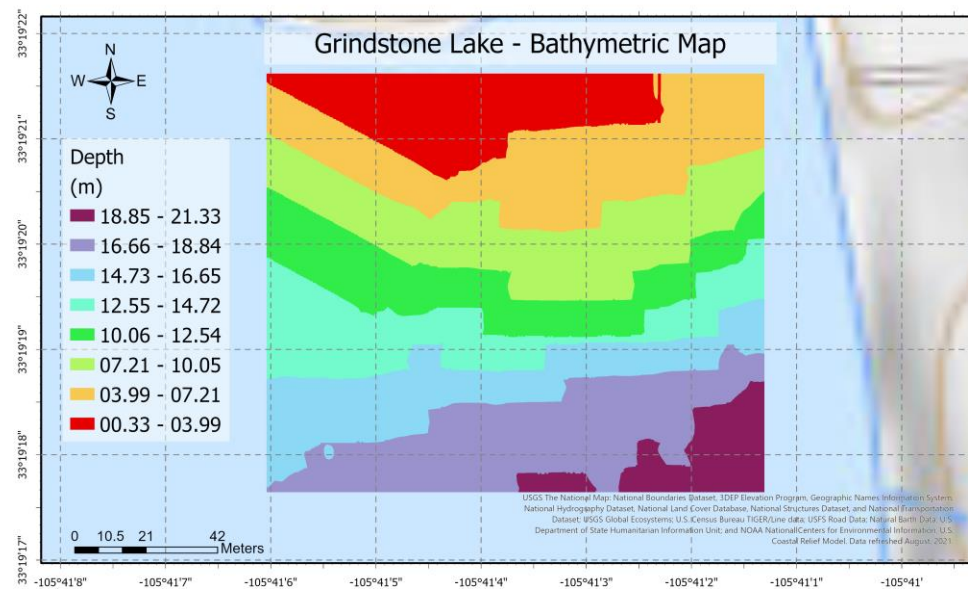
(d)

Figure 50. Bathymetric Map of the Ascarate Lake on March 03, 2022. (a) Mission 1 – Horizontal Path. (b) Mission 2 – Vertical Path. (c) Mission 3 – Spiral Path.

The data collected from the most extended successful missions generated the maps in Figure 51 using the previous interpolation method. A distance of 2,129.15 meters and 1,316.2 meters were respectively covered. The bathymetric drawings enclose an area of 28,210 m² (Figure 51 – a) and 14,400 m² (Figure 51 – b).



(a)



(b)

Figure 51. Bathymetric Maps. (a) South Section of the Ascarate Lake on May 19, 2022. (b). East Section of the Grindstone Lake on May 25, 2022.

4.5. Limitations of the Results

The two GPS systems present an offset in some path representations (Figure 39 and 40) in the previous chapter (Results and discussion) primarily due to the accuracy limitations between the two localization methods. A GPS 3D Fix positional mode that requires a minimum of four

satellites (Sager-Fradkin, et al., 2007) has been utilized in the ABES platform, supplying an accuracy from 1 to 2.5 meters in a clear sky view. In contrast, the positioning system employed in the payload used an RTK Quality GPS with accuracy from 0.03 to 1 meter. The GPS systems provided numerous accuracies in latitude and longitude, depending on cloud cover and satellite availability (Chunyue, et al., 2019). Additionally, a compass (River Surveyor M9) calibration is required prior to each discharge measurement to compensate for magnetic fields specific to the site, which has not been completed in some field campaigns.

Some study areas present a vast quantity of hydrilla. The sea submerged plants have been found inserted in the thrusters in some scenarios, which reduce the power supply to the propulsion system and control of the vehicle. An obstacle in the rudderless four thrusters system affects the boat's heading and speed since each propeller has a different throttle function. Thruster covers have been installed to prevent the adhesion of the vegetation without success because they generated considerable water resistance. In these scenarios, an increment in the required electric current to move the boat significantly reduced the operational hours. The solar power management system provides an additional power source that activates the failsafe command in a situation like the one previously described. However, the USV design may not be suitable for field studies with extensive vegetation.

The capability study shows a significant deviation in the turning points due to the inertia created by the weight of the platform; the distance between actual and desired waypoints increased to 2.5 meters in these locations. Moreover, the weather conditions influence the control capacity of the USV. Research by Wilson & Williams (2019) demonstrated that the most prominent errors pushed the Autonomous Surface Vessel (ASV) slightly outside the defined boundary due to increasing winds. The sensor integration systems prevent damage in the prototype during strong wind conditions by activating the automatic recovery system. Nevertheless, the failsafe command depends on the GPS functionality to return home. A machine learning algorithm running in the microprocessor that controls the position and direction of the vehicle might overcome the challenge of keeping the vessel safe under extreme conditions without the GPS sensor.

CHAPTER 5: FUTURE WORK

This section will provide solutions to the limitations of the platform in the previous chapter. The navigation system will be improved to reach an absolute accuracy of less than 50 centimeters by integrating an RTK-GPS module. However, to eliminate the GPS coordinate error between the platform (ABES) and the payload (River Surveyor M9), both positioning systems would be combined to reach higher levels of precision and accuracy. Data fusion of multiple sensors will develop more accurate and reliable navigation schemes and obtain the desired information worthy of further investigation (Sutton, 2011). In addition, a Maximum Power Point Tracking (MPPT) system would be incorporated to maximize the supply of solar panel power output, regardless of the temperature and irradiation conditions. Together with the integration of the second solar panel in a parallel configuration will provide the system with the double optimum operating current (5.38 Amperes) available to extend the duration of a mission and improve the battery recovery system. Furthermore, the steering control will be optimized with an improved PID algorithm model to control turning capabilities, such as the gradual decrease of the RPM supply to the thrusters at the turning points and hydro-jet thrusters to improve the propulsion system. The consolidation of the sensors and power configuration, which demonstrated strong capabilities, set the base of a reliable system that could benefit future research in adaptive path planning. Finally, the vast amount of data provided by the sensor integration systems would be utilized to implement a machine learning model to transform the preventive failsafe command into a self-navigation USV with predictive capabilities.

CHAPTER 6: SUMMARY AND CONCLUSIONS

This research studies the challenges in the development steps of an autonomous Unmanned Surface Vehicle for Bathymetric Surveys. The integration of heterogeneous sensors makes possible the effective navigation control of the platform that enables functions that deal with the communication limitations, the lack of accuracy in the data collection, and the government of the vehicle's state, such as position, orientation, and velocity. The design and integration of the Solar Power Management System (SPMS) extend the duration of the autonomous mission effectively, employing the energy of photovoltaic cells as a second power source. A transparent algorithm that analyzes real-time data collected by the sensors to make autonomous decisions that enhance the safety and coverage control of the prototype is implemented. Additionally, technical evaluation of the platform's subsystems is presented as measurable evidence of the reliability and robustness of the prototype.

The demand power of the numerous electronic components of the system was the base of the calculations for the energy requirements. Results show that a 60 Ampere-Hour battery system provides enough energy to navigate the boat for four hours. An assessment of two battery systems shows that the LiPO Battery system, usually used for drone applications, reaches the cut-off voltage in a short period compared to a LiFePO₄ battery connected to a solar controller powered by a solar panel. The Solar Power Management System (SPMS) is estimated to increment 37% of the length of a mission. Moreover, the 50-watt solar panel integrated into the vehicle does not work as a standalone cell charger due to the time constraints to completely charge a battery. However, the incorporation of the SPMS demonstrated in the field studies to be a reliable source of energy that can operate for four hours without the risk of reaching the cut-off voltage. In addition, during the pauses of a mission, it can automatically provide energy to the batteries until it overpasses the nominal operating voltage that enables the use of the vehicle in scenarios that would not be possible with the LiPO battery system.

This thesis focuses on the hardware and software design involved in making self-governing decisions. Therefore, integrating a second microprocessor into the system permitted the live monitoring of critical parameters such as battery voltage, wind speed, radio signal, and temperature. The data collected by the sensors is the support to define the capabilities of the proposed platform. For instance, the lower limit operating voltage is 11.5 volts, the maximum operating temperature in the electronic box is 45 °C, and the highest operating wind speed possible is 25 km/h. Successfully tested in the field, these values set the safety operating perimeter of the prototype, which serves as a trigger signal to deploy the failsafe command. This feature creates an unflinching system that ensures the safety of the electronic components and the payload.

The navigation and motion control system is improved with the PID parameters tuning and integrating the GPS / IMU sensors. Likewise, a capability test measures the ability to meet required programmed waypoints. As a result, the propulsion system composed of the four thrusters shows a stable performance when it moves in one direction. However, the steering control performance declines at the turning points due to the inertia created by the weight of the boat or wind conditions. Nevertheless, the distance between the desired waypoint and the actual position does not influence the collected data quality. The statistical analysis demonstrated that the USV could reach a desired waypoint and path satisfactorily with an average deviation of one meter.

The vehicle is a perfect tool for surveying shallow water zones, hard-to-reach, or dangerous areas due to its omnidirectional, flexible, and robust capabilities. The Solar Power Management System (SPMS) proved to increase the duration of a mission over the standard LiPO battery system. The platform can reach speeds up to 1.5 m/s, but for surveying purposes, the ideal speed is best at 1.2 m/s to keep the balance between measurement accuracy and propulsion speed. At an ideal speed, the ABES can cover 13,160 meters, an area of 144,000 square meters, and collect 14,400 samples in four hours of operation. Likewise, it offers an economical solution to execute lentic and lotic scientific research since it offers good navigation time and control capabilities. It is an excellent example of how engineering can enable science.

REFERENCES

- Aissi, M., Moumen, Y., Berrich, J., Bouchentouf, T., Bourhaleb, M., & Rahmoun, M. (2020). Autonomous solar USV with an automated launch and recovery system for UAV: State of the art and Design. *International Conference on Electronics, Control, Optimization and Computer Science*, 1-5.
- Alvarez, L., Moreno, H., Segales, A., Pham, T., Pillar-Little, E., & Chilson, P. (2018). Merging Unmanned Aerial Systems (UAS) Imagery and Echo Soundings with an Adaptive Sampling Technique for Bathymetric Surveys. *Remote Sensing*, 1362.
- Åström, K., & Hägglund, T. (2004). Revisiting the Ziegler–Nichols step response method for PID control. *Journal of Process Control*, 635-650.
- Beattie, S. D. (2016). Understanding capacity fade in silicon based electrodes for lithium-ion batteries using three electrode cells and upper cut-off voltage studies. *Journal of Power Sources*, 426-430.
- Bhattacharjee, A. (2012). Design and Comparative Study of Three Photovoltaic Battery Charge. *International Journal of Advanced Computer Research*.
- Boukoberine, M. N., Zhou, Z., & Benbouzid, M. (2019). Power Supply Architectures for Drones - A Review. *IEEE*, 1-4.
- Brassington, G. (2017). Mean absolute error and root mean square error: which is the better metric for assessing model performance? *EGU General Assembly Conference Abstracts*, 3574.

- Campbell, S., Naeem, W., & Irwin, G. (2012). A review on improving the autonomy of unmanned surface vehicles through intelligent collision avoidance manoeuvres. *Annual Reviews in Control*.
- Chunyue, L., Jiajia, J., Fajie, D., Wei, L., Xianquan, W., Lingran, B., . . . Guoliang, Y. (2019). Modeling and Experimental Testing of an Unmanned Surface Vehicle with Rudderless Double Thrusters. *sensors*, 1-17.
- Contreras, M. T., Gironás, J., & Escauriaza, C. (2020). Forecasting flood hazards in real time: a surrogate model for hydrometeorological events in an Andean watershed. *Nat. Hazards Earth Syst. Sci*.
- da Silveira, C., Strenzel, G., Maida, M., Araújo, T., & Ferreira, B. (2020). Multiresolution Satellite-Derived Bathymetry in Shallow Coral Reefs: Improving Linear Algorithms with Geographical Analysis. *Journal of Coastal Research*.
- Davis, D. (2003). Water Quality Assessments for Selected New Mexico Lakes. *Monitoring and Assessment Section Surface Water Quality Bureau*, 16-17.
- Ferreira, H., Martins, R., Marques, E., Pinto, J., Martins, A., Almeida, J., . . . Silva, E. (2007). SWORDFISH: an Autonomous Surface Vehicle for Network Centric Operations. 3-6.
- Furfaro, T., Dusek, J., & von Ellenrieder, K. (2009). Design, Construction, and Initial Testing of an Autonomous Surface Vehicle for Riverine and Coastal Reconnaissance. *Department of Ocean Engineering*, 2-6.
- Harvey, J., Jarvis, R., Verstraete, D., Bagg, R., Honnery, D., & Palmer, J. (2012). Development of a Hybrid-electric Power System Model for a Small Surveillance Aircraft. *International Congress of the Aeronautical Sciences*, 1-3.

- Hell, B., Broman, B., Jakobsson, L., Jakobsson, M., Magnusson, Å., & Wiberg, P. (2012). The Use of Bathymetric Data in Society and Science: A Review from the Baltic Sea.
- Horrit, M., Bates, P., & Mattinson, M. (2016). Effects of mesh resolution and topographic representation in 2D finite volume models of shallow water fluvial flow. *Journal of Hydrology*, 1-3.
- Jaw-Kuen, S., Der-Ming, M., Pin-Ying, Y., Geng-Feng, W., & Jhij Hua, G. (2009). Design of a Solar Power Management System for an Experimental UAV. *IEEE Transactions on Aerospace and Electronic Systems*, 2-3.
- Jungwook, H., Yonghoon, C., Jonghwi, K., Kinwhan, K., Nam-sun, S., & Sun, Y. (2020). Autonomous collision detection and avoidance for ARAGON. *Maritime Safety and Environmental Research*.
- K. Anderson, D. G. (2016). A Grassroots Remote Sensing Toolkit Using Live Coding, Smartphones, Kites and Lightweight Drones. *Plos One*, 2-3.
- Kebkal, K., Glushko, I., Tietz, T., Bannasch, R., Kebkal, O., Komar, M., & Yakovlev, S. (2014). SONOBOT - An Autonomous Unmanned Surface Vehicle for Hydrographic Surveys with Hydroacoustic Communication and Positioning for Underwater Acoustic Surveillance and Monitoring. 2-10.
- Khare, N., & Singh, P. (2012). Modeling and Optimization of a Hybrid Power System for an Unmanned Surface Vehicle. *Journal of Power Sources*, 368-377.
- Kislik, C., Dronova, I., & Kelly, M. (2018). UAVs in Support of Algal Bloom Research: A Review of Current Applications and Future Opportunities. *drones*, 2-3.

- Kok Ping, J., Ling, A. E., Quan, T. J., & Dat, C. Y. (2012). Generic Unmanned Aerial Vehicle (UAV) for civilian application. *IEEE Conference on Sustainable Utilization and Development in Engineering and Technology*, 2-4.
- Kum, B.-C., Shin, D.-H., Jang, S., Lee, S., Lee, J., Moh, T., . . . Cho, J. (2020). Application of Unmanned Surface Vehicles in Coastal Environments: Bathymetric Survey using a Multibeam Echosounder. *Journal of Coastal Research*.
- Legleiter, C., & Kinzel, P. (2021). Improving Remotely Sensed River Bathymetry by Image-Averaging. *Water Resources Research*, 1-2.
- Liu, Z., Zhang, Y., Yu, X., & Yuan, C. (2016). Unmanned surface vehicles: An overview of developments and challenges. *Annual Reviews in Control*, 2-10.
- Morten, B. (2010). Topics in Guided Motion Control of Marine Vehicles. *Tapir Uttrykk*.
- O'Neill, B. (2006). Euclidean Distance. *International Encyclopedia of Education*.
- Osaretin, C. (2015). Design and Implementation of a Solar Charge Controller with Variable Output. *Electrical and electronic engineering*, 41-43.
- Rashid, M. (2001). *Power Electronic Handbook*. San Diego: Academic Press.
- Roberts, G., & Sutton, R. (2006). *Advances in unmanned marine vehicles*. London: The Institution of Engineering and Technology.
- Roy, N., & Sinha, R. (2007). Understanding confluence dynamics in the alluvial Ganga–Ramganga valley, India: An integrated approach using geomorphology and hydrology. *Geomorphology*, 1-2.
- Sager-Fradkin, K., Jenkins, K., Hoffman, R., Happe, P., Beecham, J., & Wright, G. (2007). Fix Success and Accuracy of Global Positioning System Collars in Old-Growth Temperate Coniferous Forests. *The Journal of Wildlife Management*, 1298--1308.

- Savitz, S., Blickstein, I., Buryk, P., Button, R., DeLuca, P., Dryden, J., . . . Potter , A. (2013). US Navy Employment Options for Unmanned Surface Vehicles (USVs). *Rand National Defense Reasearch Inst Santa Monica*.
- Sharma, S., Naeem, W., & Sutton, R. (2012). An Autopilot Based on a Local Control Network Design for an Unmanned. *J. Navig.*, 281-301.
- Šiljeg, A., Lozic, S., & Šiljeg, S. (2015). A comparison of interpolation methods on the basis of data obtained from a bathymetric survey of Lake Vrana, Croatia. *Hydrol. Earth Syst. Sci.*, 1-5.
- Skinner, K. (2011). Evaluation of LiDAR-Acquired Bathymetric and Topographic Data Accuracy in Various Hydrogeomorphic Settings in the Deadwood and South Fork Boise Rivers. *US Geological Survey: Reston, VA, USA*.
- Sonnenburg, C., & Woolsey, C. (2013). Modeling, Identification, and Control of an Unmanned Surface Vehicle. *Department of Aerospace & Ocean Engineering*.
- Sutton, R. a. (2011). Adaptive navigation systems for an unmanned surface vehicle. *Journal of Marine Engineering \& Technology*, 3--20.
- Tejado, I., Vinagre, B., Traver, J., Prieto-Arranz, J., & Nuevo-Gallardo, C. (2019). Back to Basics: Meaning of the Parameters of Fractional Order PID Controllers. *Mathematics*, 1-5.
- Traganos, D., & Reinartz, P. (2018). Mapping Mediterranean seagrasses with Sentinel-2 imagery. *Marine Pollution Bulletin*.
- Versini, P.-A., Gires, A., Schertzer, D., & Tchiguirinskaia, I. (2020). Measurements of the water balance components of a large green roof in the greater Paris area. *Earth Syst. Sci. Data*, 2-4.

Villa, J., Aaltonen, J., & Koskinen, K. (2020). Path-Following With LiDAR-Based Obstacle Avoidance of an Unmanned Surface Vehicle in Harbor Conditions. *IEEE Transactions on Mechatronics*.

Viney, I., & Kirk, G. (2000). Remote control and viewing for a total station.

Wilson, T., & Williams, S. (2017). Adaptive path planning for depth-constrained bathymetric mapping with an autonomous surface vessel. *Australian Centre for Field Robotics*, 1-13.

GLOSSARY

ABES: Autonomous Bathymetric Exploration System

ACDP: Acoustic Current Doppler Profiler

Ah: Ampere-Hour

DOF: Degrees of Freedom

GPS: Global Positioning System

IMU: Inertial Measurement Unit

LiFePO₄: Lithium Iron Phosphate Battery

LiPO: Lithium-Polymer

MAE: Mean Absolute Error

PID: Proportional Integral Derivative

PCB: Printed Circuit Board

PV: Photovoltaic

PWM: Pulse-Width Modulation

RF: Radio-Frequency

RTK: Real-Time Kinematic

RPM: Revolutions Per Minute

RMSE: Root Mean Square Error

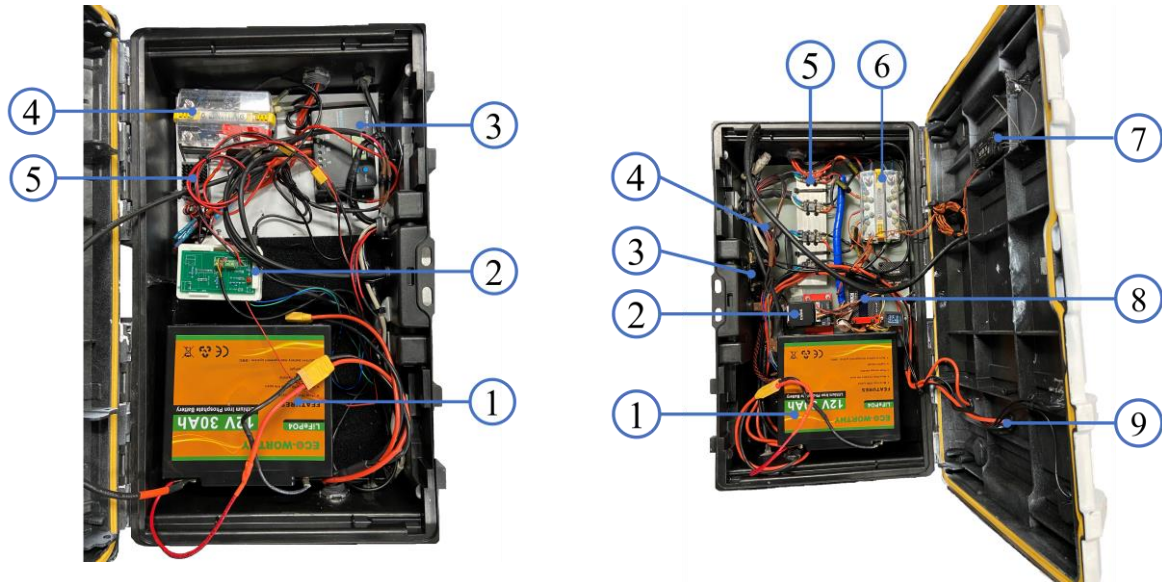
SOC: State of Charge

SPMS: Solar Power Management System

USV: Unmanned Surface Vehicle

APPENDIX

I. Electronic Enclosure Box Configuration



Left Enclosure Box	Right Enclosure Box
<ol style="list-style-type: none"> 1. LiFePO4 30Ah Battery 2. Sensor Integration. Microprocessor (Raspberry Pi 4) + PCB Design 3. Wanderer Solar Charge Controller 4. Dual Bus Bar Terminal 5. Voltage Regulator (Castle CC Bec Pro) 	<ol style="list-style-type: none"> 1. LiFePO4 30Ah Battery 2. Flight Controller (Pixhawk 2.1) 3. Telemetry Modem (RFD900+) 4. Buzzer 5. Speed Controller - Driver (Basic ESC) 6. Dual Bus Bar Terminal 7. Radio Receiver (FrSky Taranis) 8. Current / Voltage Control Board 9. Circuit Breaker

II. Sensor Integration Module



III. Cost Estimation

Item	Quantity	Unit Cost (USD)	Total Cost (USD)
Flight Controller (Pixhawk 2.1 and GPS Here 2)	1	\$ 330.00	\$ 330.00
Mauch Power Supply x8	1	\$ 142.00	\$ 142.00
Mauch 017 BEC	1	\$ 66.99	\$ 66.99
Muach PL 200	3	\$ 40.48	\$ 121.44
Radio Receiver (FrSky)	1	\$ 37.00	\$ 37.00
Telemetry (RFD900+)	1	\$ 107.00	\$ 107.00
Thruster T200	4	\$ 169.00	\$ 676.00
Thruster Controller (Basi ESC)	4	\$ 25.00	\$ 100.00
Cable (12 AWG)	1	\$ 29.98	\$ 29.98
150 A Circuit Breaker	1	\$ 25.57	\$ 25.57
Enclosure Box (Dewalt IP 65)	2	\$ 29.99	\$ 59.98
2.4 Antenna Extension	1	\$ 8.99	\$ 8.99
900 rpsma extension	2	\$ 5.98	\$ 11.96
20 A Castel Bec	1	\$ 37.00	\$ 37.00
River Surveyor Battery Mod / Plug	1	\$ 190.00	\$ 190.00
Bulkhead	1	\$ 10.49	\$ 10.49
Boat Dock Bumper	4	\$ 9.99	\$ 39.96
Boat Float	4	\$ 9.99	\$ 39.96
Extension Cable	1	\$ 12.49	\$ 12.49
U.FL Mini PCI to Reverse Polarity SMA Antenna	1	\$ 4.99	\$ 4.99
Cable Glands	1	\$ 9.99	\$ 9.99
Tube	1	\$ 37.89	\$ 37.89
USB bulkhead	1	\$ 16.98	\$ 16.98
Clamp RS	1	\$ 10.90	\$ 10.90
Clamp 2	1	\$ 37.90	\$ 37.90
Cables for Pixhawk	1	\$ 31.15	\$ 31.15
Metal For Frame	0.66	\$ 754.44	\$ 497.93
Zinc Alloy Flexible Hinge	2	\$ 17.68	\$ 35.36
XT-90 Female Connectors	1	\$ 9.98	\$ 9.98
ECO-WORTHY 5Amp 12V Battery Charger	1	\$ 55.99	\$ 55.99
Weather Meter Kit - Station	1	\$ 79.95	\$ 79.95
ECO-WORTHY 12V Lithium Battery - 30Ah	2	\$ 139.99	\$ 279.98
Raspberry Pi 4 Cable USB-C - 5.1V	1	\$ 8.00	\$ 8.00
2 Inch Adhesive Black Hook and Loop Tape	1	\$ 12.42	\$ 12.42
TYUMEN 100FT 20 Gauge 2pin 2	1	\$ 15.99	\$ 15.99
Cable Connect Charge 10 AWG	1	\$ 27.99	\$ 27.99
Resistant Black Cable Ties	1	\$ 8.99	\$ 8.99
Cable Ties (25.6")	1	\$ 27.99	\$ 27.99
Screw M8-1.25 x 14mm	1	\$ 7.81	\$ 7.81
Screw - M8 x 16mm	1	\$ 8.66	\$ 8.66
Small Bubble Level Frame	1	\$ 6.98	\$ 6.98
Solar Panel 50W + Controller	1	\$ 89.99	\$ 89.99
1000mm 4040 Aluminum Profile	1	\$ 33.99	\$ 33.99

M8 Thread T Spring Nut	1	\$	21.99	\$	21.99
Aluminum Extrusion Profile - (Color: 4040)	2	\$	17.68	\$	35.36
Raspberry Pi 4	1	\$	109.99	\$	109.99
INA219 - Sensor	1	\$	12.99	\$	12.99
DS18B20 - Sensor	1	\$	10.58	\$	10.58
4S Balance Plug Extension	1	\$	8.99	\$	8.99
<hr/>					
Total	68				\$3,604.51
<hr/>					

VITA

Fernando holds a bachelor's degree in Mechatronics Engineering from the ITESM in Mexico. He has five years of experience in the automotive manufacturing industry as a process engineer. Currently, in the last term of the M.S. in Electrical Engineering, conducting a study on the integration of an autonomous system. His research interests are sensor integration, mobile robots, data acquisition, automation, and positioning systems.

Contact Information: fsotelotor@miners.utep.edu